NIST Technical Note 1992

Impact of Ground Motion Selection Methods on the Seismic Assessment of Steel Special Moment Frames

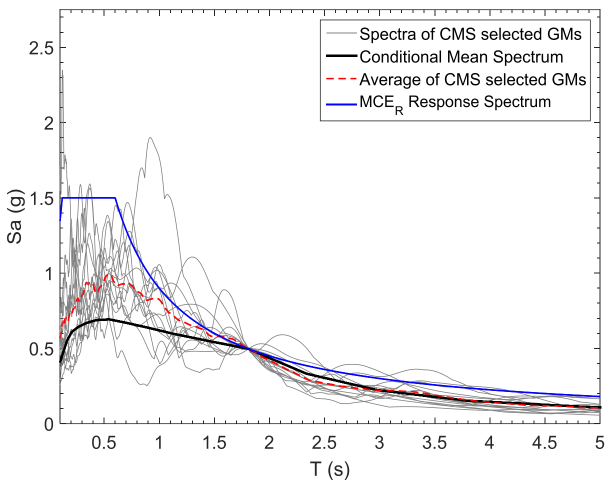

Raul Uribe
Siamak Sattar
Matthew S. Speicher
Luis Ibarra

This publication is available free of charge from:
https://doi.org/10.6028/NIST.TN.1992

National Institute of Standards and Technology
U.S. Department of Commerce

NIST Technical Note 1992

Impact of Ground Motion Selection Methods on the Seismic Assessment of Steel Special Moment Frames

Raul Uribe
Siamak Sattar
Matthew S. Speicher
Luis Ibarra

This publication is available free of charge from:
https://doi.org/10.6028/NIST.TN.1992

September 2018

U.S. Department of Commerce
Wilbur L. Ross, Jr., Secretary

National Institute of Standards and Technology
Walter Copan, NIST Director and Undersecretary of Commerce for Standards and Technology

National Institute of Standards and Technology Technical Note 1992
Natl. Inst. Stand. Technol. Tech. Note 1992, 108 pages (September 2018)
CODEN: NTNOEF

This publication is available free of charge from:
https://doi.org/10.6028/NIST.TN.1992

Abstract

This study quantifies the impact of different ground motion selection methods on the seismic performance evaluation of steel special moment frames. Two methods are investigated: a "traditional" approach, herein referred to as the Pacific Earthquake Engineering Research (PEER) method, and a newer approach known as the Conditional Mean Spectrum (CMS) method. The PEER method selects ground motions using the Risk-based Maximum Considered Earthquake (MCE_R) as the target spectrum, while the CMS method uses the conditional mean spectrum that anchor to the MCE_R at multiple conditioning periods. Three special moment frames of 4-, 8-, and 16-stories are designed in accordance with ASCE/SEI 7-10 to represent archetype steel frame buildings as found in regions of high seismicity. The seismic performance of these frames is assessed with the nonlinear dynamic procedure prescribed in ASCE/SEI 41-13, using ground motions selected and scaled in accordance with both methods. The performance of the buildings is evaluated at the Collapse Prevention (CP) performance level for a far-field site located in Los Angeles, CA. The CMS method results in lower mean and median response in terms of demand-to-capacity ratios in the reduced beam sections and column hinges. Ground motions selected and scaled using CMS result in a smaller dispersion of the output parameters in most of the beam and column elements, if the conditioning period that results in the highest mean demand-to-capacity ratio is the fundamental period, T_1. The results of this study show that the ground motion selection process can cause significant differences in structural response that may lead to different retrofitting decisions. These results provide motivation for engineers to consider the use of the CMS method as an alternative ground motions selection approach when assessing building performance.

Keywords:

ASCE/SEI 41, conditional mean spectrum, ground motion selection, performance-based seismic design, steel moment frame, seismic assessment.

TABLE OF CONTENTS

CHAPTER 1:

INTRODUCTION

Nonlinear dynamic analysis has become more popular among practitioners, mainly due to advancements in the simulation and computational capabilities, as well as the increasing use of performance-based seismic design approaches. One of the main steps in assessing the response of a building using nonlinear dynamic procedures is to analyze the building model for a suite of ground motions. Several ground motion selection methods have been developed that vary in terms of the selection criteria, error computation, target spectrum, etc. The premise of all ground motion selection methods is to select records that reasonably estimate ground motions anticipated to occur in a future earthquake at a specific site. Different ground motion selection methods lead to different nonlinear response results. For new buildings, the difference in structural response caused by these methods could lead to buildings being either over or under designed, which is less than ideal in either scenario. For the evaluation of existing buildings, differences in the selected ground motion method may lead to different retrofitting decisions that also may or may not be ideal.

In general, ground motion selection and scaling methods can be categorized as either a) amplitude scaling, or b) spectral matching (i.e., modification of frequency content). This study focuses on methods in the former category. A comprehensive list of various approaches to select and scale ground motions is reported in Haselton et al. (2009). One of the most commonly used methods involves scaling the records to match a specific intensity level at a given period, e.g., the spectral acceleration at the fundamental period, $S_a(T_1)$. The typical spectra used as targets are the Maximum Considered Earthquake (MCE_R)

spectrum, which is developed using parameters from ASCE/SEI 7-10 (ASCE, 2010), or the Uniform Hazard Spectrum (UHS), which is constructed from hazard curves from probabilistic seismic hazard analyses. These selection methods often give the ground motions that best match the target spectrum after they have been scaled. The basis for selecting the best match is to minimize the "error" (i.e., the difference) between the target spectrum and the selected ground motion. However, both the error and the target spectrum can be obtained in different ways, potentially leading to significantly different results.

This study focuses on two ground motion selection methods: 1) the PEER method, a well-established method widely used in research and practice; and 2) the Conditional Mean Spectrum (CMS) method, a newer method that has been employed primarily in research. In the PEER method, ground motions are selected to minimize the error between each ground motion spectrum and the target spectrum, MCE_R in this study, across a range of periods. The approach is referred to as the PEER method because it is implemented using the PEER online tool (PEER, 2016). Other studies have used methods similar to the PEER method that match records to the MCE_R spectrum while minimizing the error in a specified range for use in nonlinear analyses (Harris and Speicher, 2015; Kalkan and Chopra, 2010). In contrast, the CMS method uses the conditional mean spectrum as the target for selecting and scaling the ground motions at the selected conditioning period. Therefore, the CMS method can be considered a single target spectral acceleration approach in which the spectral accelerations at the conditioning period will exhibit no dispersion (Adam et al., 2016).

To investigate the effects of these ground motion selection methods, newly designed 4-, 8- and 16-story structural steel buildings with special moment frames are assessed using the nonlinear dynamic procedure outlined in ASCE/SEI 41-13 (ASCE, 2014) for ground motions selected using the CMS and PEER methods. These buildings come from a series of reports and papers that highlighted the need to investigate the effects of ground motion selection and scaling methods on nonlinear dynamic assessment results as it pertains to ASCE 41 (Harris and Speicher, 2015; Speicher and Harris, 2016a, 2016b; Sattar, 2018). The predicted performance of the buildings, in terms of nonlinear hinge deformations and their corresponding dispersion, is compared for the two selection methods.

CHAPTER 2:

BACKGROUND ON GROUND MOTION SELECTION AND SCALING METHODS

2.1 Conditional Mean Spectrum Method

The CMS method is a site-specific ground motion selection method in which scaled ground motion records are selected based on how closely they match a conditional mean target spectrum across a range of structural vibration periods (Baker, 2011). The CMS method was developed as an alternative to the more conservative uniform hazard spectrum (UHS). The UHS is constructed from spectral acceleration values of hazard curves developed using probabilistic seismic hazard analysis at a selected probability of exceedance (e.g., 2 % in 50 years) with every value of the UHS having the same exceedance probability. The CMS is a more realistic target for selecting and scaling ground motions because of the intrinsic conservatism in the UHS due to the unlikely scenario of all the “high” spectral accelerations occurring in a single event (Baker, 2011). Instead, the CMS is conditioned, or anchored, to a single spectral acceleration at a period of significance, such as the building’s fundamental period.

In this study, the risk-targeted maximum considered earthquake (MCE_R) is selected as the spectrum to anchor the CMS, and it is computed following ASCE/SEI 7-10 recommendations. Once the spectral acceleration at the conditioning period (i.e., the period in which the spectral acceleration of the CMS matches the MCE_R) is determined, the median ground motion spectrum is calculated using the Campbell and Bozorgnia ground motion prediction model (GMPM) (Campbell and Bozorgnia, 2008). The CMS spectrum, is then computed using Eq. (1):

$$\mu_{\ln Sa(T_i)|lnSa(T^*)} = \mu_{\ln Sa}(M, R, T_i) + \rho(T_i, T^*)\varepsilon(T^*)\sigma_{\ln Sa}(T_i) \tag{1}$$

where $\mu_{\ln Sa(T_i)|\ln Sa(T^*)}$ is the logarithmic mean S_a at period T_i, for a given S_a at period T^*, $\mu_{\ln Sa}(M, R, T_i)$ is the median ground motion spectrum, also denoted as the logarithmic mean of S_a, M and R are the earthquake mean magnitude and mean distance from deaggregation, respectively, $\rho(T_i, T^*)$ is the correlation coefficient between ε at T_i and T^*, $\varepsilon(T^*)$ represents the number of standard deviations the target spectral acceleration differs from the median ground motion at the conditioning period (Baker, 2011), and $\sigma_{\ln Sa}(T_i)$ is the standard deviation of $\ln S_a$ at period T_i from the GMPM. Additional information regarding the calculation of the CMS target spectrum is provided in (Lin et al., 2013). The computed CMS has lower spectral accelerations than the MCE_R spectrum, except for the acceleration at the conditioning period, which matches the MCE_R as shown in Figure 1. These lower spectral values are more noticeable at shorter periods, where structural higher modes are located, but can also be observed at longer periods. This implies that use of the ground motions matched to the CMS provides a more realistic basis to evaluate the structural performance.

Once the CMS target spectrum is developed, the ground motions are selected based on how similar their spectrum is to the CMS. The degree of similarity is based on the smallest sum of squared errors (SSE) as defined in Eq. (2):

$$SSE = \sum_{i=1}^{n} \left(\ln S_a(T_i) - \ln {S_a}^{CMS}(T_i)\right)^2 \tag{2}$$

$\rho(T_i, T^*)\varepsilon(T^*)$where S_a is the individual record spectral acceleration, S_a^{CMS} is the CMS spectral acceleration, and T_i is the period. The upper limit n in the summation refers to the number of partitions of the period interval of interest. The ground motions with the least amount of error are chosen, resulting in a mean ground motion spectrum that closely matches the conditional mean spectrum. There are other methods in which ground motions are selected to match both the variance, $\sigma_{lnSa}(T_i)$, and mean of the ground motion spectra computed from a ground motion prediction model (e.g. conditional spectra (CS) method (Lin et al., 2013)), but they are not part of this study.

2.2 PEER Method

The second method used in this study scales ground motions to minimize the error between each ground motion spectrum and the target spectrum, MCE_R, across a range of periods. The difference in acceleration amplitude at selected periods between the target spectrum and each individual spectrum is defined as an error, and computed using the mean squared error (MSE) as follows in Eq. (3):

$$MSE = \frac{\sum_i w(T_i)\left\{\ln\left[S_a^{target}(T_i)\right] - \ln\left[f * S_a^{record}(T_i)\right]\right\}^2}{\sum_i w(T_i)} \tag{3}$$

where $w(T_i)$ is the weight assigned to the period, T_i; S_a^{target} is the target spectral acceleration; S_a^{record} is the individual record spectral acceleration, and f is the linear scale factor assigned to the entire ground motion.

In this study, period weighting factor, w, is set to 1.0 across the range of interest from $0.2T_1$ to $2T_1$, as specified by ASCE/SEI 7 for matching ground motions. The scale factor

f in Eq. (1) is optimized to have the smallest MSE achievable within the same range of periods as the weight function. With this method, the smaller the error, the better the individual ground motion spectrum matches the target spectrum over the range of interest.

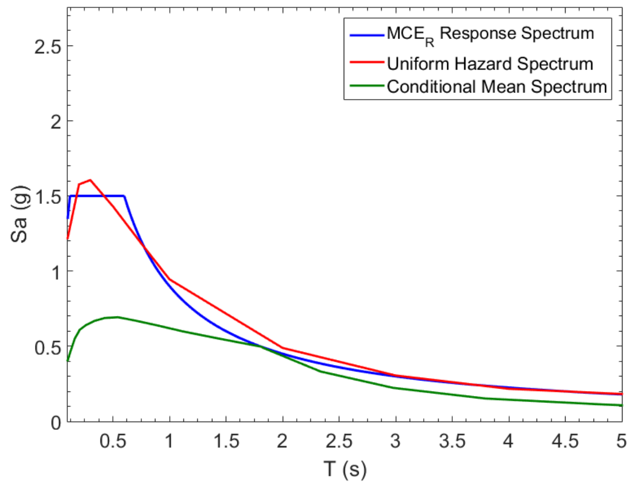

Figure 1. Comparison of the UHS, MCE$_R$ spectrum, and CMS conditioned at T_1 = 1.81 s for the 4-story SMF

CHAPTER 3:

BUILDING DESCRIPTION AND MODELING

3.1 Design and Configuration

Three archetype buildings (4-, 8-, and 16-stories) are evaluated in this study. The buildings are designed in accordance with the 2012 International Building Code (IBC) (ICC, 2012), and its referenced standards ASCE/SEI 7-10 and AISC 341-10 (AISC, 2010). The seismic force-resisting system (SFRS) is an exterior three-bay special moment frame (SMF) in the east-west direction and an exterior two-bay special concentrically braced frame (SCBF) in the north-south direction. This study focuses only on the SMF performance. Figure 2 shows a typical building floor plan and Figure 3 shows the SMF elevations for the 4-, 8-, and 16-story buildings. Reduced beam sections (RBSs) are used for the SMF beam-to-column connections, and columns are sized to satisfy strong-column/weak-beam requirements. Additionally, columns are upsized where necessary to avoid the use of doubler plates to strengthen/stiffen the column webs, to reflect what is done in practice. Detailed information regarding building properties, materials, and the design process can be found in Harris and Speicher (2015).

The building is assumed to be located on a site with stiff soil (Site Class D), and is assigned to Seismic Design Category D with spectral accelerations S_S = 1.5 g at T_s = 0.2 s., and S_1 = 0.59 g at T_1 = 1.0 s. The equivalent lateral force (ELF) procedure of ASCE/SEI 7-10 is used to determine the seismic design loads. The frames are also designed to resist wind loads, in which the basic wind speeds are set to 177 km/h (110 mph) for the 700-year wind (strength) and 116 km/h (72 mph) for the 10-year wind (drift).

3.2 Overview of PERFORM-3D Model

The buildings are modeled in three dimensions using PERFORM-3D (CSI, 2011). The special moment frame (SMF) models used for the nonlinear analysis are the same as those used in the Harris and Speicher (2015) study. For the gravity framing system, the beams and columns are modeled with elastic elements, and the beam-to-column connections as pinned. For the SFRS, each potential nonlinear action is modeled with a discrete nonlinear element. The nonlinear behavior of the beams is modeled with moment-curvature hinges that are placed at the centerline of each RBS. The reduced stiffness of the RBS is captured by using a prismatic section over the entire length of the RBS with cross-sectional properties equal to those at one-third of the length of the RBS from the center of the RBS. The nonlinear behavior of the columns is modeled with moment-curvature hinges that account for axial-moment interaction (i.e., referred to as PMM hinges in PERFORM-3D). These column hinges are placed at one-half the column depth away from the face of the beam. The column base is modeled as fixed. Lastly, the nonlinear behavior in the panel zones is modeled with PERFORM-3D's panel zone element, which is based on the Krawinkler model (Krawinkler, 1978). Each one of these nonlinear component models is initially constructed using ASCE/SEI 41-13 modeling parameters defined in ASCE/SEI 41-13 Table 9-6, and then qualitatively calibrated against experimental tests (see Harris and Speicher, 2015).

The nonlinear analysis is set to terminate when the solution fails to converge or when an arbitrary roof drift ratio of 20 percent is reached. Collapse modes not modeled herein (e.g., failures in the gravity framing system) would likely occur well before a 20 percent drift is reached. The impact of modeling uncertainty is not considered in this study, but has been shown that it can influence results in other studies (e.g., Sattar et al. (2013)).

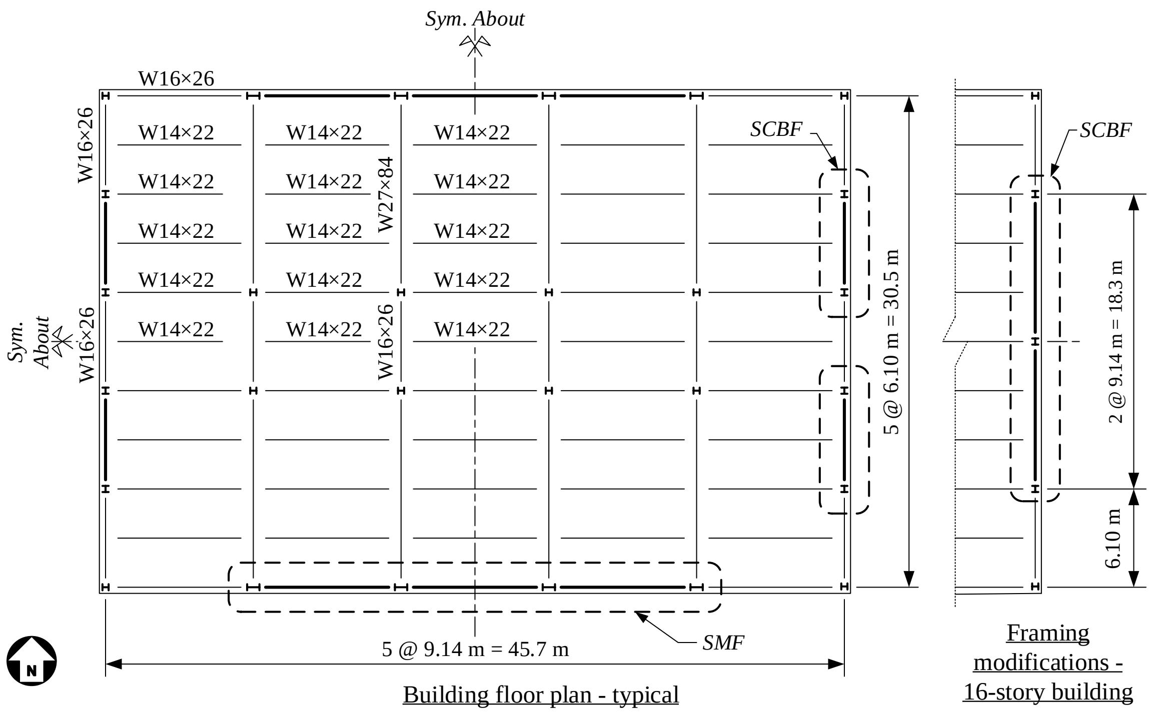

Figure 2. Floor plan for the archetype buildings used in this study (note: member section sizes are given in US customary units).

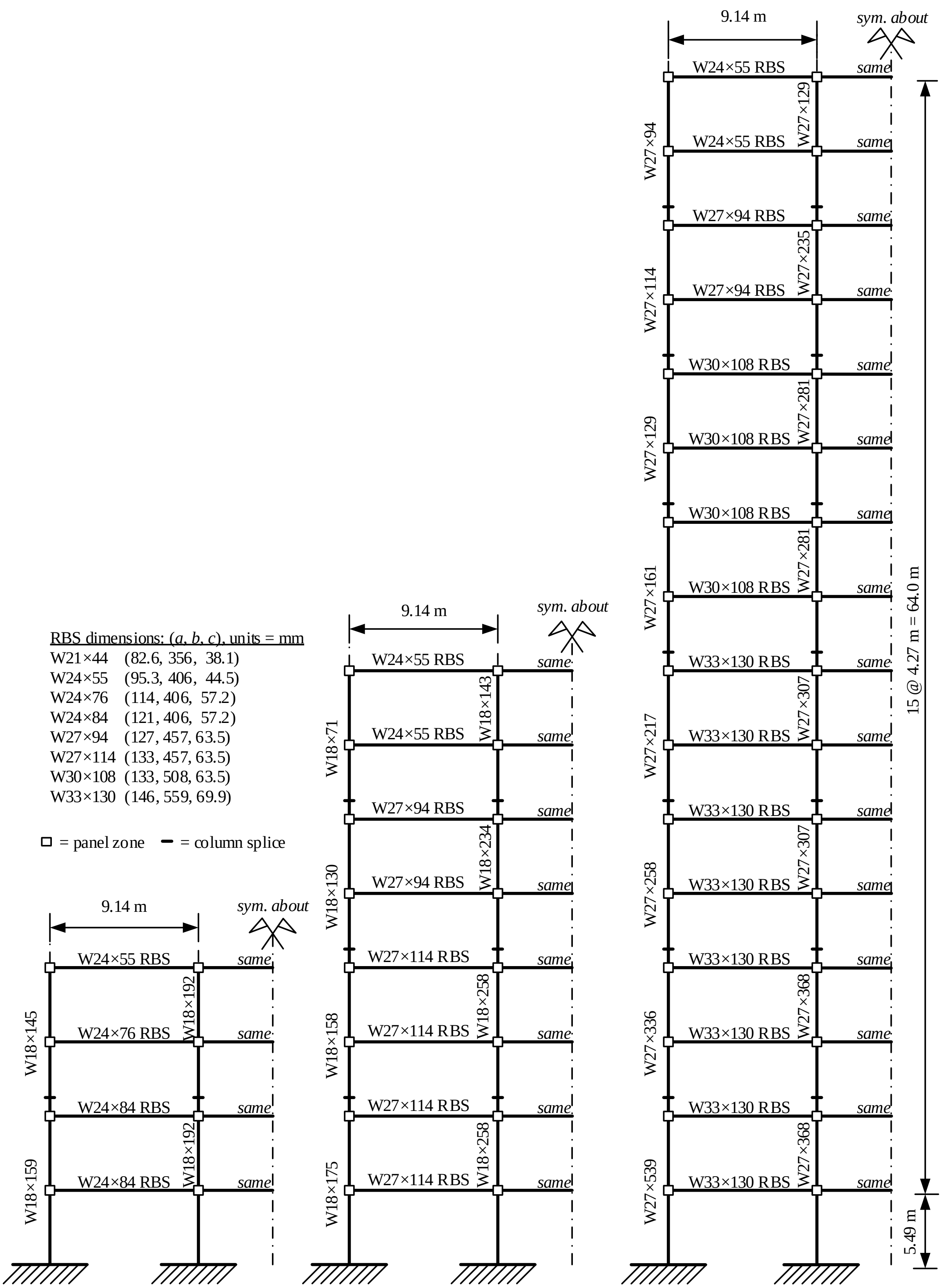

Figure 3. SMF elevations for the 4-, 8-, and 16-story building used in this study (note: member section sizes are given in English units).

CHAPTER 4:

IMPLEMENTATION OF THE GROUND MOTION SELECTION

4.1 Site Selection

The archetype buildings are assumed to be located in Los Angeles, CA, a densely populated city with a large and diverse building stock located in an area of high seismicity. A far-field site within the Los Angeles area is selected based on the soil classification and the mean rupture distance. The soil type is selected to match the site class used in the archetype building design, i.e., soil type D with an average shear wave velocity (V_{s30}) of 180-360 $\mathrm{m/s}$ (USGS, 2016a). The selected site has a V_{s30} value of 300 m/s to 360 m/s. The site is selected to satisfy the ASCE/SEI 7-10 requirements for a far-field site, i.e., located more than 15 km (9.3 miles) from a rupture plane. A site can also be considered far-field in the 10 km to 15 km range as long as the Richter magnitude of the earthquake produced at the site is less than 7.0 (ASCE, 2016). The selected far-field site (latitude/longitude = 34.197 degrees/ -118.645 degrees) has a mean rupture distance from the assumed site of 17.2 km according to the deaggregation computed with the USGS deaggregation tool (USGS, 2016b).

4.2 General Criteria for Ground Motion Selection

The criteria for the selection and scaling of ground motions meet or exceed ASCE/SEI 7-16 requirements. For example, the selection of 14 records exceeds ASCE/SEI 7-16 requirements of 11 records for a nonlinear dynamic analysis. ASCE/SEI 7-16 is used for the ground motion selection (rather than ASCE/SEI 7-10) because it is the first reference standard that includes a set of recommendations for use of the CMS method. The selection and scaling implemented include the following stipulations for the two methods investigated:

1. Fourteen ground motions records are selected (ASCE/SEI 7-16 requires 11 records)
2. The scale factor on individual records is no greater than 2.5 (ASCE/SEI 7-16 limits the scale factor to 4.0)
3. No more than one record is selected from any one recording station
4. No more than three records are selected from the same earthquake event

The scale factor cap of 2.5 keeps the ground motion characteristics and shape closer to what may be expected based on the recorded motions. The limitations on the amount of records included in the ground motion suite from a certain recording station or event prevents the suite from being overly influenced by a single event.

4.3 Implementation of Conditional Mean Spectrum Ground Motion Selection

The first step in implementing the CMS method is to choose the conditioning periods. The fundamental period of the system, T_1, is the main conditioning period, but additional conditioning periods are selected to account for different structural performance aspects (NIST, 2011). A short conditioning period is used to account for higher mode contributions, while a long conditioning period accounts for period elongation effects (Lin et al., 2013). This study follows the suggestions of ASCE/SEI 7-16 that recommend using a lower limit of no more than $0.2T_1$ and an upper limit of no less than $2T_1$ for the bounds of the period range. Accordingly, periods of $0.2T_1, T_1$, and $2T_1$ are initially selected as the conditioning periods. A fourth conditioning period of $0.4T_1$ is added to satisfy the

ASCE/SEI 7-16 requirement for having the envelope of the target spectra exceed 75 % of the MCE_R between $0.2T_1$ and $2T_1$. The selection of these four conditioning periods is employed on the 4- and 8-story buildings. For the 16-story building, only the $0.2T_1, 0.4T_1$, and T_1 conditioning periods are necessary to meet the 75 % envelope criteria.

Ground motions are selected following the procedure developed by Jayaram et al. (2011). In this study, the tool developed by Baker (2016) is used to automate this process, as described in detail in Appendix A. The tool first constructs the target CMS based on the structural properties and the site's hazard deaggregation, and then selects a set of ground motions from the PEER NGA-West2 ground motion database (PEER, 2016) with the least amount of error (SSE; Eq. (2)) with respect to the target conditional mean spectrum. The scale factor for each ground motion is determined by dividing the spectral acceleration value of the CMS at the conditioning period by the acceleration value of the selected ground motion at the same period. This method of scaling ensures that every selected ground motion, for a given target spectrum, has the same S_a at the conditioning period, thus creating a "pinch point". Figure 4(a) shows the 14 ground motions selected using the CMS method for the 4-story building conditioned at the fundamental period, T_1. Figure 4(b) presents the target and the average mean spectra for the four conditioning periods used in this study (i.e., $0.2T_1, 0.4T_1, T_1$, and $2T_1$). The frames are evaluated for the ground motion sets selected at the conditioning periods to identify the maximum mean demand. Appendix B summarizes the records selected using the CMS method for the three buildings.

4.4 Implementation of PEER Ground Motion Selection

The PEER NGA-West2 database tool (PEER, 2016) is used in this study to select ground motions based on minimizing the error (MSE, Eq. (3)) across the period range of $0.2T_1$ and $2T_1$ with respect to the MCE_R target spectrum (see Appendix A). The tool input parameters include magnitude, rupture distance, shear wave velocity, scale factor, weight function, and type fault. No restriction is considered for fault type or ground motion shape. The desirable rupture distance is selected between 10 km and 110 km to ensure the tool selects only far-field ground motions with no forward directivity effects. Note that ground motions with a distance between 10 km and 15 km must have a magnitude lower than 7.0 to be selected. The shear wave velocity (V_{s30}) is chosen between 300 m/s and 360 m/s to select records that occurred in soil conditions similar to the selected site. A uniform weight (w = 1.0 in Eq. (3)) is considered for computing the error at various periods in the range of interest. Ground motions are selected independent of component direction, and the 14 scaled records with the minimum MSE are selected with the condition that no more than one record is selected from the same station and seismic event. The selected ground motions, which are already scaled once to minimize the MSE, are scaled for a second time using a single scale factor applied to all records in the set, to ensure that the arithmetic mean of the ground motions does not drop below the target spectrum between $0.2T_1$ and $2T_1$ (ASCE/SEI 7-16). In the PEER method, the maximum scale factor to minimize the MSE for *individual* ground motions is set as 2.5. However, this limit may be exceeded when the arithmetic mean (average) spectrum of the 14 individual records is scaled to ensure the mean spectrum is equal to or larger than the MCE_R target spectrum, but even in this case the scale factor is still less than four, as recommended by ASCE/SEI 7-16. Figure 4(b) shows the average of 14 ground motions selected using the PEER method for the 4-story building. Figure 4(c) shows the spectra of a set of ground motions selected for the 4-

story frame using the PEER method. To see the records selected with the PEER method for all three buildings, refer to Appendix B. As observed, PEER method is not a single target spectral acceleration approach, and the average acceleration of PEER records is higher than that of CMS records between $0.2T_1$ and $2T_1$. This difference implies that PEER ground motions may lead to larger inelastic building responses than CMS records.

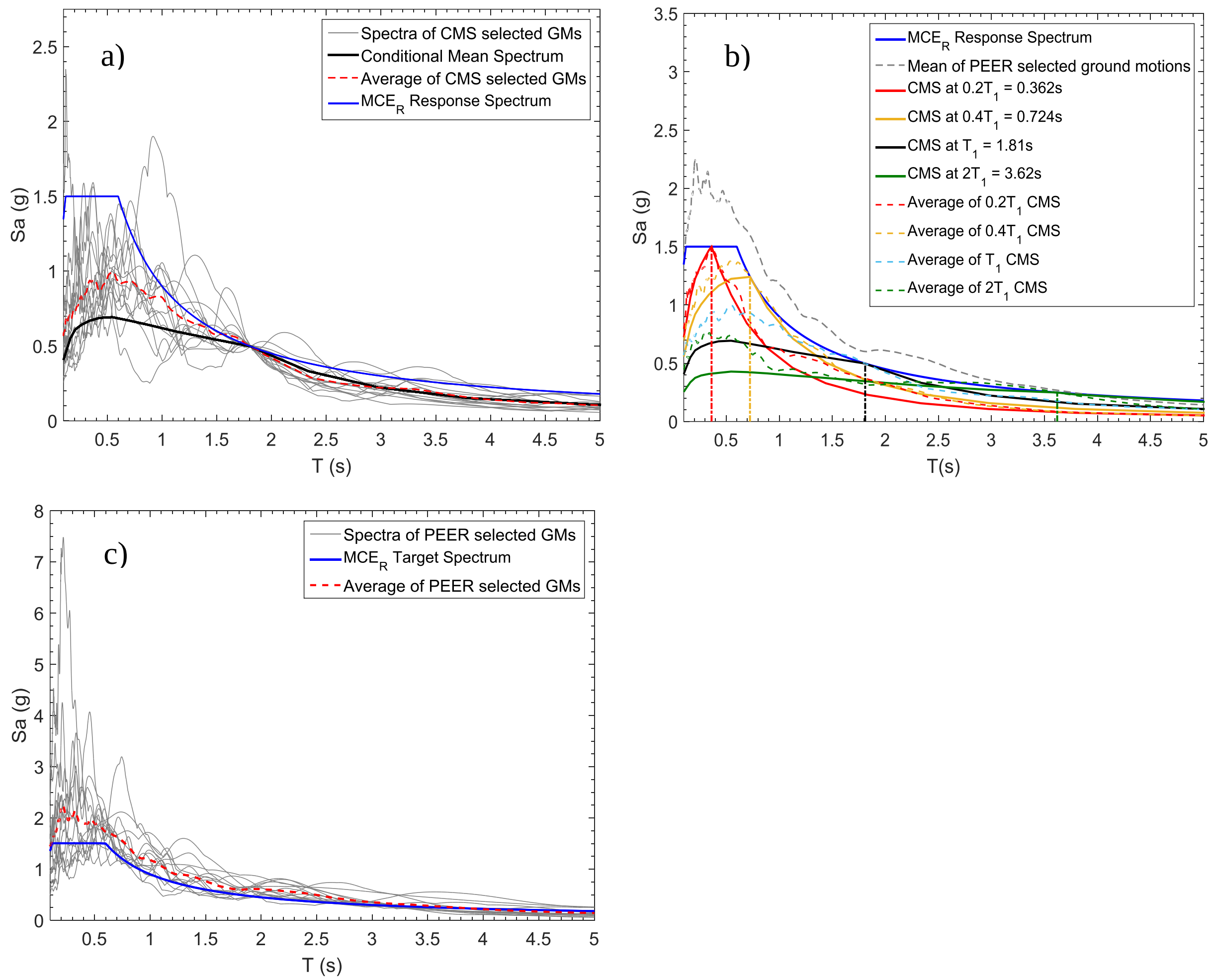

Figure 4. For the 4-story building, (a) the response spectra of ground motions selected using the CMS method conditioned at $T_1 = 1.81$ s; (b) the target and average CMS spectra for four conditioning periods in comparison with the average of the PEER spectra; and (c) response spectra of ground motions selected using the PEER method.

CHAPTER 5:

ASSESSMENT OF MOMENT FRAMES

An ASCE/SEI 41-13 seismic performance assessment using the nonlinear dynamic procedure is conducted in this study with the structural performance evaluated at the Collapse Prevention (CP) level. The following section briefly describes the nonlinear model. Additional details on carrying out the ASCE/SEI 41 assessment on these archetype buildings can be found in Harris and Speicher (2015).

5.1 Format for Results Presentation

The results are presented in terms of a *normalized* demand-to-capacity ratio, DCR_N (the N subscript is added to distinguish it from the *DCR* defined in ASCE/SEI 41-13 §7.3.1.1, which is the unreduced demand-capacity ratio in a linear analysis). A DCR_N value greater than unity indicates that a component does not satisfy the acceptance criteria. The DCR_N is computed as shown in Eq. (4) and Eq. (5)(Harris and Speicher, 2015):

Deformation-controlled action:

$$DCR_N = \frac{\theta_{total}}{\kappa\left(\theta_y + \theta_{pe} + \theta_{p,AC}\right)} \tag{4}$$

Force-controlled action:

$$DCR_N = \frac{\theta_{total}}{\kappa\theta_y} \tag{5}$$

where θ_y is the yield deformation, θ_{pe} is the post-yield elastic deformation, θ_{total} is the total deformation, $\theta_{p,AC}$ is the acceptance criterion based on plastic deformation defined in ASCE/SEI 41, and κ is the knowledge factor. The total deformation is used because the PERFORM 3D moment-curvature output is in terms of total (elastic + plastic) curvature (moment-curvature hinges are used for the columns and beams). Figure 5 illustrates the variables on a generalized backbone curve for a component required for the calculation of DCR_N. The acceptance criteria for all elements are set to the Collapse Prevention performance level for the three buildings. The knowledge factor is taken as unity since all the buildings are new and all their respective information is known.

ASCE/SEI 41-13, Chapter 9, defines which actions are force- versus deformation-controlled in an SMF. In general, an action is considered deformation-controlled if inelastic response is expected and the component exhibits ductile behavior. In contrast, an action is considered force-controlled if inelastic action is not desired or if the component exhibits non-ductile behavior. Beam-to-column connections and panel zone rotations are generally considered deformation-controlled, while column rotations classification depends on the level of axial load, which must reach approximately 50 % of column axial capacity under static conditions for the component to be considered a force-controlled action. Axial deformations in columns are always considered force-controlled. Note that for the column hinges, the fact that some hinges may be considered force-controlled and, therefore, should be checked to see if they have yielded, is reflected in the results.

5.2 Central Measures of Dispersion using ASCE 41 Approach

In this section the DCR_N plots for nonlinear dynamic analysis of the 4-, 8-, and 16-story moment frames are presented for the arithmetic mean and median response of the RBS and column hinge components. The arithmetic mean response is considered because ASCE/SEI 41-13 Table 7-1 indicates that the average response should be reported for a far-field site when 10 or more records are used in the time history analysis. In calculation of the arithmetic mean and median, all analysis results, including the "collapsed" cases, are used. A case is considered to have "collapsed" when the 20 % drift limit is reached in the analysis. This does not mean that collapse occurs at a 20 % drift; collapse is expected to occur before the roof reaches this drift limit. Therefore, this drift limit is simply a trigger to terminate the analysis. If the solution algorithm fails to converge, the maximum DCR_N response attained from the record is used, which may or may not be "collapse". The DCR_N results at the CP performance level for Bay D-E of the moment frame are presented in this section. To see the results for the other bays, refer to Appendix C.

Figure 6(a) shows the mean DCR_N values for the RBS hinges over the height of the 4-story building using the PEER and CMS methods. The DCR_N values for the CMS method correspond to the controlling period for which the analysis produced the largest mean DCR_N at each floor. In the case of the 4-story building, the controlling period for all the RBS elements is the $0.4T_1$ conditioning period. The results presented in Figure 6(a) show that the CMS method provides lower DCR_N than those obtained from the PEER method at every floor level, with the maximum difference of about 55 % in mean and median with respect to the PEER values. Figure 6(a) also shows that the RBS connections do not pass the ASCE/SEI 41-13 acceptance criteria, i.e., the mean DCR_N value is greater than 1.0, when PEER method ground motions are employed. Conversely, the same components show satisfactory performance when CMS method ground motions are used. More importantly, some of the 14 ground motions records may produce collapse, and in these cases a roof drift limit of 20 % is used in the calculations, significantly increasing the mean demands.

As shown in Figure 6(b), the column hinges of the 4-story present a similar pattern as the RBS connections, in which the CMS method results in lower DCR_N than the PEER method, with maximum differences in the mean and median of approximately 60 % and 45 %, respectively. There are three different controlling periods for columns: $0.4T_1$ for the first story, T_1 for the second and third stories, and $0.2T_1$ for the 4th story. The largest difference between the $\mathrm{DCR_N}$ of column hinges computed using the two methods occurs at the base of the building, where columns are expected to yield first and experience larger inelastic deformation. The PEER ground motions are expected to induce a higher level of nonlinearity in the building components than the CMS method, because the PEER ground motions have higher average spectral acceleration values, as shown in Figure 4b. These higher nonlinearities occurring from using the PEER method lead to more collapse cases, as reported in Table 1, increasing the average DCR_N. Table 1 summarizes the number of CMS and PEER ground motions that lead to collapses for the three buildings considered in this study. In the table, for the computation of the DCR_N dispersion later, cases where the solution fails to converge are treated as collapse.

The results of the 8-story building are similar to those of the 4-story building with the CMS selected ground motions providing lower DCR_N values than those from the PEER method, as shown in Figure 7(a). For the 8-story RBS components, the mean and median of the DCR_N results for the CMS method are lower than those obtained with the PEER method by 70 % and 55 %, respectively. The controlling period for the beam elements are T_1 for the 2nd through 6th floors, $0.4T_1$ for the 7th floor, and $0.2T_1$ for the last two floors. The column hinges in the 8-story frame also show the CMS records provide a lower response with the maximum difference in the mean and median of about 60 % and 40 %, respectively, with respect to the PEER values. The results for the column hinges in the 8-story frame are presented in Figure 7(b). Similar to the RBS, the columns are mostly controlled by the T_1 conditioning period, which controls from the base up to the 5th story. The 6th and 7th stories are controlled by the $0.4T_1$ and the 8th story by the $0.2T_1$ conditioning period. The lower stories of the building are controlled by the first-mode while the upper stories are controlled by higher modes, e.g. $T_2 = 0.98$ s., which is expected (Baker, 2011). Note that the RBS or column hinge (CH) components that exceeded the acceptance criteria, i.e. mean $DCR_N > 1.0$, for the CMS records are those in the lower floors controlled by the T_1 conditioning period. The 16-story building shows a similar trend to the 4- and 8-story results with lower mean and median demands in DCR_N coming from the CMS selected ground motions. As shown in Figure 8, the RBS components show a lower CMS mean DCR_N with a maximum difference of approximately 95 % in comparison with PEER results. The difference between the CMS and PEER mean results is larger for the 16-story frame, compared to the 4- and 8-story, because the CMS method does not lead to any collapse in this building, whereas the PEER method has one realization that collapses and one that does not converge, as reported in Table 1. An important reason for such a large difference is that the response of most of the beams in the CMS method is controlled by the T_1 conditioning period, which has an average spectrum with significantly lower spectral accelerations than the PEER spectrum, as shown in Figure 9. For instance, at T_1 = 4.12 s., the PEER spectral acceleration is nearly 200 % larger than that of the CMS spectrum. Therefore, the CMS records produced lower DCR_N values, and collapse is less likely to occur. The median DCR_N for the CMS records has a maximum difference of 70 % with respect to that obtained from PEER records. Figure 8(b) presents mean and median DCR_N results for the column hinges which are lower when the CMS method is used. The CMS results satisfy ASCE/SEI 41-13 acceptance criteria, while the PEER method has all but three columns satisfy the criteria. The column DCR_N mean and median percent difference, with respect to the PEER results, are 75 % and 97 %, respectively. Table 2 summarizes the percent difference in mean and median DCR_N values for the CMS method of the RBS and CH elements with respect to the PEER values of the three structures. The percentage differences reported are computed as follows:

$$\%\, Difference = \frac{DCR_{N,PEER} - DCR_{N,CMS}}{DCR_{N,PEER}} \times 100 \qquad (6)$$

where $DCR_{N,PEER}$ corresponds to the demand-to-capacity ratio for the PEER method of a component and $DCR_{N,CMS}$ corresponds to the ratio for the CMS method for a component.

A comparison of the 4-, 8-, and 16-story results show an increase in the percentage difference of the predicted mean response as the building height increases. Meanwhile, the difference in the median is about the same except in the 16-story building where the difference in the median response is 15 % larger. The larger difference in the mean response of the 8-story building, in comparison to the 4-story building, occurs mainly because more realizations reach the 20 % drift limit for the PEER records. The 8-story frame has four total collapses from PEER selected ground motions, while collapse in the 4- and 16-story occurred only twice in each, as reported in Table 1. In the 16-story building, the larger difference in the mean and median occurs because there are no collapses for any of the CMS records, as previously mentioned. Thus, in the cases of analyses that include collapse cases, the mean response recommended by ASCE/SEI 41-13 largely depends on the arbitrary upper limit assumption of 20% for the drift at collapse which can cause the mean to provide misleading results. The median, on the other hand, is a more stable central measure of dispersion because it does not depend on the assumed probabilistic distribution function, and is not affected by a small percentage of realizations.

For the archetype buildings considered in this study, T_1 is the only conditioning period in the CMS method that causes any components in all three frames to not meet the acceptance criteria, i.e. mean DCR_N is greater than 1.0, as the response of buildings is dominated by the first-mode. This finding may imply that for regular code-compliant steel moment frame buildings, we may only need to consider one conditioning period at T_1. However, more archetype buildings especially with greater height need to be analyzed to generalize this finding. The rest of the conditioning periods, $0.2T_1$, $0.4T_1$, and $2T_1$, are used to comply with ASCE/SEI 7-16 to ensure the effects of shorter modes and period elongation are captured. In this particular study, those conditioning periods do not cause the acceptance criteria to be exceeded in any of the three buildings' components, even when they produce the highest mean DCR_N. However, in buildings with different structural systems or heights, other conditioning periods may trigger the response of the components in the building.

5.3 Central Measures of Dispersion using a Lognormal Distribution

A series of Kolmogorov-Smirnov (K-S) tests on the DCR_N data demonstrated that the lognormal distribution fits a majority of the data more appropriately than a normal distribution (see Appendix D). This was expected given that the data has only positive values, and it is skewed to the right end of the distribution (Shome and Cornell, 1999). Based on this outcome, the DCR_N statistical output parameters are computed in this section assuming the data is lognormally distributed. Note, that the input ground motions do not change in this section and are the same as the ones in Section 5.2, and shown in Figure 9. The only difference is how the mean DCR_N results are calculated. Rather than using a simple arithmetic average, by assuming the data is lognormally distributed, the mean of the data can be computed as:

$$\mu_x = e^{\mu_{\ln x}} * e^{\frac{\sigma_{\ln x}^2}{2}} = x_{50} * e^{\frac{\sigma_{\ln x}^2}{2}} \tag{7}$$

where $\mu_{\ln x}$ is the mean of the natural logarithm of DCR_N values, $x_{50}$is the median of the data, and $\sigma_{\ln x}$ is the standard deviation of the natural logarithm of DCR_N values, which can be calculated as:

$$\sigma_{\ln x} = \ln\left(\sqrt{\frac{x_{84}}{x_{16}}}\right) \tag{8}$$

where x_{84} and x_{16} represent the 84$^{\text{th}}$ and 16$^{\text{th}}$ percentile of the 14 DCR_N values for each element, respectively (Ibarra and Krawinkler, 2005). Note that $\sigma_{\ln x}$ and μ_x are computed in such a way that collapse of a couple of realizations does not force the use of the arbitrary roof drift limits. Since 14 realizations are considered in the evaluation, collapse cases are not used in the calculations if no more than two records cause collapse. If more than two records cause collapse, the 84th percentile will have to include collapse cases. If a set of ground motions produces more than two collapses, but no more than seven, then the following equation would be used to calculate the dispersion instead (Ibarra and Krawinkler, 2005):

$$\sigma_{\ln x} = \ln\left(\frac{x_{50}}{x_{16}}\right) \tag{9}$$

where the values are defined previously. The major difference between Eq. (8) and Eq. (9) is the use of the 50th percentile instead of the 84th. It is preferable to use Eq. (8) because the results are more consistent, since the density interval spans two standard deviations, instead of one. Note that Eq. (9) can ignore up to six collapse cases, which may not be acceptable from a practical point of view; the maximum number collapse cases observed in this study was four. Figure 10a, b, and c plot the mean and median response for the beams using the lognormal distribution assumption. The DCR_N values in these figures are computed using Eq. (7) and Eq. (8) or Eq. (9) and are labeled as "lognormal mean". As observed in Figure 10, the median values did not change when the lognormal probability density function is used. However, the mean values are lower than those computed using an arithmetic mean. In fact, the CMS mean computed based on the lognormal distribution assumption is close to the CMS median values. The CMS lognormal mean is reduced because it is computed based on the median, x_{50}, and standard deviation of the log of the data, $\sigma_{\ln x}$, which are calculated using the 84th, 50th and 16th percentiles. As a result, extreme values that may arise due to building collapse for some realizations are not considered in the median computation. In this section, the results for Bay D-E of the SMF are shown.

For the results of the other bays, refer to Appendix C.

PEER mean DCR_N values are still larger than those obtained from the CMS method, in part because $S_a(T_1)$ is larger for the PEER method (Figure 4b). However, the mean response for the RBS elements in the 4- and 8-story frames pass the ASCE/SEI 41-13 acceptance criteria when the mean is computed based on the lognormal distribution using Eqs. (7) and (8). A few components in the 16-story frame still exceed the acceptance criteria, but in general more components pass the expected performance when Eqs. (7) and (8) are employed. This result demonstrates that post-processing the results using different approaches, in this case using a different probability distribution for mean calculation, may lead to a different retrofitting approach. Figure 11(a), 10(b), and 10(c) present similar results for the 4, 8, and 16-story building columns computed with a lognormal distribution. Employing the lognormal distribution reduces the mean demand to be closer to the median for almost all elements, because $\sigma_{\ln x}$ and μ_x calculations (Eq. (7) and (8)) do not force the use of arbitrary roof drift limits. Overall, the lognormal distribution provides lower mean demands than using an arithmetic mean. The maximum percentage difference of the mean DCR_N between the normal and lognormal distribution for each method is reported in Table 3. The results show that the DCR_N of the beams and columns in the CMS method assuming the lognormal distribution is 65 % and 95 %, respectively, lower than the case using an arithmetic mean. For the PEER method, the difference in DCR_N can be as large as 80 % in the beams and 95 % in the columns between the mean of the lognormal distribution and the arithmetic mean. The percentages are calculated in a similar way as in Eq. (6), but instead using the normal and lognormal values for each method so the difference in DCR_N from different distributions can be compared.

5.4 Uncertainty in Response Prediction Using CMS and PEER

One of the primary goals of efficient ground motion selection methods is to predict the numerical structural seismic response with the smallest possible number of records. The methods evaluated in this study select ground motions that closely match the prescribed target spectrum, and the selection procedure that leads to a smaller variability on the structural response can help a method be considered more suitable. To determine the uncertainty associated with the results produced by each ground motion selection approach, the DCR_N dispersion (standard deviation) is computed for each element using Eq. (8).

To establish a fair comparison between the statistical results obtained from the two methods, the PEER spectrum is scaled down to match the MCE_R spectral acceleration at T_1, because the use of a larger $S_a(T_1)$ in the PEER spectrum leads to larger nonlinear excursions and more collapses, increasing the dispersion of the response. Therefore, the results presented in this section correspond to the lowered PEER input, denoted as PEER scaled down at T_1. Then, the only input that remains the same as the previous sections is that of the CMS method. Figure 12(a)-(c) present the average spectra of the scaled down PEER records when compared to the average CMS records for the 4-, 8-, and 16-story buildings, respectively. As can be seen, the scaled down PEER average spectral value at T_1 of the input for this section matches the value from the MCE_R and CMS curves. Figure 13(a)-(c) compare the means and medians of the beam DCR_N obtained from the CMS and the scaled down PEER ground motions for the 4-, 8-, and 16-story buildings, respectively. As observed in Figure 14, the lognormal mean results for the PEER spectrum scaled down at T_1 are about 30 % , 85 %, and 70 % lower for the 4-, 8-, and 16-story building, respectively, than those obtained from using the original PEER spectrum ground motions, showing the effect of the spectral acceleration at T_1 which differ in approximately 20 %, 70 %, and 95 % for the 4-, 8-, and 16-story, respectively, from the original to the reduced spectrum. As observed, the CMS and scaled down PEER results are closer to each other than the results from using PEER ground motions that are not scaled down from the previous sections. As observed, the CMS and scaled down PEER results are closer to each other than the results from using PEER ground motions that are not scaled down from the previous sections. Scaling down the average PEER spectrum to $S_a(T_1)$ results in lower median and mean demand to capacity ratios, due to a lower $S_a(T_1)$ value, resulting in smaller inelastic excursions and less collapse cases than those presented in Table 1. The dispersion for the scaled down PEER ground motions is compared to the CMS results at the controlling conditioning period of each element. The dispersion of the RBS connections located at the bay D-E and the columns of Col. Line E of the 4-, 8-, and 16-story buildings are presented in Figure 15, Figure 16, and Figure 17 respectively. To see the results for the other bays and column lines, refer to Appendix C. The second column in the tables reported in Figure 15-Figure 17 show the standard deviation obtained from the CMS method, as well as the conditioning period with the largest mean demand (shown in parenthesis). The third column shows the dispersion derived from the scaled down PEER method, and the fourth column is the ratio of the standard deviation between the CMS at the controlling period and the scaled down PEER method.

According to Figure 15a, the CMS method leads to a higher structural response dispersion for the DCR_N of RBS connections of the 4-story frame for all floors, with only one exception at the fourth floor. The dispersion can be almost four times larger than the dispersion using the PEER method. For the 8-story building the opposite trend is observed, and the PEER method results in a dispersion that is about twice that of the CMS method at all floors, with the exception of demands at the roof level, as shown in Figure 16a. For the 16-story building, the RBS connection dispersion is slightly smaller for the CMS method, except at the 10th and 12th floors, as shown in Figure 17a. The factor that apparently determines whether the CMS method has smaller dispersion is the controlling period. For the 4-story frame, the controlling period is $0.4T_1$, whereas most floors in the 8- and 16-story building have T_1 as the controlling period. Figure 16(a) and Figure 17(a) show that when the mean demand parameter is controlled by the conditioning period T_1, the CMS method generally leads to smaller dispersion. The 16-story results show there are only a couple cases where T_1 controls yet the CMS dispersion is higher.

For the column hinge elements, the results show that the CMS method also leads to lower dispersion for most cases. For the 4-story frame, the CMS records have a lower dispersion in the 2nd and 3rd story columns, as shown in Figure 15(b), where both stories have a controlling period of T_1. The 8-story column hinge results resemble those of the RBS connections with most columns controlled by T_1. Figure 16(b) shows that the CMS ground motions lead to a lower dispersion in most columns in the 8-story building, where the 6th and 7th floor columns are the exceptions. The dispersion for the 16-story frame columns is similar to those of the 8-story frame with a majority of the elements having a T_1 controlling period. The DCR_N dispersion is lower with the CMS selected records for a majority of the elements, as observed in Figure 17(b). The PEER method provides lower DCR_N dispersion in the 10th, 11th, 13th, and 16th floors, but only the 11th and 13th story are controlled by the first-mode. The data suggests that if T_1 is the CMS controlling period, the dispersion is more likely to be lower than the dispersion obtained from the PEER method for the same element. This means that for buildings whose response is dominated by the first-mode there is a higher chance to have lower dispersion for the CMS records if T_1 is the controlling period.

The collapse capacity uncertainty is related to the ground motion variability at T_1, higher order periods (i.e., shorter periods), and inelastic periods longer than T_1. For cases where the CMS controlling period is T_1, the spectra for the CMS method has no dispersion at T_1 while the PEER method does. However, the CMS dispersion is mostly lower because the contribution to collapse capacity uncertainty from higher modes and inelastic longer period is less relevant on the overall response because the average accelerations at these other periods are smaller than those of the target spectrum, MCE_R (see Figure 1 and Figure 4a). However, when the mean demand is controlled by a different conditioning period, other than T_1, the dispersion of $S_a(T_1)$ is not zero, and there is a collapse capacity uncertainty contribution even within the elastic system performance. Moreover, the dispersion at higher modes is also different from zero, unless the controlling period (e.g., $0.4T_1$) coincidentally corresponds to one of these higher modes. These trends are shown in Figure 18, where the shaded areas correspond to the maximum and minimum spectral values for spectra anchored at the 8-story building T_1 and $0.2T_1$ periods. If the controlling period is T_1, the standard deviation at T_1 is obviously $\sigma_{T_1} = 0$, and for $T_2 = 0.35T_1$, $\sigma_{T_2} = 0.34$. Thus, from the first two elastic modes, only T_2 contributes to collapse capacity uncertainty. Furthermore, this contribution from T_2 dispersion is less significant for CMS because of the average lower $S_a(T_2)$. However, if the controlling period is $0.2T_1$, $\sigma_{T_1} = 0.61 \neq 0$, as expected, but $\sigma_{T_2} = 0.41$ is also different from zero because $T_2 = 0.35T_1 \neq$

$0.2T_1$, as well as the rest of higher mode period dispersion. A similar trend is found for the 4- and 16-story buildings as well. This dispersion is more noticeable if the short controlling period is anchored close to the plateau of the MCE_R spectrum. Overall the CMS method provides lower dispersions for a majority of RBS and CH elements of the three frames evaluated. Thus if T_1 is the controlling period, then collapse capacity uncertainty is likely to be lower for the CMS method than for cases where another conditioning period controls the mean response.

Table 1. Total collapse cases caused by CMS and PEER selected ground motions.

Building	GM Selection Method	No. of GMs that lead to collapse	Controlling Period
4-story	CMS	1	$0.4T_1$
	PEER	2	N/A
	PEER scaled down at T_1	1	N/A
8-story	CMS	1	T_1
	PEER	4	N/A
	PEER scaled down at T_1	1	N/A
16-story	CMS	0	N/A
	PEER	2*	N/A
	PEER scaled down at T_1	0	N/A

*For this case only one collapse occurred. The other case did not converge therefore it is treated as a collapse.

Table 2. Maximum difference of DCR_N between CMS and PEER median and mean demands of the three SMFs for the RBS and CH elements.

Building	Maximum Percent Difference of DCR_N in			
	Reduced Beam Sections		Column Hinges	
	Median	Mean	Median	Mean
4-story	55 %	55 %	45 %	60 %
8-story	55 %	70 %	40 %	60 %
16-story	70 %	95 %	75 %	97 %

Table 3. Maximum difference of DCR_N between the normal and lognormal distribution mean demands of the three SMFs for the RBS and CH elements for both GM selection methods.

Building	DCR_N Percent Difference in			
	Reduced Beam Sections Lognormal Mean vs arithmetic Mean		Column Hinges Lognormal Mean vs arithmetic Mean	
	CMS	PEER	CMS	PEER
4-story	55 %	55 %	95 %	95 %
8-story	65 %	80 %	95 %	95 %
16-story	10 %	80 %	10 %	90 %

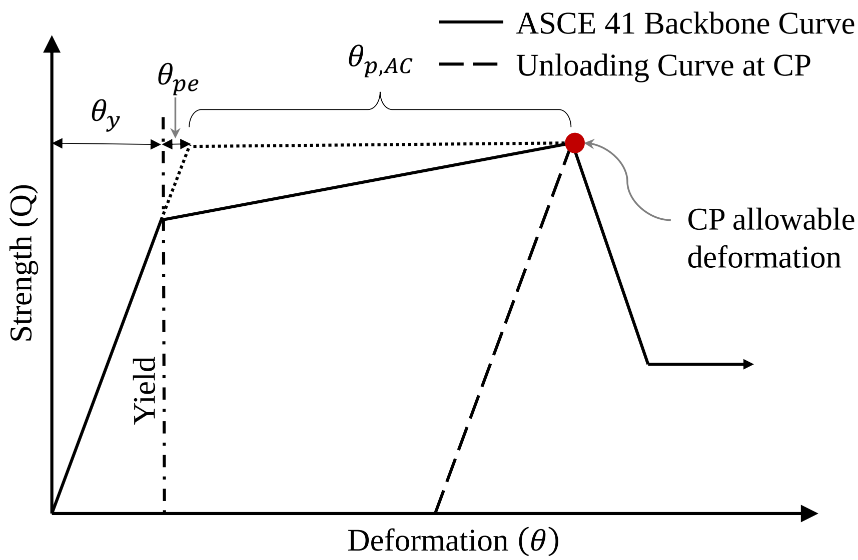

Figure 5. Generalized Component Backbone Curve.

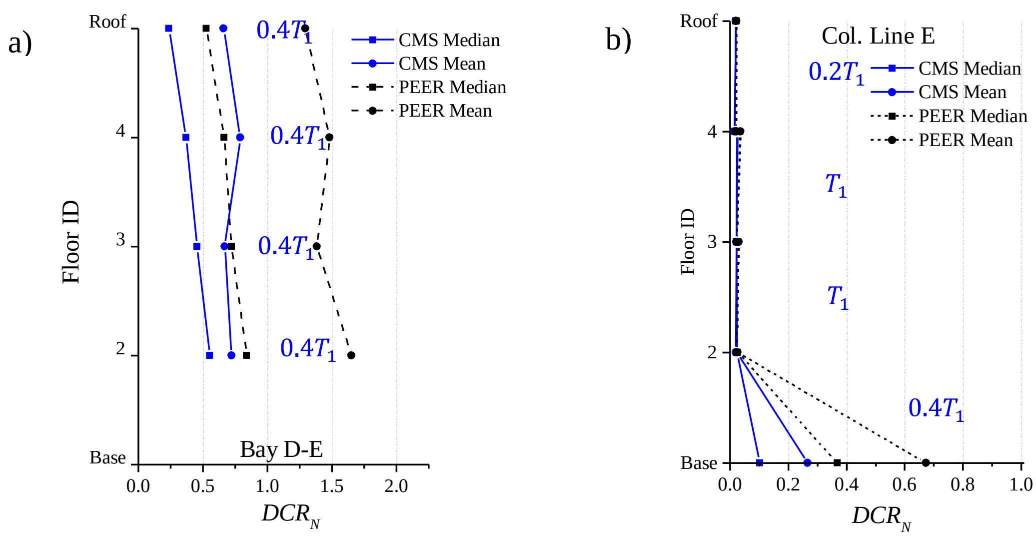

Figure 6. Comparison of max DCR_N values of the 4-story building for the (a) reduced beam sections and (b) the column hinges computed for ground motions selected using the CMS and PEER methods. The controlling period of the element at each story/floor is reported on the figure.

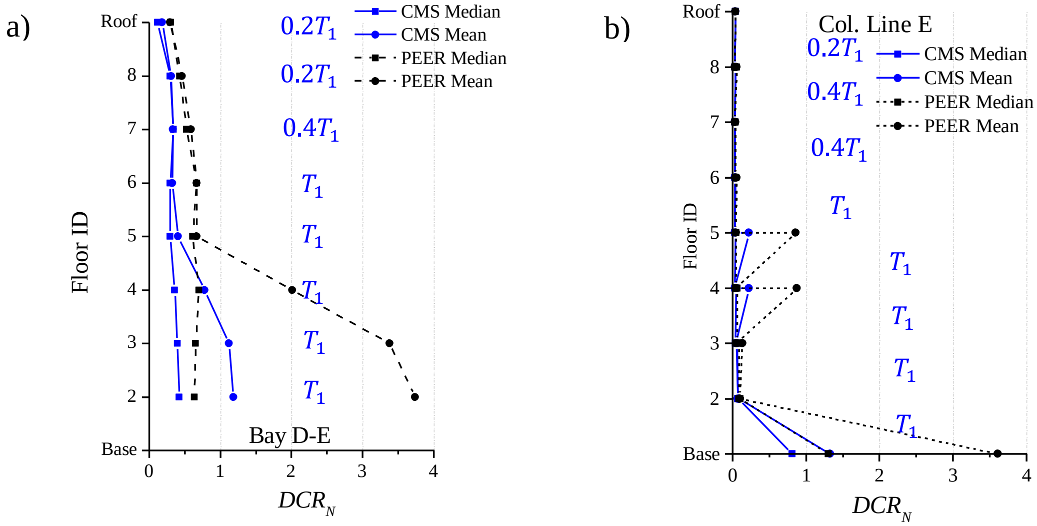

Figure 7. Comparison of max DCR_N values of the 8-story building for the (a) reduced beam sections and (b) the column hinges computed for ground motions selected using the CMS and PEER methods.

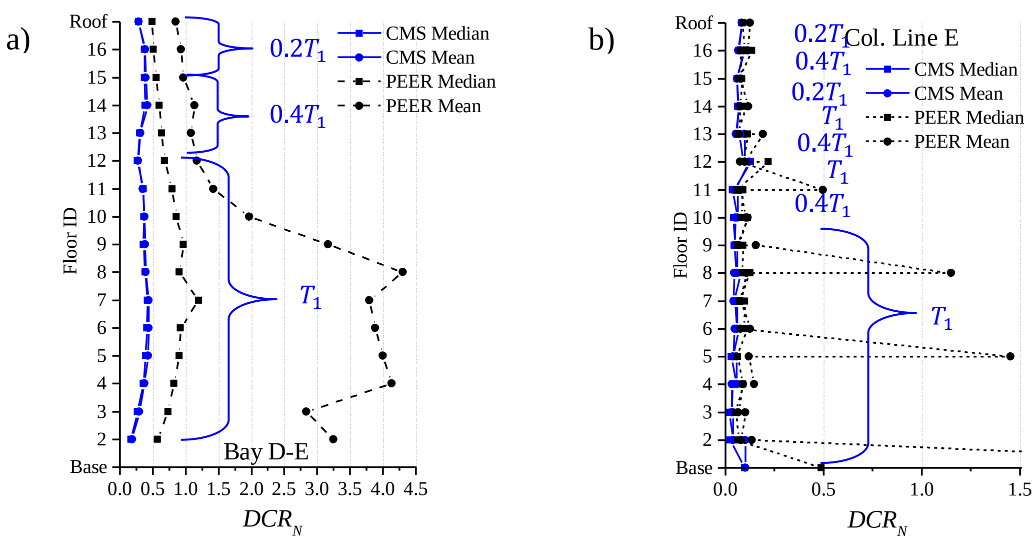

Figure 8. Comparison of max DCR_N values of the 16-story building for the (a) reduced beam sections and (b) the column hinges computed for ground motions selected using the CMS and PEER methods.

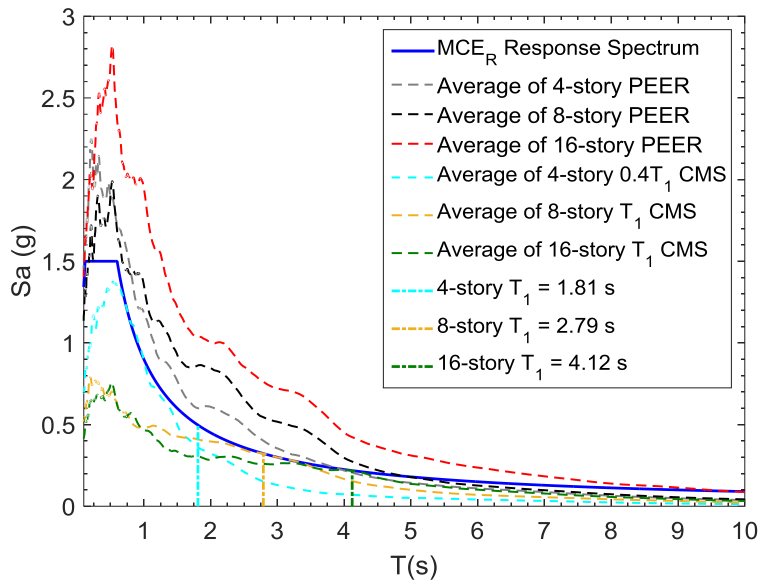

Figure 9. Comparison of average S_a values of the ground motions selected using the CMS and PEER ground motion selection methods of the 4-, 8-, and 16-story buildings. The CMS ground motions reported only for the controlling period which controlled most the elements.

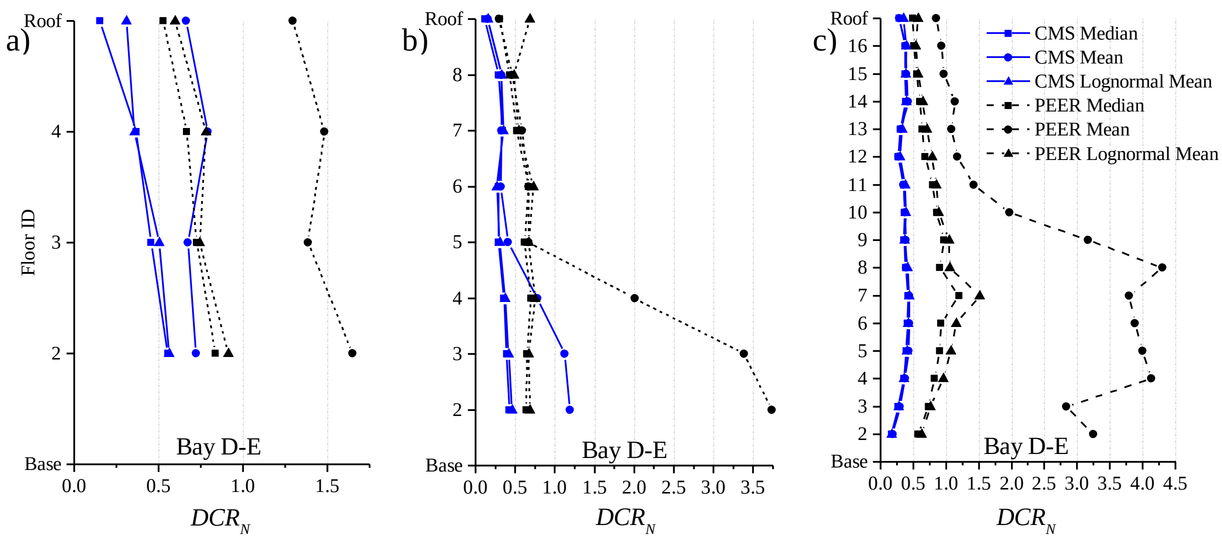

Figure 10. Comparison of max DCR_N values of the reduced beam sections computed for ground motions selected using the CMS and PEER selection methods for the (a) 4-story (b) 8-story and the (c) 16-story buildings. [The "lognormal mean" is calculated using Eq (7), and represents the mean of the max DCR_N values assuming the lognormal distribution, see discussion in Section 5.3].

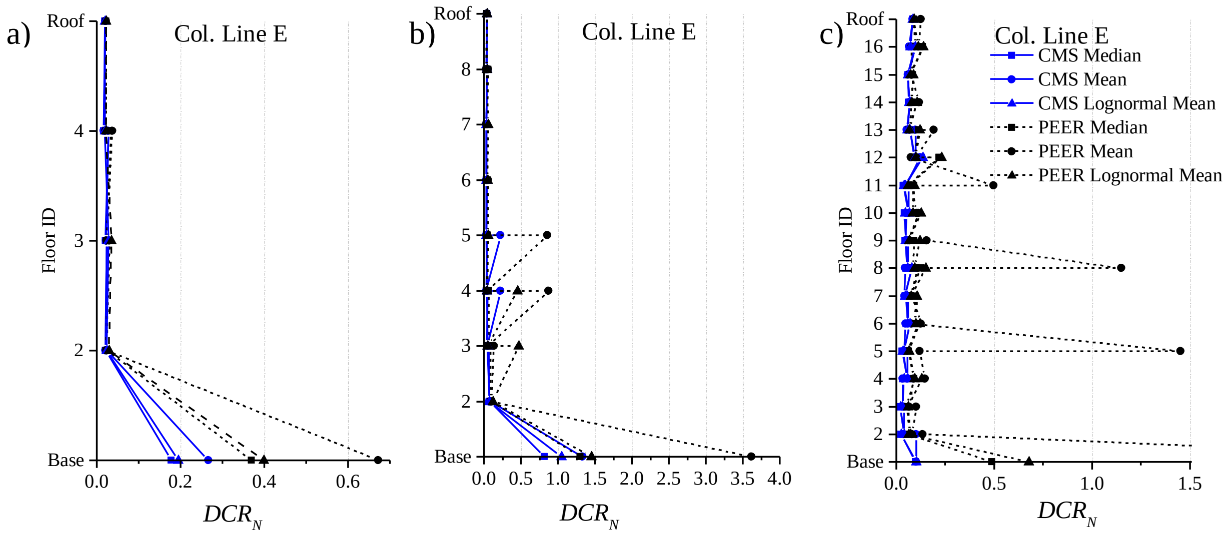

Figure 11. Comparison of max DCR_N values of the column hinges computed for ground motions selected using the CMS and PEER selection methods for the (a) 4-story (b) 8-story and the (c) 16-story buildings. [The "lognormal mean" is calculated using Eq (7), and represents the mean of the max DCR_N values assuming the lognormal distribution, see discussion in Section 5.3].

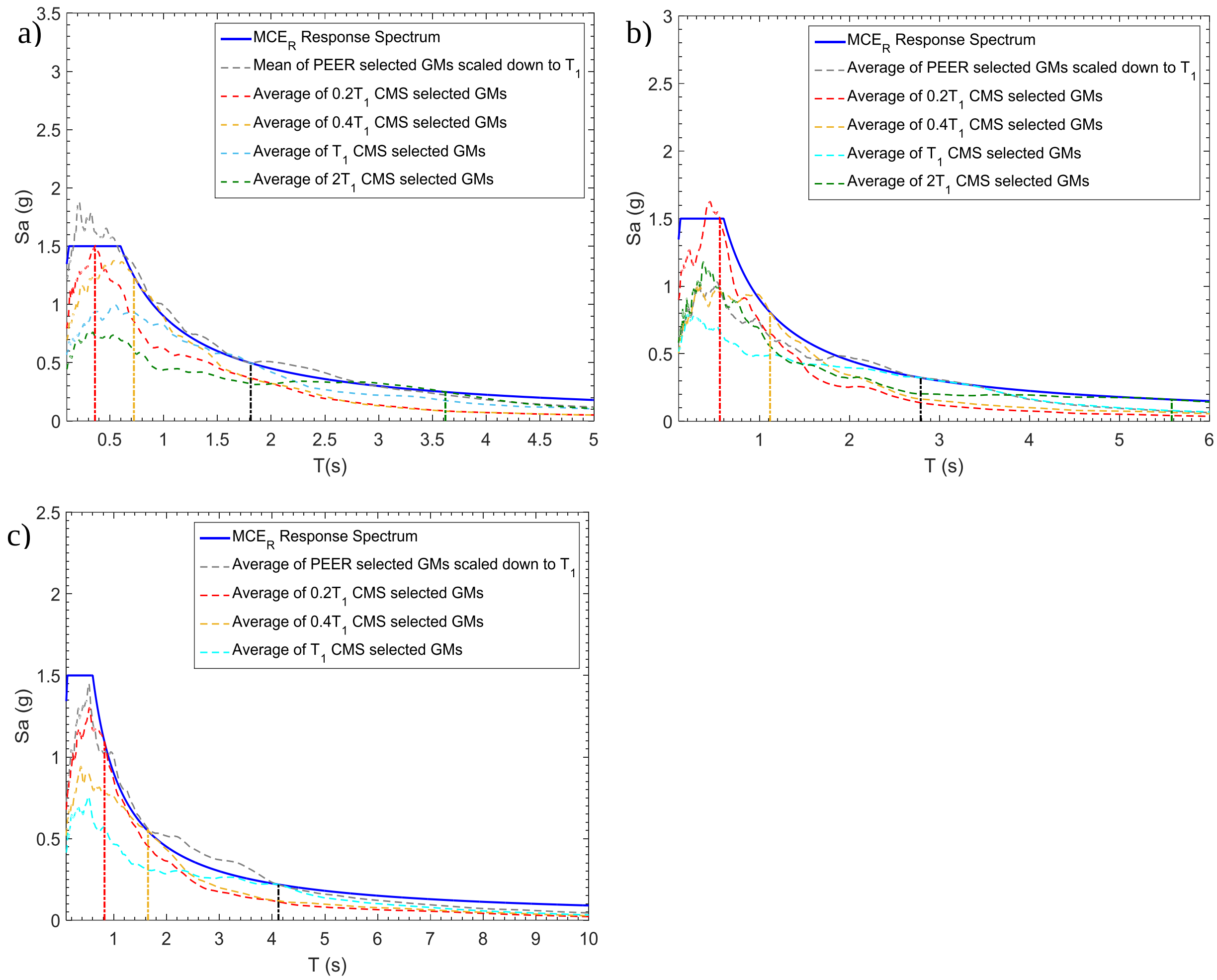

Figure 12. The average CMS spectra for four conditioning periods in comparison with the average of the PEER spectra scaled down to the MCE$_R$ at T_1 for the (a) 4-story (b) 8-story and (c) 16-story building.

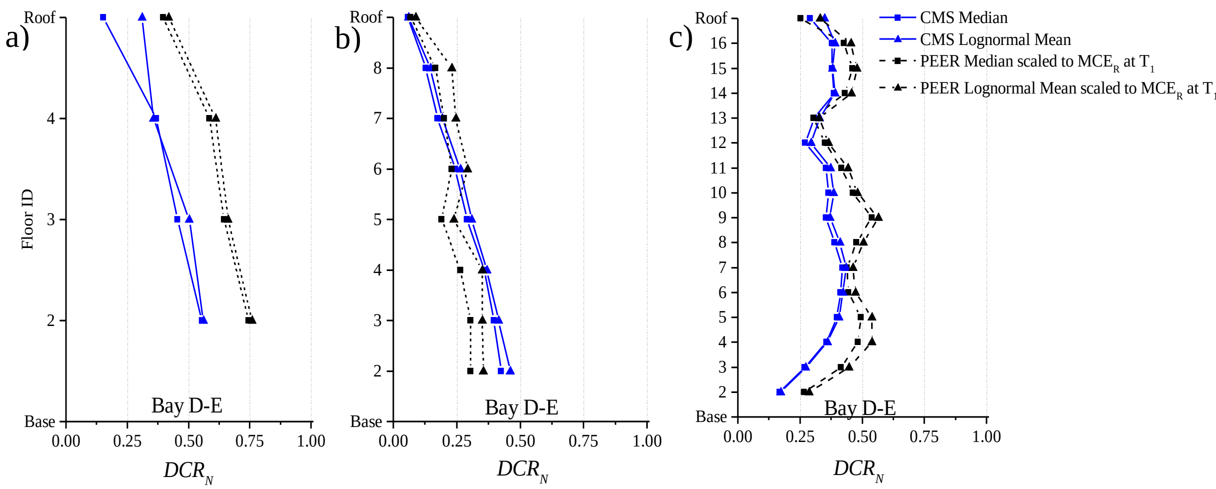

Figure 13. Comparison of max DCR_N values of the reduced beam sections computed for the CMS and PEER scaled down at T_1 ground motions for the (a) 4-story, (b) 8-story and (c) 16-story building. [The "lognormal mean" is calculated using Eq (7), and represents the mean of the max DCR_N values assuming the lognormal distribution, see discussion in Section 5.3].

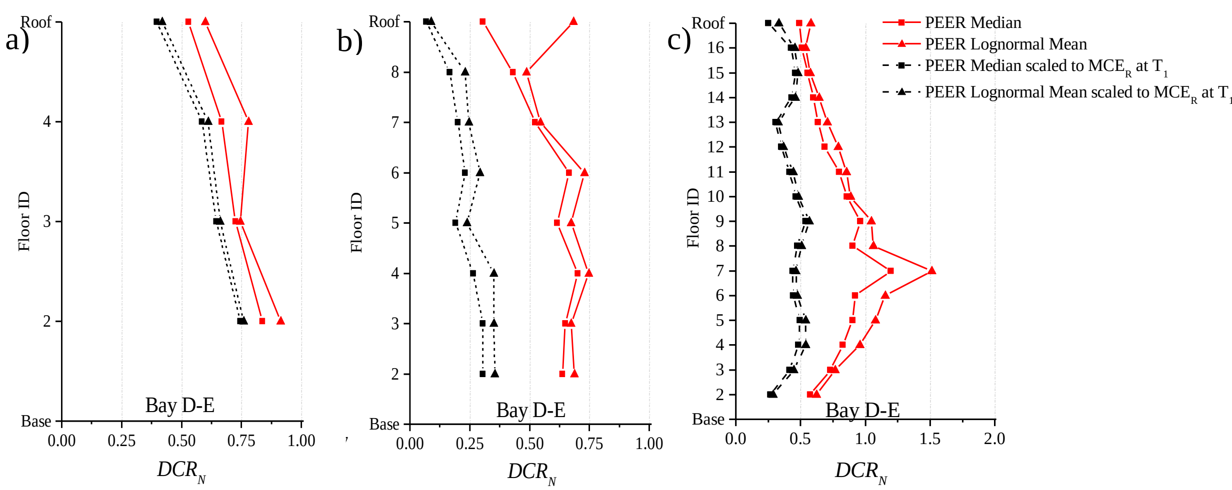

Figure 14. Comparison of max DCR_N values of the reduced beam sections computed for the PEER and PEER scaled down at T_1 ground motions for the (a) 4-story, (b) 8-story and (c) 16-story building. [The "lognormal mean" is calculated using Eq (7), and represents the mean of the max DCR_N values assuming the lognormal distribution, see discussion in Section 5.3].

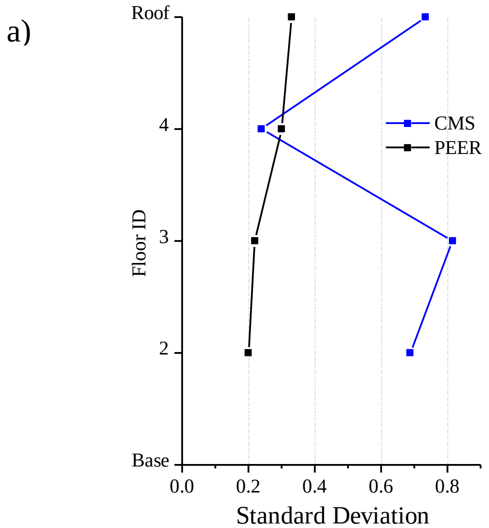

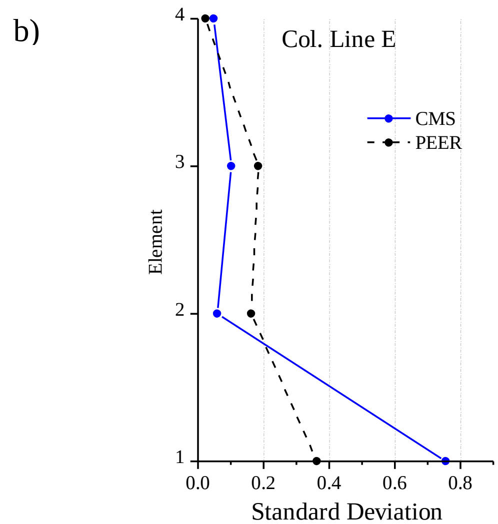

Story Number	$\sigma_{CMS}{}^{*}$	$\sigma_{PEER\ @\ T_1}$	$\frac{\sigma_{CMS}{}^{*}}{\sigma_{PEER\ @\ T_1}}$
2	0.69 (0.4T_1)	0.20	3.48
3	0.82 (0.4T_1)	0.21	3.85
4	0.24 (0.4T_1)	0.29	0.82
Roof	0.73 (0.4T_1)	0.33	2.24

Story Number	$\sigma_{CMS}{}^{*}$	$\sigma_{PEER\ @\ T_1}$	$\frac{\sigma_{CMS}{}^{*}}{\sigma_{PEER\ @\ T_1}}$
1	0.75 (0.4T_1)	0.36	2.08
2	0.059 (T_1)	0.16	0.37
3	0.10 (T_1)	0.18	0.55
4	0.048 (0.2T_1)	0.023	2.06

* σ_{CMS} is computed for the controlling conditioning period.

Figure 15. Standard deviation of the DCR_N results for the 4-story building of the (a) RBS connections in bay D-E and (b) column hinges in the column located on column line E using CMS at the controlling period and PEER methods. (The controlling period is reported in parenthesis next to the dispersion).

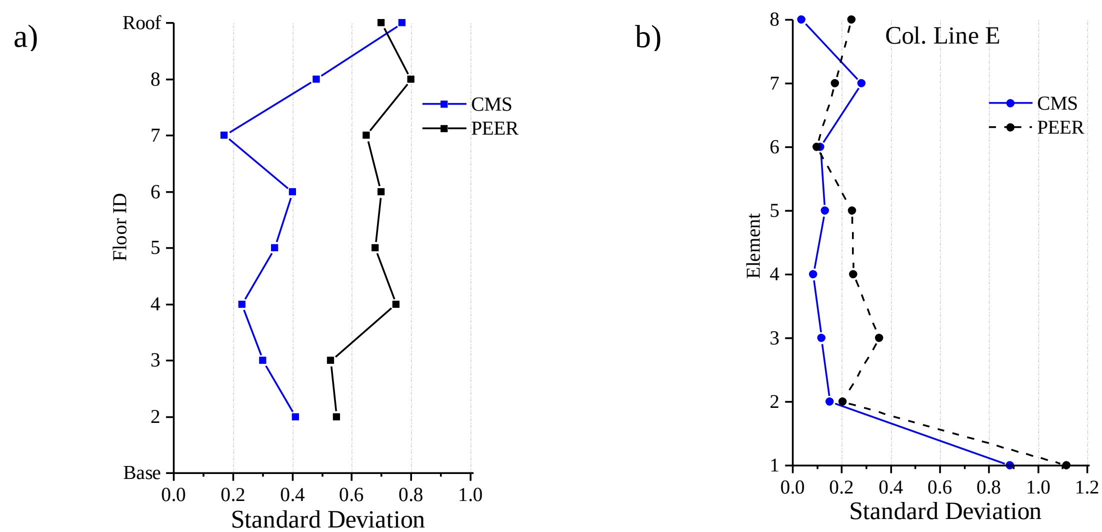

Story Number	$\sigma_{CMS}{}^{*}$	$\sigma_{PEER\ @\ T_1}$	$\frac{\sigma_{CMS}{}^{*}}{\sigma_{PEER\ @\ T_1}}$
2	0.41 (T_1)	0.55	0.74
3	0.30 (T_1)	0.53	0.56
4	0.23 (T_1)	0.75	0.31
5	0.34 (T_1)	0.68	0.50
6	0.40 (T_1)	0.70	0.57
7	0.17 (0.4T_1)	0.65	0.26
8	0.48 (0.2T_1)	0.80	0.60
Roof	0.77 (0.2T_1)	0.70	1.09

Story Number	$\sigma_{CMS}{}^{*}$	$\sigma_{PEER\ @\ T_1}$	$\frac{\sigma_{CMS}{}^{*}}{\sigma_{PEER\ @\ T_1}}$
1	0.88 (T_1)	1.12	0.79
2	0.15 (T_1)	0.20	0.75
3	0.12 (T_1)	0.35	0.34
4	0.085 (T_1)	0.25	0.34
5	0.13 (T_1)	0.24	0.54
6	0.11 (0.4T_1)	0.099	1.11
7	0.28 (0.4T_1)	0.17	1.64
8	0.036 (0.2T_1)	0.24	0.15

* σ_{CMS} is computed for the controlling conditioning period.

Figure 16. Standard deviation of the DCR_N results for the 8-story building of the (a) RBS connections in bay D-E and (b) column hinges in the column located on column line E using CMS at the controlling period and PEER methods. (The controlling period is reported in parenthesis next to the dispersion).

a)

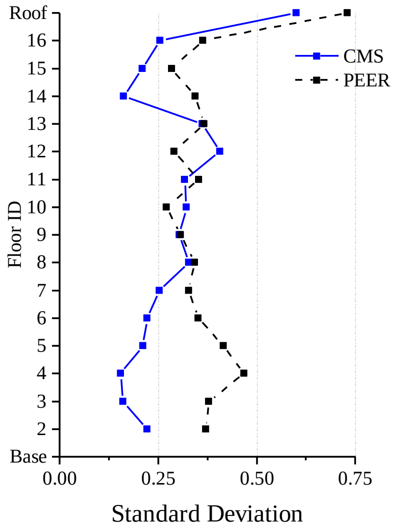

b)

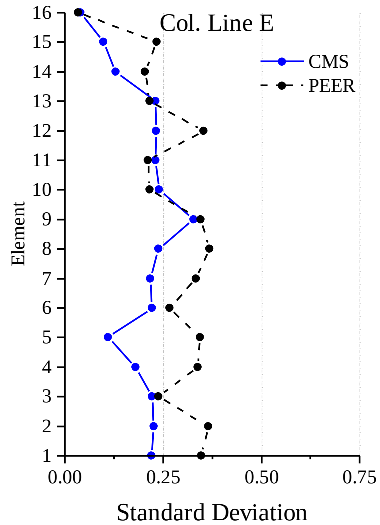

Story Number	$\sigma_{CMS}{}^{*}$	$\sigma_{PEER\ @\ T_1}$	$\frac{\sigma_{CMS}{}^{*}}{\sigma_{PEER\ @\ T_1}}$
2	0.22 (T_1)	0.37	0.59
3	0.16 (T_1)	0.38	0.43
4	0.15 (T_1)	0.47	0.33
5	0.21 (T_1)	0.42	0.51
6	0.22 (T_1)	0.35	0.63
7	0.25 (T_1)	0.33	0.77
8	0.33 (T_1)	0.34	0.95
9	0.30 (T_1)	0.31	0.99
10	0.32 (T_1)	0.27	1.19
11	0.32 (T_1)	0.35	0.90
12	0.41 (T_1)	0.29	1.40
13	0.36 (0.4T_1)	0.37	0.99
14	0.16 (0.4T_1)	0.34	0.47
15	0.21 (0.4T_1)	0.28	0.74
16	0.54 (0.2T_1)	0.36	0.70
Roof	0.60 (0.2T_1)	0.73	0.82

* σ_{CMS} is computed for the controlling conditioning period.

Story Number	$\sigma_{CMS}{}^{*}$	$\sigma_{PEER\ @\ T_1}$	$\frac{\sigma_{CMS}{}^{*}}{\sigma_{PEER\ @\ T_1}}$
1	0.22 (T_1)	0.35	0.63
2	0.22 (T_1)	0.36	0.61
3	0.22 (T_1)	0.24	0.93
4	0.18 (T_1)	0.34	0.53
5	0.11 (T_1)	0.34	0.32
6	0.22 (T_1)	0.27	0.83
7	0.22 (T_1)	0.33	0.66
8	0.24 (T_1)	0.37	0.65
9	0.33 (T_1)	0.35	0.94
10	0.24 (0.4T_1)	0.22	1.11
11	0.23 (T_1)	0.21	1.10
12	0.23 (0.4T_1)	0.35	0.66
13	0.23 (T_1)	0.22	1.07
14	0.13 (0.2T_1)	0.20	0.63
15	0.099 (0.4T_1)	0.23	0.42
16	0.040 (0.2T_1)	0.033	1.21

Figure 17. Standard deviation of the DCR_N results for the 16-story building at bay D-E of the (a) RBS connections and (b) column hinges in the column located on column line E using CMS at the controlling period and PEER methods. (The controlling period is reported in parenthesis next to the dispersion).

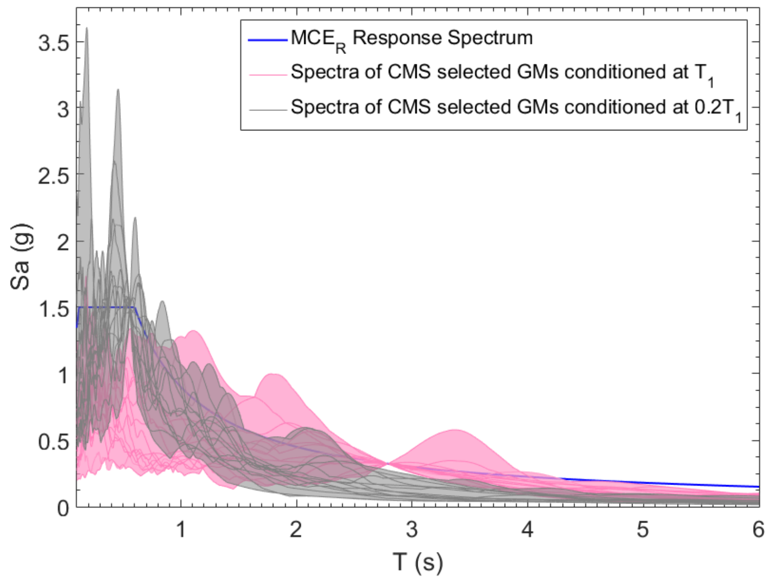

Figure 18. Ground motions selected for conditioning periods of T_1 and $0.2T_1$ for the 8-story building. The shaded area shows the bandwidth of the spectra set.

CHAPTER 6:

CONCLUSIONS

This study evaluates the effect of ground motion selection methods on the response of steel buildings. For this purpose, the response of a set of 4-, 8- and 16-story steel special moment frames, located at a far-field site in Los Angeles, CA, are assessed according to ASCE/SEI 41-13 nonlinear procedure using the CMS and PEER methods to select 14 ground motions records. The mean and median normalized demand-to-capacity ratios are calculated assuming normal and lognormal distributions for various components, and the results from the two ground motion selection methods are compared. The results show that the average (i.e., arithmetic mean) demand-to-capacity ratios (DCR_N) of the reduced beam section and column hinge components predicted by using the CMS ground motions are approximately 55 % to 95 % lower than the ones from PEER ground motions for the beams, depending on the number of stories in the frame being evaluated, and approximately 60 % to 97 % lower for the columns. Similar results are observed for the median of the demand-to-capacity ratios where the median DCR_N from CMS method is approximately 55 % to 70 % lower than PEER for the beams and 45 % to 75 % lower for the columns. The lower mean and median demands are mainly caused by a lower average intensity of the CMS selected ground motions in comparison to the PEER ground motions.

A comparison between the mean and median response of the reduced beam sections and column hinges is conducted using the lognormal distribution for DCR_N. Assuming a lognormal distribution for the demand-to-capacity ratios can cause a significant difference in the predicted average DCR_N, that may lead to different retrofitting decisions for the building. For the CMS method, the DCR_N values are reduced from 10 % to 65 % in the beams and from 10 % to 95 % in the columns, by simply calculating the mean assuming a lognormal distribution instead of calculating the mean using the arithmetic average . For the PEER method, the adoption of a lognormal distribution reduced the DCR_N values from 55 % to 80 % in the beams and from 90 % to 95 % in the columns. The reason for this DCR_N reduction is that the normal distribution assigns a roof drift ratio of 20 % for collapsed frame realizations when computing the arithmetic mean. On the other hand, collapse values are excluded from the calculation of the mean response when the data are assumed lognormally distributed, and the mean and dispersion are computed based on the 16th and 84th or 50th percentiles of the data points. Therefore, if collapse capacity is expected for a few realizations, the mean and dispersion may best be calculated assuming a lognormal distribution and a mean estimate that relies on the 16th and 84th percentiles. However, the median is a more robust central measure of dispersion, and is not influenced by a small number of collapsed frame realizations, even if the data is assumed to be normally distributed. These findings illustrate the importance of identifying probabilistic distributions that appropriately represent the analysis results to make a more informed retrofitting decision.

As shown in Figure 9, the PEER mean $S_a(T_1)$ values are larger than $S_a(T_1)$ for the MCE_R spectrum. To have a fair comparison of the structural response dispersion, the PEER ground motions are scaled down to have the average $S_a(T_1)$ match the MCE_R spectrum at

T_1 for each building. The *DCR$_N$* results from lowering the spectral acceleration for the PEER records are closer to the CMS results and sometimes are even lower. The resulting mean *DCR$_N$* for the reduced PEER spectrum ground motions are approximately 45 % lower than those obtained for the original PEER spectrum. The results showed that the CMS method can provide lower dispersion, i.e. higher confidence, in the predicted response than the PEER ground motions scaled down at T_1, especially when the controlling period is T_1. Since both CMS and modified PEER spectra have the same average spectral acceleration at T_1, the reduction in *DCR$_N$* dispersion is only attributed to the more realistic CMS spectra. Approximately 88 % of the building elements have lower *DCR$_N$* dispersion in the CMS method when T_1 is the controlling period. However, the CMS has the lower dispersion in only 55 % of the elements when the controlling period is not T_1. If the conditioning period is T_1, the CMS is expected to lead to less collapse capacity uncertainty because there is no ground motion variability at T_1 (as in the PEER method), and the mean spectrum exhibits less energy than PEER spectrum at higher modes and at longer nonlinear periods of vibration. Consequently, the CMS dispersion is higher in components that are located in the upper stories where higher modes are more likely to control. Overall, the CMS method provides a lower *DCR$_N$* dispersion 75 % of the time across the results of the three buildings, regardless of controlling period, when compared to the dispersion provided by the PEER method. Note that ASCE/SEI 7-16 prescribes the use of other conditioning periods to ensure that the CMS envelope spectrum does not fall below 75 % of the MCE_R spectrum.

In conclusion, this study showed that the ground motion selection methodology has an impact on the assessment outcome. Although the CMS method requires more effort in the selection and assessment process it provides a ground motion set that is considered more realistic than that of the PEER method, and also provides less dispersion in the results. The results of this study are valid for steel special moment frames that are within the range of 4- to 16-stories.

DISCLAIMER

Certain commercial software, equipment, instruments, or materials may have been used in the preparation of information contributing to this paper. Identification in this paper is not intended to imply recommendation or endorsement by NIST, nor is it intended to imply that such software, equipment, instruments, or materials are necessarily the best available for the purpose.

APPENDIX A:

TOOLS USED TO IMPLEMENT SELECTION METHODS

The tools developed by Baker et al. (2016) are used to implement the ground motion selection methods. This appendix shows the scaling and selection ground motion process based on these tools.

A.1 Tools used to implement the CMS Method

To implement the CMS method, MATLAB scripts developed by Baker et al. (Baker, 2016) are used to develop the target CMS, select and scale ground motions to match the CMS, graph the selected ground motions' response spectra, and download the ground motion data (e.g. acceleration time history, etc.). There are two main files used in this study: "BackCalcEpsilon" and "Select_Ground_Motions". The first file back-calculates the epsilon associated with the conditioning period, allowing the user to condition the CMS at multiple periods of the maximum considered earthquake, $MCE_{R,}$ spectrum. The script calculates the ε by generating the median response spectrum and the standard deviation, σ, for the site using a ground motion prediction model (GMPM). The following equation (Baker, 2011) back-calculates ε at the conditioning period:

$$\varepsilon(T) = \frac{\ln\big(S_a(T)\big) - \mu_{lnSa}(M,R,T)}{\sigma_{lnSa}(T)} \tag{10}$$

where $\ln\big(S_a(T)\big)$ is the natural log of the spectral acceleration of the MCE_R at period T, $\mu_{lnSa}(M,R,T)$ is the median spectral acceleration, in normal space, at T from the GMPM, and $\sigma_{lnSa}(T)$ is the predicted standard deviation in log space, also from the GMPM. The second file, "Select_Ground_Motions", is used to construct the CMS, select the ground motions to match that CMS, and create the output needed for the nonlinear dynamic analysis. The output consists of scaled acceleration time histories that are used to input into PERFORM-3D along with figures of the response spectra of the scaled ground motions. This file uses the ε, calculated using Eq. (10), from the "BackCalcEpsilon" file to determine the correlation coefficient, ρ, at all other periods and computes the CMS over the entire period range of interest. The file algorithm scales and selects records from the PEER Ground Motion Database, also referred to as PEER NGA-West 2, a database of approximately 3,200 ground motions, based on how close the spectra match the CMS. Recall that the similarity between the spectra and the target spectrum is measured based on the amount of difference, "error", between the ground motion spectrum and the target spectrum. For the CMS method, this error is computed as the sum of squared errors, SSE, from Eq. (2).

To utilize the MATLAB scripts mentioned above, a series of steps needs to be taken to obtain the necessary deaggregation input parameters required by both files. Deaggregation is the breakdown of the total seismic hazard to its total contributions from individual components, such as magnitude and rupture distance. The first step is to select the conditioning period. The fundamental period of vibration T_1 is usually the first point where the CMS will be anchored to the MCE_R spectrum, although other conditioning periods may be needed to meet standards requirements. Once the conditioning period is selected, the deaggregation information pertaining to that conditioning period is needed, specifically: the spectral acceleration of the MCE_R at the conditioning period; the mean magnitude, M, and mean rupture distance, R, for the site; and the depth to the 2.5 km/s shear wave velocity

Z_{vs}. This information is used in the "BackCalcEpsilon" script to obtain the parameter epsilon, ε, at the conditioning period needed by the "Select_Ground_Motions" script to construct the target CMS for the site.

The spectral acceleration at the conditioning period is taken directly from the MCE_R spectrum or whichever spectrum is used for anchoring. The mean M and mean R for the site are retrieved from the USGS web tool deaggregation output (USGS, 2016b), as shown in Figure 19 underlined in red. To obtain the deaggregation output, the web tool requires the site's coordinates, V_{s30}, the exceedance probability, and approximate period desired for conditioning as input, as shown in Figure 20. If the period of interest is in between the spectral period choices, interpolation can be used to obtain the mean M and mean R. The exceedance probability input in the tool is 2 % in 50 years, which is roughly the same probability used for the MCE_R spectrum.

The next variable in the "BackCalcEpsilon" script is Z_{vs}, which is the depth to the 2.5 km/s shear-wave velocity horizon. The Z_{vs} is obtained from the OpenSHA "Site Data Viewer/Plotter" application (OpenSHA, 2016) by inputting the coordinates and the minimum and maximum V_{s30} of the selected site, similar to the USGS web tool. As observed in Figure 21, the output of the OpenSHA application provides the parameter Z_{vs}. Once the deaggregation information is collected, it is input into the "BackCalcEpsilon" script, as seen in Figure 22(a), that will back-calculate the parameter epsilon, ε, at the conditioning period. For the V_{s30} variable, the minimum value applicable to the soil type is entered. Other parameters presented in Figure 22(a), but not discussed in this description, are set to the default values given in the script. The output ε is presented in Figure 22(b).

Once M, R, Z_{vs}, V_{s30} and ε are known, they are input into the

"Select_Ground_Motions" script where the target CMS is constructed and ground motions are selected. Figure 23 is an example of the deaggregation input needed by the "Select_Ground_Motions" script to construct the CMS and select ground motions. Because the CMS is a site-specific selection method, the shape of the CMS changes if different site information is used; or even if the same site is used with different building information leading to a different conditioning period.

Figure 23(a) shows where the deaggregation information is input into "Select_Ground_Motions". To have the script select ground motions based only on error and disregard the variance, the useVar variable is set to zero. Otherwise, the script will select ground motions based on the Conditional Spectrum method and not the Conditional Mean Spectrum method Figure 23(b) shows that the script also gives the user the options of how many ground motions can be selected, the period of the building, and the max scale factor for the ground motions. Once the desired ground motions settings are input, then the script can be run to scale and select ground motions.

The "Select_Ground_Motions" script outputs several files, the most important files contain the selected records with their respective scale factors (this file is saved in the MATLAB script directory) and the response spectra plot of the CMS selected ground motions. In this study, four conditioning periods are used to meet the requirements set by ASCE/SEI 7-16 to have the envelope of the spectra be greater than 75 % of the MCE_R spectrum. The exception is the 16-story building which required only 3 conditioning periods to meet this criterion. The response spectra generated by the "Select_Ground_Motions" script for the 4-, 8-, and 16-story buildings are presented in Figure 24 (a), (b), and (c), respectively. The records are also selected to ensure that a set did not have more than three records from the same event and that no more than one record came from an individual station. A summary of the records for the three frames can be seen in Appendix B.

A.2 Tools used to implement the PEER Method

The tools used to select ground motions for the PEER method are provided by the PEER NGA-West2 (PEER, 2016) database. For this reason, this method is referred to as the PEER method. This tool is accessed by logging into the open database at PEER's website. Once logged into the PEER's website (PEER, 2016), the spectrum type that will be used to match ground motions is selected. The "ASCE Code Spectrum" option is selected to use the MCE_R spectrum. The user must then input the S_{DS}, S_{D1}, and T_L acceleration parameters from ASCE/SEI 7, shown in Figure 25. The information can be obtained from a USGS web tool (USGS, 2016c). As shown in Figure 26, the needed information includes the reference source (e.g., ASCE/SEI 7) from which the spectrum will be developed, the site's soil classification, the buildings' risk category, and the site coordinates. Since the MCE_R spectrum is desired, the S_{MS} and S_{M1} acceleration parameters are input instead of the design parameters S_{DS} and S_{D1}. The S_{MS} and S_{M1} are then input into the PEER web tool, as shown in Figure 25, which will generate the target spectrum in the tool. Once generated the user may search for records to match the MCE_R spectrum by selecting the "Search Records" option.

The parameters are selected to most closely match those of the selected site as shown in Figure 27. It can be seen that the "Initial Scale Factor" sets the minimum scale factor to 0.25 with a maximum of 2.5, therefore when the ground motions are scaled for a second time they do not exceed the upper bound limit of 4.0. For the “Suite” section, both the H1 and H2 options are selected but run individually because the tool can only run one spectral ordinate at a time. Under the “Scaling” section the “Minimize MSE” option is selected with the “weight function” set to minimize the MSE uniformly between the range of $0.2T_1$ and $2T_1$. Note, that if the input is too general, e.g. magnitude or rupture distance range is too large or left empty, the tool may crash. The output generated by the tool is presented in Figure 28.

Once the tool is run for the H1 and H2 spectral ordinates, the output is saved to an Excel spreadsheet where it is processed with a MATLAB script to sort the ground motions by error and select the fourteen ground motions with the least amount of mean squared error. The average spectrum for selected records is then calculated and scaled with a second scale factor, referred to as the “Suite Scale Factor”, to ensure the average (arithmetic mean) does not fall below the target spectrum in the period range of $0.2T_1$ and $2T_1$. After the Excel file is processed, the selected records now have a “combined” scale factor that minimizes the error and ensures the average is above the target spectrum. Shown in Figure 29, the combined scale factor is a product of the individual scale factor and the suite scale factor.

Once the ground motions are scaled and selected, their spectra and average are plotted as a “visual” check to ensure their average is above the target spectrum for the $0.2T_1$ to $2T_1$ period range. Figure 30(a) presents the spectra for records selected with the PEER method for the 4-story frame, showing that the average of the ground motions is above the target spectrum for the aforementioned period range, therefore meeting the selection criteria. The spectra of the selected records for the 8-, and 16-story frames can be seen in Figure 30(b) and (c), respectively. Records seen in Figure 30 are the input used to compare the demand-to-capacity ratios, DCR_N, with those produced by the CMS method. The PEER records used to compare dispersion are scaled to match the average spectral acceleration at T_1 to that of the target spectrum. These records are shown in Figure 31(a), (b), and (c) for the 4-, 8-, and 16-story buildings, respectively. PEER selected ground motions are included in Appendix B.

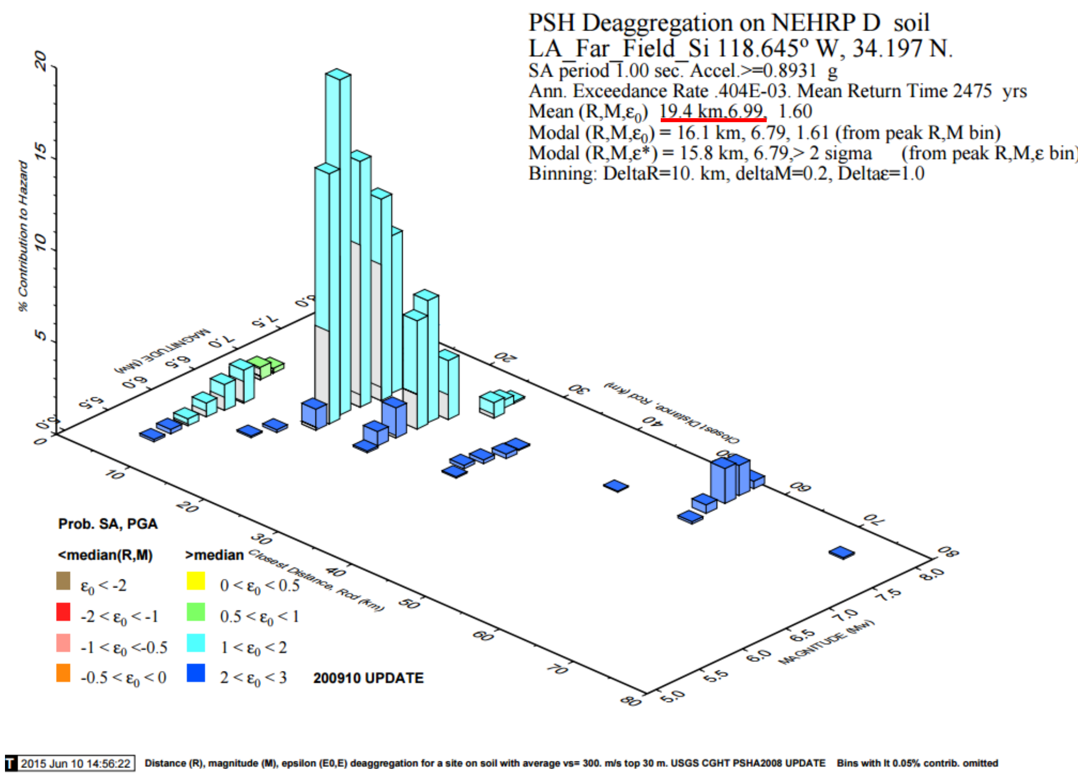

Figure 19. Example deaggregation information for a building where T_1 = 1.00 s.

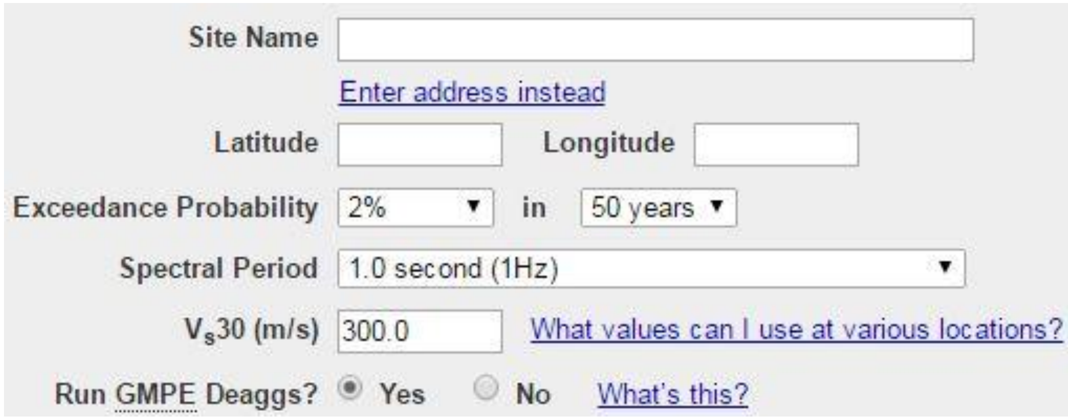

Figure 20. USGS web tool input fields for deaggregation.

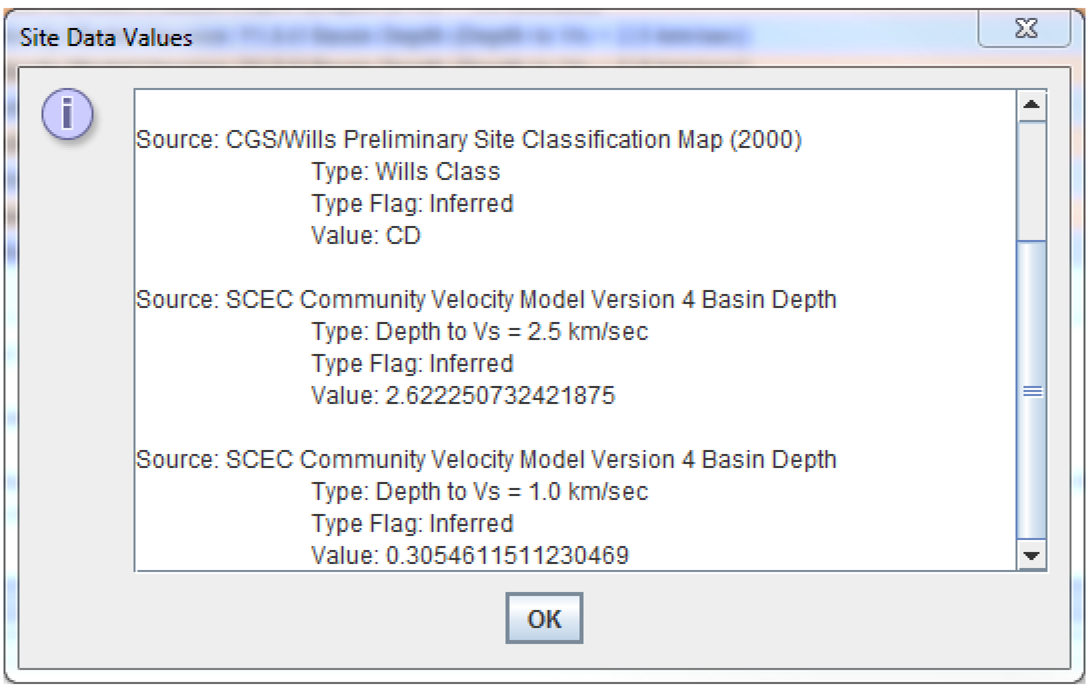

Figure 21. Example output of Z_{vs} from OpenSHA application.

a)

```
Ztor = 0;
delta = 90;
lambda = 180;
Vs30 = 300;
Zvs = 2.61480;
% arb = 0; % geometric mean
arb = 1; % arbitrary component

% USGS hazard and deaggregation inputs:
T1 = 1.0; % Period of interest
M_bar = 6.99; % Mean magnitude, "M"
R_bar = 28.6; % Mean rupture distance, "R"
Sa_star = 0.4500; % Sa value at conditioning period
```

b)

```
eps_bar =

    2.6338
```

Figure 22. (a) Sample input for the "BackCalcEpsilon" script to determine epsilon at the conditioning period and (b) the output epsilon.

a)

```
hazardLevel = 1;
M_bar       = 6.99;
R_bar       = 28.6;
eps_bar     = 2.6338;
Vs30        = 300;
Ztor        = 0;
delta       = 90;
lambda      = 180;
Zvs         = 2.61480;
arb         = 1; % Arbitrary component
PerTgt      = logspace(-1,log10(10),20);
showPlots = 1;
useVar      = 0;
```

b)

```
perKnown    = Periods;
nGM         = 14;
T1          = 1.00;
building    = 1;
isScaled    = 1;
maxScale    = 2;
weights     = [1.0 2.0];
nLoop       = 2;
penalty     = 0;
notAllowed = [];
checkCorr   = 1;
seedValue   = 1;
outputFile = 'Output File.dat';
```

Figure 23. Example of a) deaggregation information input and b) user selected input required for the "Select_Ground_Motions" script to select ground motions to match the CMS for a building where T_1 = 1.00 s.

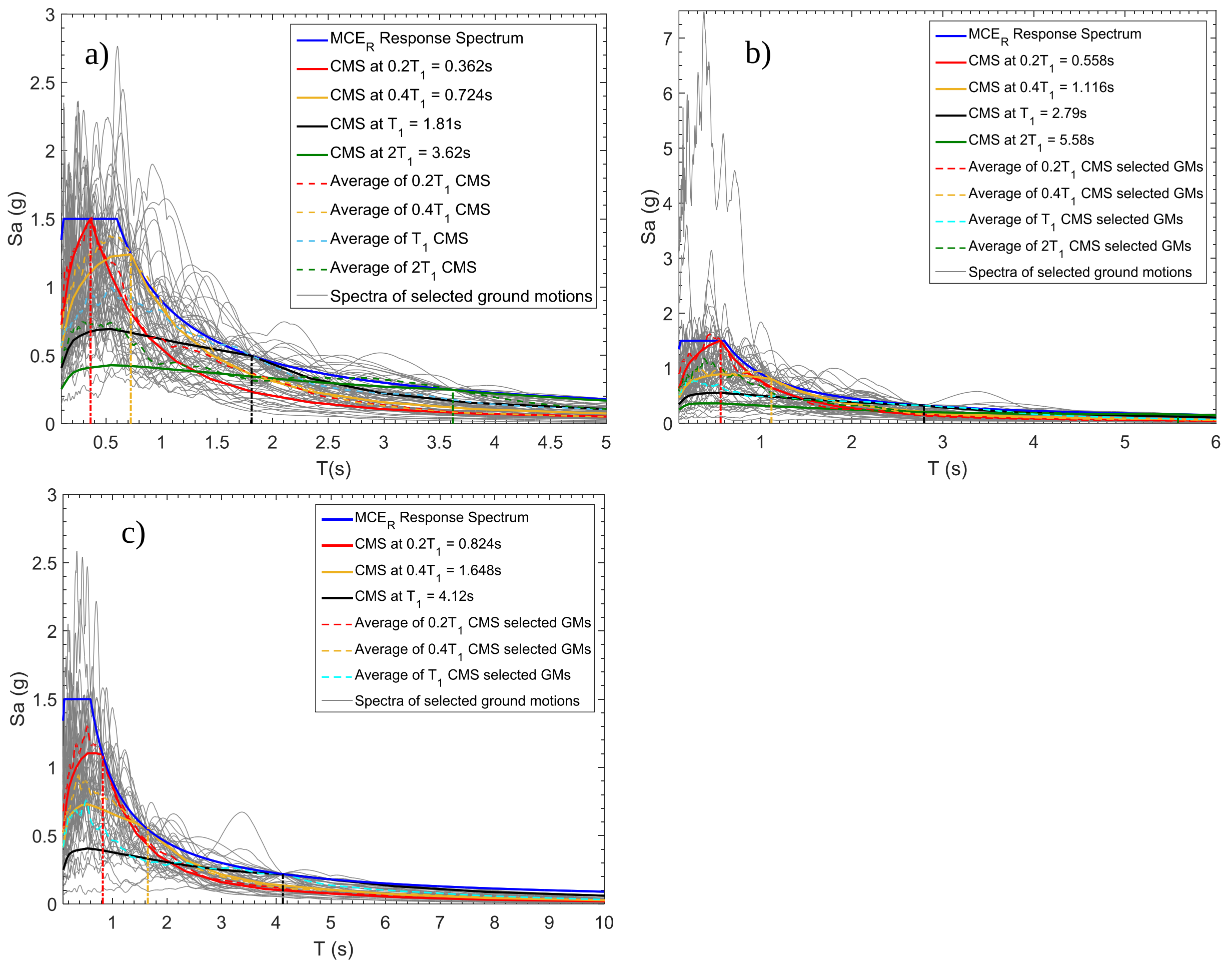

Figure 24. Ground motion spectra at the conditioning periods, their average, and the MCE$_R$ spectrum for the a) 4-, b) 8- and c) 16-story buildings using the CMS method.

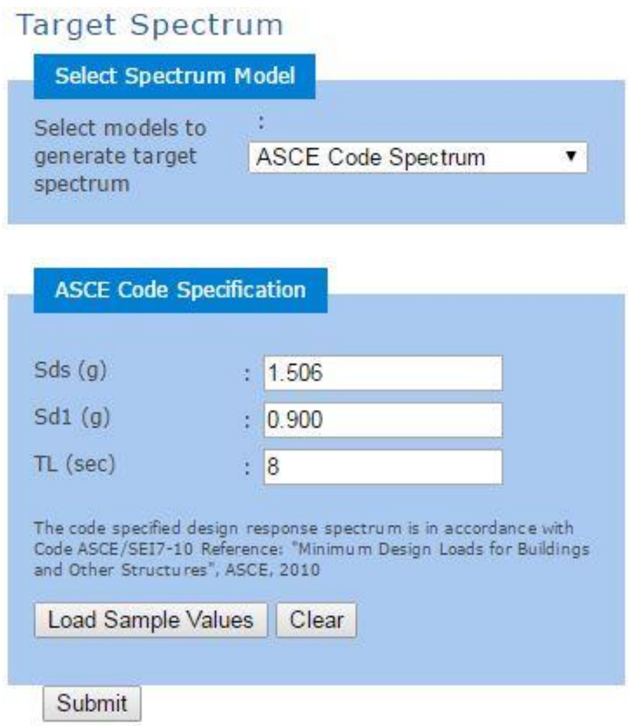

Figure 25. Target spectrum input for PEER ground motion selection tool.

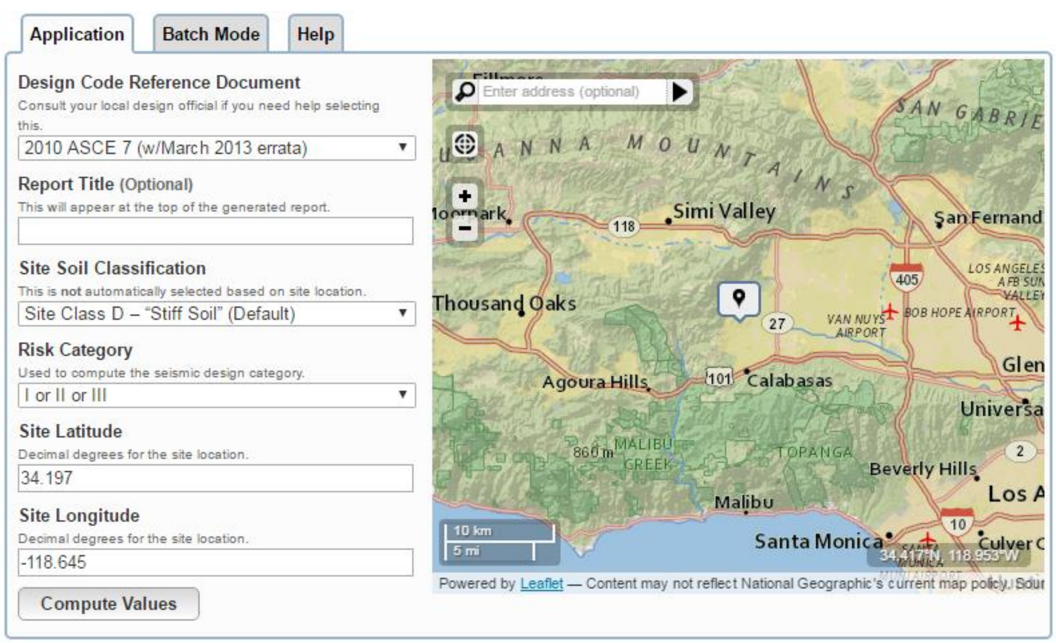

Figure 26. Input to generate MCE_R target spectrum via the PEER method for the selected site.

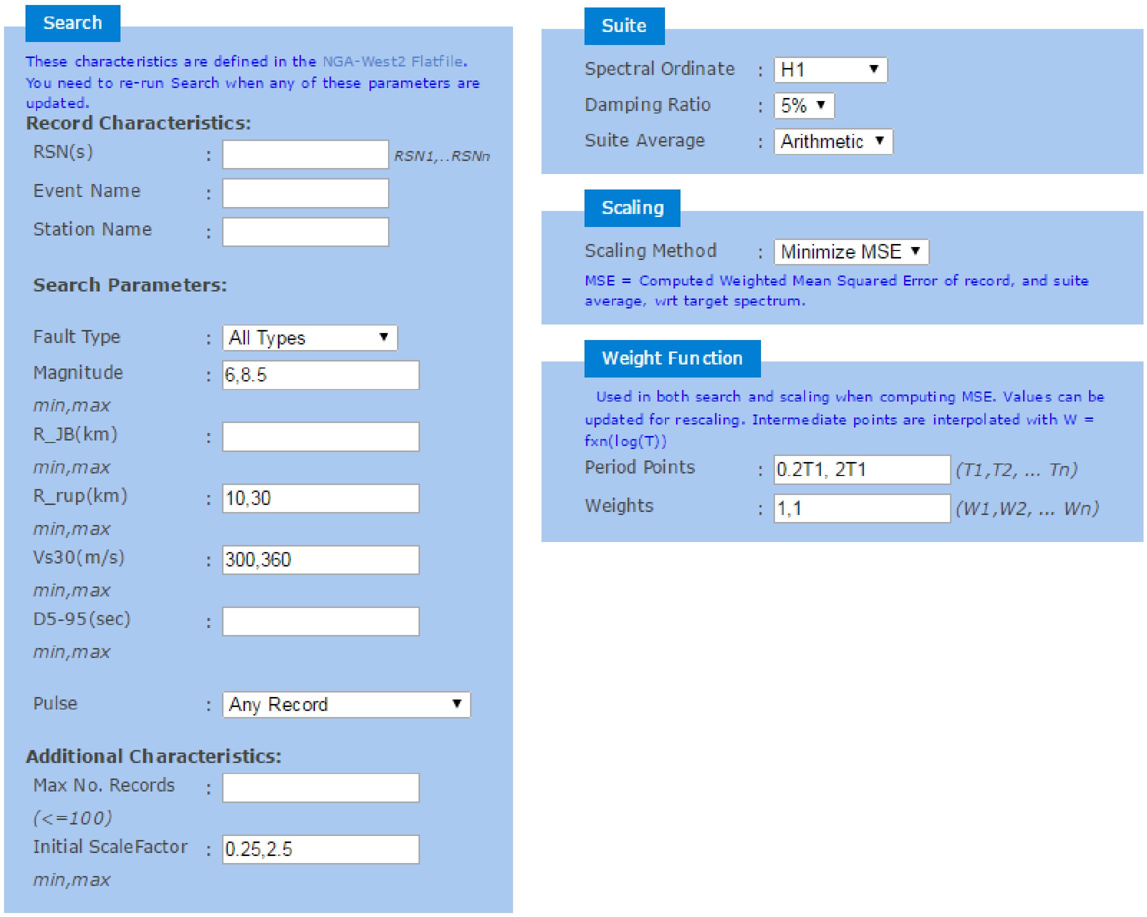

Figure 27. PEER web tool search parameters for ground motion selection.

Result ID	Spectral Ordinate	Record Seq. #	MSE	Scale Factor	Tp(s)	D5-75(s)	D5-95(s)	Arias Intensity (m/s)	Event	Year	Station	Mag	Mechanism
1	H1	725	0.1234	2.1989	-	11.2	13.7	2.1	Superstition Hills-02	1987	Poe Road (temp)	6.54	strike slip
2	H1	900	0.0798	2.2616	7.504	10.9	18.9	0.9	Landers	1992	Yermo Fire Station	7.28	strike slip
3	H1	953	0.1863	1.4372	-	6.0	9.3	4.5	Northridge-01	1994	Beverly Hills - 14145 Mulhol	6.69	Reverse
4	H1	960	0.1115	1.8288	-	3.2	6.3	2.0	Northridge-01	1994	Canyon Country - W Lost Cany	6.69	Reverse
5	H1	1077	0.0608	2.0853	-	6.9	10.7	2.8	Northridge-01	1994	Santa Monica City Hall	6.69	Reverse
6	H1	3749	0.1742	1.9414	-	6.1	15.0	1.3	Cape Mendocino	1992	Fortuna Fire Station	7.01	Reverse
7	H1	4861	0.1539	2.2307	-	10.7	19.5	2.1	Chuetsu-oki, Japan	2007	Nakanoshima Nagaoka	6.8	Reverse
8	H1	4886	0.5647	1.6697	-	7.4	12.9	4.9	Chuetsu-oki, Japan	2007	Tamati Yone Izumozaki	6.8	Reverse
9	H1	4894	0.0825	0.894	-	6.0	10.4	16.5	Chuetsu-oki, Japan	2007	Kashiwazaki NPP, Unit 1: ground surface	6.8	Reverse

Figure 28. Output generated by PEER web tool for ground motion selection.

Record Nc	SpectralID	Ordinate	MSE	Indiv. Scale Factor	Combined Scale Factors	Event	Station	Acc. FileName	Suite Scale Factor
1	RSN-5780	H2	0.0363	1.95	2.36	Iwate, Jap	Iwadeyam	RSN5780_IWATE_54015EW.AT2	1.21
2	RSN-4866	H2	0.0505	2.49	3.01	Chuetsu-c	Kawanishi	RSN4866_CHUETSU_65039EW.AT2	
3	RSN-1048	H1	0.0547	2.34	2.83	Northridg	Northridg	RSN1048_NORTHR_STC090.AT2	
4	RSN-4894	H2	0.0581	0.59	0.72	Chuetsu-c	Kashiwaza	RSN4894_CHUETSU_1-G1EW.AT2	
5	RSN-1077	H1	0.0608	2.22	2.69	Northridg	Santa Mor	RSN1077_NORTHR_STM090.AT2	
6	RSN-1158	H1	0.065	1.94	2.35	Kocaeli, T	Duzce	RSN1158_KOCAELI_DZC180.AT2	
7	RSN-582 H	H2	0.0676	2.44	2.95	Taiwan SN	SMART1 C	RSN582_SMART1.45_45O08NS.AT2	
8	RSN-1082	H2	0.073	2.05	2.48	Northridg	Sun Valley	RSN1082_NORTHR_RO3090.AT2	
9	RSN-776 H	H1	0.0742	1.41	1.70	Loma Prie	Hollister -	RSN776_LOMAP_HSP000.AT2	
10	RSN-767 H	H2	0.0766	2.33	2.81	Loma Prie	Gilroy Arr	RSN767_LOMAP_G03090.AT2	
11	RSN-900 H	H1	0.0798	2.41	2.92	Landers	Yermo Fir	RSN900_LANDERS_YER270.AT2	
12	RSN-316 H	H1	0.0893	2.47	2.99	Westmorl	Parachute	RSN316_WESMORL_PTS225.AT2	
13	RSN-4861	H2	0.1149	2.07	2.51	Chuetsu-c	Nakanosh	RSN4861_CHUETSU_65034EW.AT2	
14	RSN-725 H	H1	0.1234	2.34	2.83	Superstiti	Poe Road	RSN725_SUPER.B_B-POE270.AT2	

Figure 29. Ground motion information for PEER selected records in Excel.

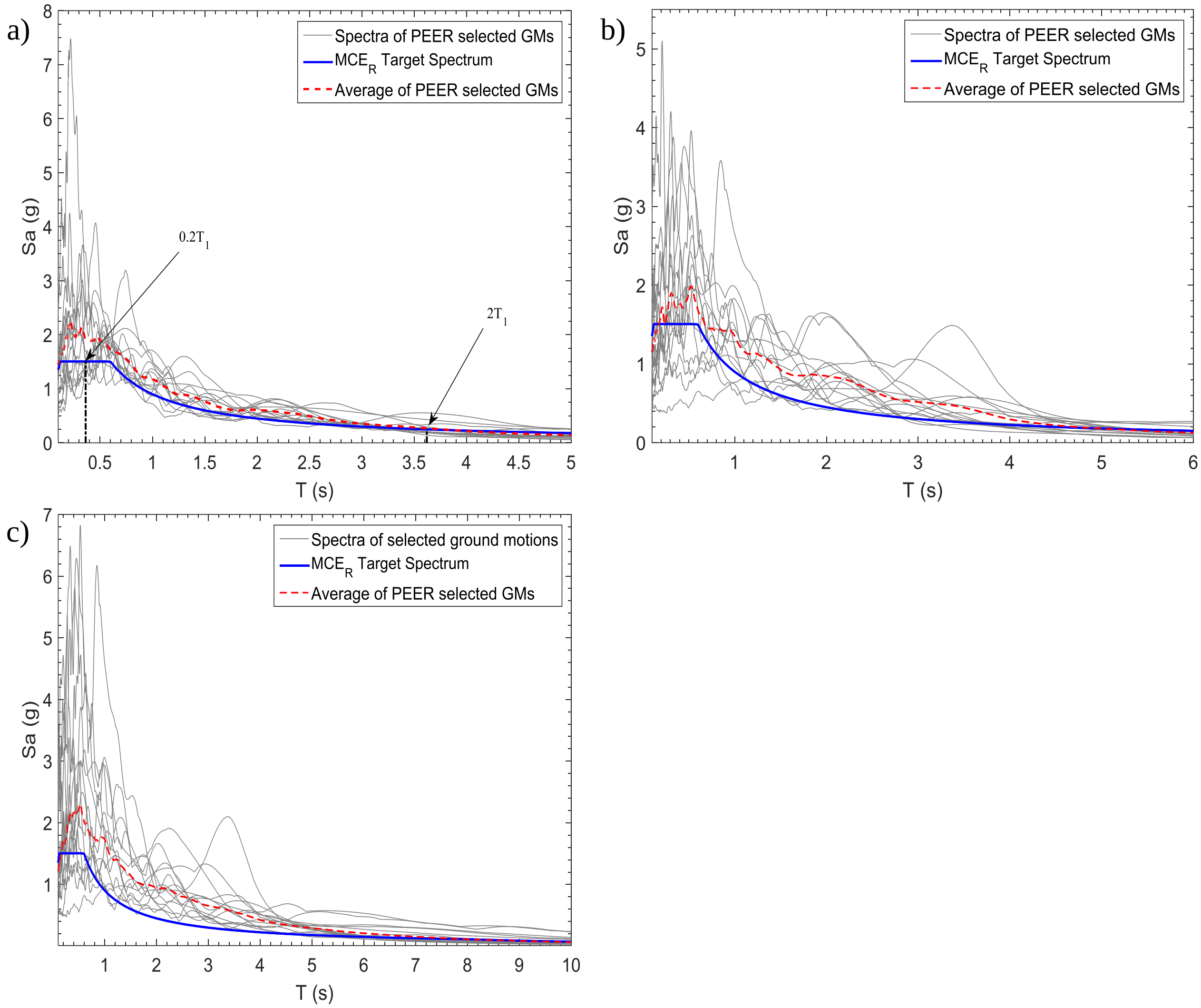

Figure 30. Spectra of PEER selected ground motions for the a) 4-story, b) 8-story, and c) 16-story ELF designed frames.

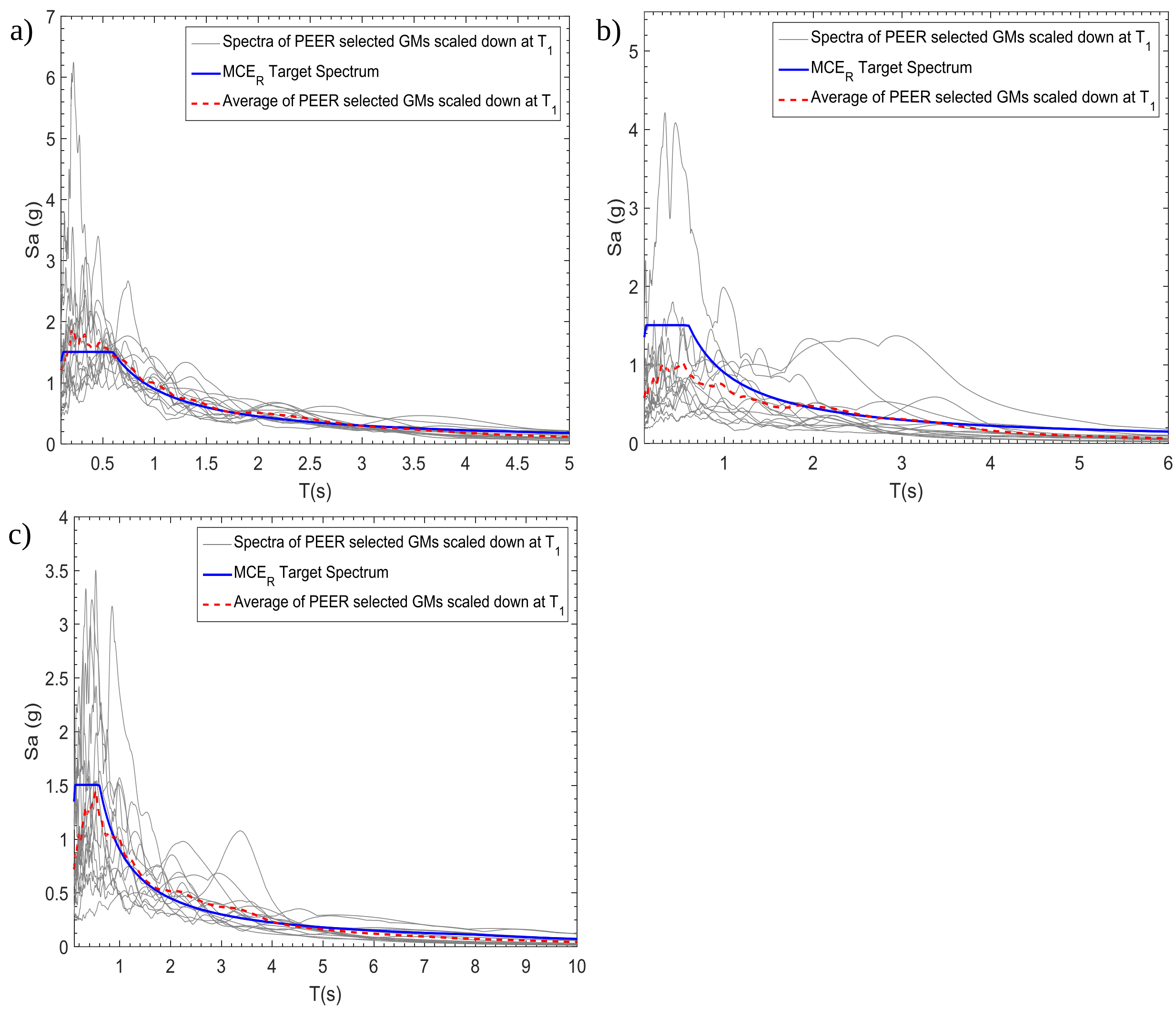

Figure 31. Spectra of PEER selected ground motions scaled down to match the MCE_R target spectrum at T_1 for the a) 4-story, b) 8-story, and c) 16-story buildings.

APPENDIX B:

GROUND MOTIONS FOR TIME HISTORY ANALYSIS

The tables and figures presented in this appendix summarize the records used for time history analysis on the frames. The tables report the event name, station, component, scale factor, time-step, and duration of the ground motions. The duration of the ground motions is rounded to the nearest tenth of a second. Tables 4-14 and Figures 32-42 summarize the ground motions selected using the CMS method at the four different conditioning periods for the 4-story building followed by the 8- and 16-story buildings. The PEER ground motions for the same frames are reported in Tables 15-17 and Figures 43-45. The combined scale factors for PEER ground motions are reported in lieu of reporting both the individual scale factor and suite scale factor.

Table 4. Ground Motion Records used for the $0.2T_1$ conditioning period for the 4-story frame.

Record No.	Event Name	Station Name	Comp.	Scale Factor	Time Step (s)	Duration (s)
1	Tabas, Iran	Dayhook	2	1.46	0.020	23.84
2	Loma Prieta	Coyote Lake Dam - Southwest Abutment	2	1.74	0.005	39.955
3	Imperial Valley	Calexico Fire Station	1	1.74	0.005	37.80
4	Northridge	Saticoy	2	1.01	0.010	29.99
5	Superstition Hills	Poe Road (Temp)	2	1.77	0.010	22.30
6	Chi-Chi, Taiwan	TCU045	2	1.67	0.005	90.00
7	Northridge	Castaic - Old Ridge Route	1	1.14	0.020	40.00
8	Northridge	Canyon Country - W Lost Canyon	1	1.30	0.010	19.99
9	Cape Mendocino	Rio Dell Overpass	1	2.00	0.020	36.00
10	Kocaeli, Turkey	Duzce	2	1.15	0.005	27.18
11	New Zealand	Matahina Dam	1	1.80	0.020	27.00
12	Loma Prieta	Gilroy Array	2	1.83	0.005	39.95
13	Kobe	Kakogawa	2	1.59	0.010	40.96
14	Irpinia, Italy	Sturno	1	1.74	0.0024	39.34

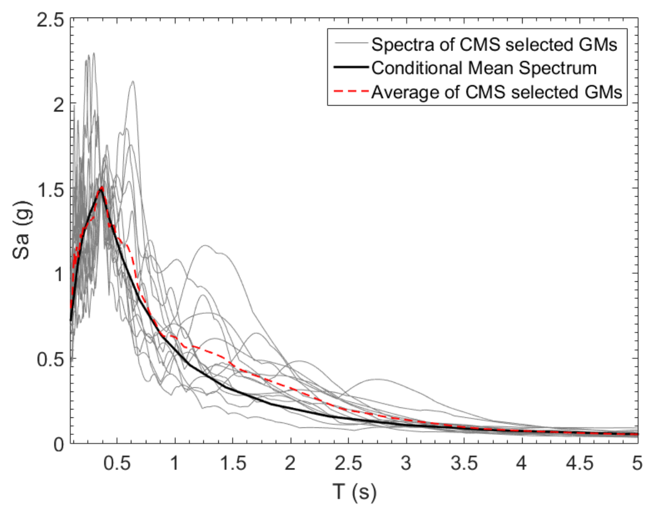

Figure 32. Ground motions selected using CMS method for the 4-story ELF-designed building at the selected site for $T = 0.2T_1 = 0.362\ s$.

Table 5. Ground Motion Records used for the $0.4T_1$ conditioning period for the 4-story frame.

Record No.	Event Name	Station Name	Comp.	Scale Factor	Time Step (s)	Duration (s)
1	Loma Prieta	Hollister Diff. Array	1	1.49	0.005	39.64
2	Loma Prieta	Hollister - South & Pine	1	1.25	0.005	59.95
3	Northridge	Saticoy	2	1.17	0.010	29.99
4	Cape Mendocino	Rio Dell Overpass	1	1.79	0.020	36.00
5	Kobe	Shin-Osaka	2	1.92	0.010	40.96
6	Northridge	Castaic - Old Ridge Route	2	1.33	0.020	40.00
7	Kobe	Amagasaki	2	1.23	0.010	54.00
8	Loma Prieta	Oakland - Outer Harbor Wharf	1	1.98	0.020	40.00
9	Northridge	Canoga Park - Topanga Canyon	2	1.86	0.010	24.99
10	Chi-Chi, Taiwan	CHY080	2	1.19	0.005	75.00
11	Landers	Coolwater	2	1.07	0.0025	27.96
12	Chi-Chi, Taiwan	TCU076	2	1.22	0.005	96.00
13	Whittier	Compton - Castlegate St	1	1.76	0.020	31.18
14	Whittier	Santa Fe Springs - E.Joslin	1	1.81	0.020	37.82

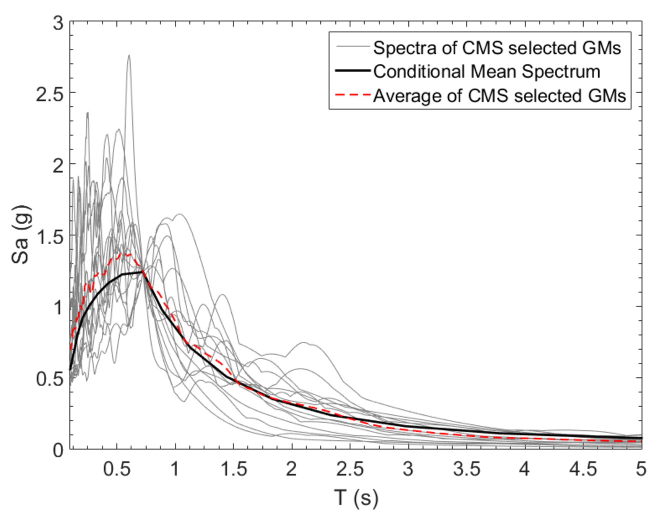

Figure 33. Ground motions selected using CMS method for the 4-story ELF-designed building at the selected site for $T = 0.4T_1 = 0.724\ s$.

Table 6. Ground Motion Records used for the T_1 conditioning period for the 4-story frame.

Record No.	Event Name	Station Name	Comp.	Scale Factor	Time Step (s)	Duration (s)
1	Loma Prieta	Hollister City Hall	2	1.34	0.005	39.09
2	Chi-Chi, Taiwan	ILA013	2	1.78	0.004	117.00
3	Chi-Chi, Taiwan	ALS	2	1.75	0.005	59.00
4	Kobe	Amagasaki	1	1.13	0.010	54.00
5	Superstition Hills	El Centro Imp. Co. Cent	2	1.56	0.005	40.00
6	Loma Prieta	Hollister - South & Pine	1	1.01	0.005	59.95
7	Loma Prieta	Hollister Diff. Array	1	1.76	0.005	39.64
8	Superstition Hills	Wildlife Liquef. Array	2	1.60	0.005	44.00
9	Chi-Chi, Taiwan	CHY036	2	1.47	0.005	90.00
10	Kocaeli, Turkey	Duzce	2	1.19	0.005	27.185
11	Kobe	Fukushima	1	2.01	0.010	80.00
12	Landers	Yermo Fire Station	1	2.02	0.020	44.00
13	Irpinia, Italy	Sturno (STN)	1	1.83	0.0024	39.34
14	Imperial Valley	Delta	2	1.85	0.010	99.92

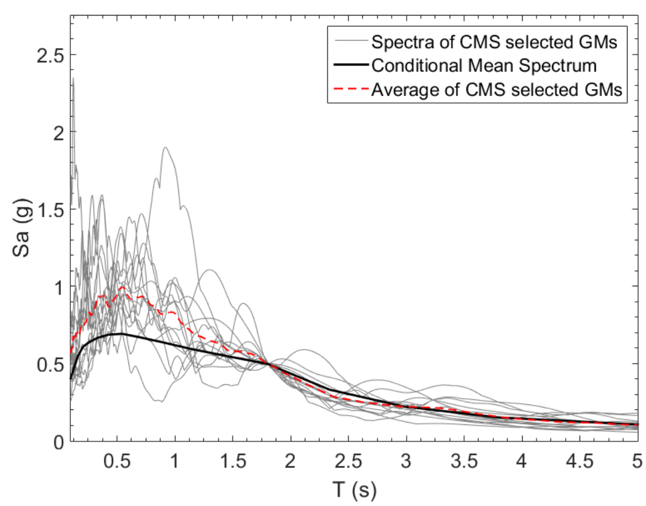

Figure 34. Ground motions selected using CMS method for the 4-story ELF-designed building at the selected site for $T = T_1 = 1.81\ s$.

Table 7. Ground Motion Records used for the $2T_1$ conditioning period for the 4-story frame.

Record No.	Event Name	Station Name	Comp.	Scale Factor	Time Step (s)	Duration (s)
1	Chi-Chi, Taiwan	CHY025	2	1.78	0.005	102.00
2	Kocaeli, Turkey	Duzce	1	1.05	0.005	27.18
3	St. Elias	Yakutat	1	1.58	0.005	82.97
4	Loma Prieta	Sunnyvale - Colton Ave.	1	1.54	0.005	39.25
5	Chi-Chi, Taiwan	CHY024	2	1.87	0.005	99.04
6	Chi-Chi, Taiwan	CHY101	2	1.89	0.005	103.00
7	Superstition Hills	Wildlife Liquef. Array	2	1.29	0.005	44.00
8	Westmorland	Parachute Test Site	1	1.79	0.005	40.00
9	Loma Prieta	Palo Alto - 1900 Embarc.	1	1.37	0.005	40.00
10	Irpinia, Italy	Sturno (STN)	2	1.20	0.0024	39.34
11	Loma Prieta	Foster City - APEEL 1	2	1.83	0.005	59.99
12	Manjil, Iran	Abhar	1	1.73	0.010	29.50
13	Kocaeli, Turkey	Yarimca	2	0.84	0.005	35.00
14	Imperial Valley	El Centro Array #10	1	1.63	0.005	36.97

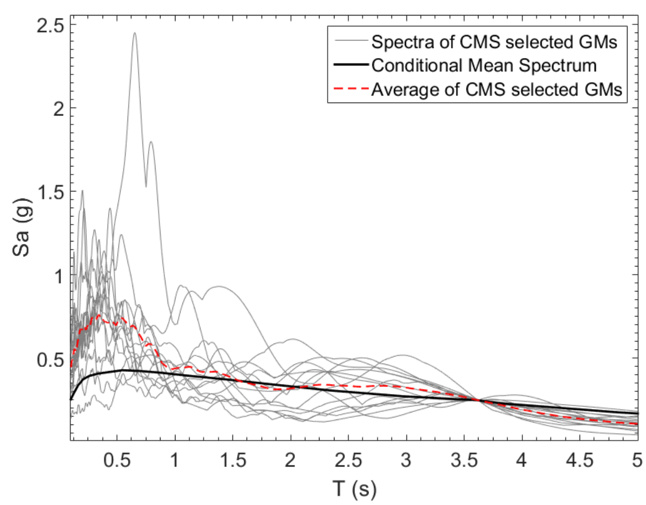

Figure 35. Ground motions selected using CMS method for the 4-story ELF-designed building at the selected site for $T = 2T_1 = 3.62\ s$.

Table 8. Ground Motion Records used for the $0.2T_1$ conditioning period for the 8-story frame.

Record No.	Event Name	Station Name	Comp.	Scale Factor	Time Step (s)	Duration (s)
1	Northridge	Saticoy	2	1.24	0.010	29.99
2	Loma Prieta	Coyote Lake Dam (SW Abut)	2	1.43	0.005	39.95
3	Loma Prieta	Hollister Diff. Array	2	1.61	0.005	39.64
4	Northridge	Castaic - Old Ridge Route	2	1.06	0.020	40.00
5	Northridge	Canoga Park - Topanga Canyon	2	1.47	0.010	24.99
6	Victoria, Mexico	Cerro Prieto	1	1.65	0.010	24.45
7	Superstition Hills	Poe Road (Temp)	1	2.12	0.010	22.30
8	Landers	Coolwater	2	1.17	0.0025	27.96
9	Loma Prieta	Gilroy Array #4	2	1.46	0.005	39.95
10	Kobe	Morigawachi	1	1.67	0.010	198.06
11	Chi-Chi, Taiwan	TCU076	1	1.36	0.005	96.00
12	Chi-Chi, Taiwan	TCU129	1	1.79	0.005	104.03
13	Friuli, Italy	Tolmezzo-Diga Ambiesta (Base)	2	1.62	0.005	36.345
14	Cape Mendocino	Rio Dell Overpass	2	1.17	0.020	36.00

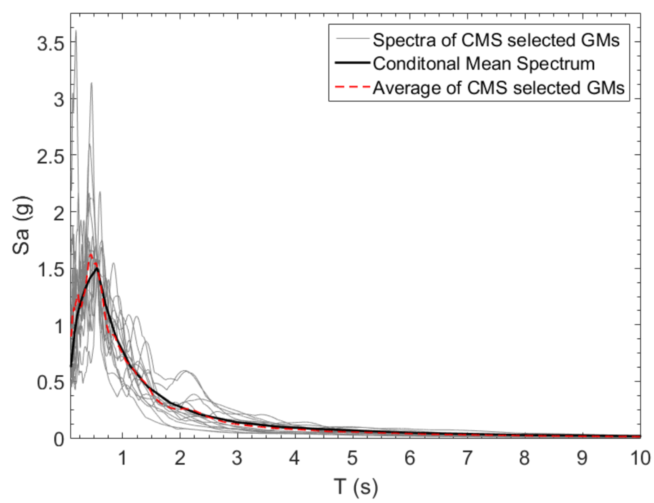

Figure 36. Ground motions selected using CMS method for the 8-story ELF-designed building at the selected site for $T = 0.2T_1 = 0.558\ s$.

Table 9. Ground Motion Records used for the $0.4T_1$ conditioning period for the 8-story frame.

Record No.	Event Name	Station Name	Comp.	Scale Factor	Time Step (s)	Duration (s)
1	Loma Prieta	Hollister - South & Pine	1	0.92	0.005	59.95
2	Kobe	Amagasaki	1	1.08	0.010	54.00
3	Kocaeli, Turkey	Duzce	2	1.28	0.005	27.18
4	Kobe	Fukushima	2	1.93	0.010	80.00
5	Loma Prieta	Palo Alto - SLAC Lab	1	1.72	0.005	39.575
6	Loma Prieta	Hollister City Hall	2	1.15	0.005	39.09
7	Superstition Hills	Westmorland Fire Station	2	1.58	0.005	40.00
8	Kobe	Yae	1	1.83	0.010	89.03
9	Kocaeli, Turkey	Ambarli	2	1.32	0.005	150.40
10	Coalinga	Parkfield - Fault Zone 1	1	1.98	0.010	40.00
11	Cape Mendocino	Rio Dell Overpass	1	1.63	0.020	36.00
12	Northridge	Castaic - Old Ridge Route	2	1.2	0.020	40.00
13	Palm Springs	Morongo Valley	1	1.89	0.005	20.16
14	Northridge	Sun Valley - Roscoe Blvd	2	1.56	0.010	30.28

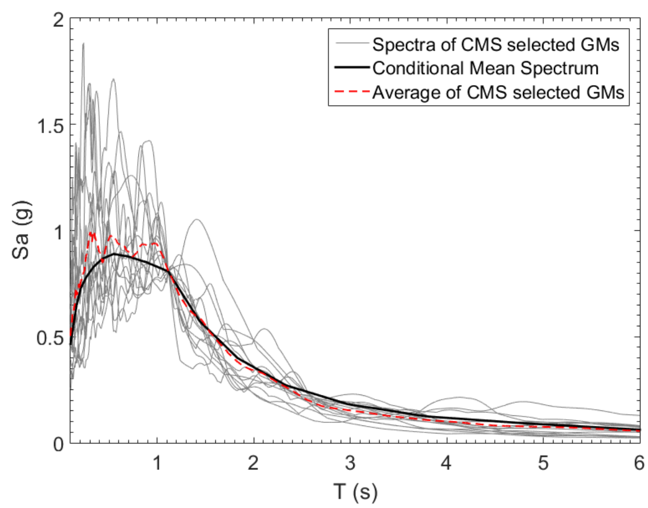

Figure 37. Ground motions selected using CMS method for the 8-story ELF-designed building at the selected site for $T = 0.4T_1 = 1.116\ s$.

Table 10. Ground Motion Records used for the T_1 conditioning period for the 8-story frame.

Record No.	Event Name	Station Name	Comp.	Scale Factor	Time Step (s)	Duration (s)
1	Chi-Chi, Taiwan	CHY025	1	1.68	0.005	102.00
2	Westmorland	Parachute Test Site	1	1.62	0.005	40.00
3	Chi-Chi, Taiwan	TCU122	1	1.89	0.005	97.00
4	Superstition Hills	El Centro Imp. Co. Cent	2	1.87	0.005	40.00
5	Imperial Valley	Brawley Airport	1	1.98	0.005	37.82
6	Superstition Hills	Westmorland Fire Station	2	1.54	0.005	44.00
7	Chi-Chi, Taiwan	CHY104	2	1.81	0.004	117.00
8	Loma Prieta	Sunnyvale - Colton Ave.	2	1.11	0.005	39.25
9	Loma Prieta	Hollister City Hall	2	1.9	0.005	39.09
10	Palm Springs	Morongo Valley	2	1.94	0.005	20.16
11	Irpinia, Italy	Sturno (STN)	2	0.93	0.0024	39.34
12	Loma Prieta	Palo Alto - 1900 Embarc.	2	1.41	0.005	40.00
13	Manjil, Iran	Abhar	2	1	0.010	29.49
14	Imperial Valley	El Centro Array #3	1	1.74	0.005	39.54

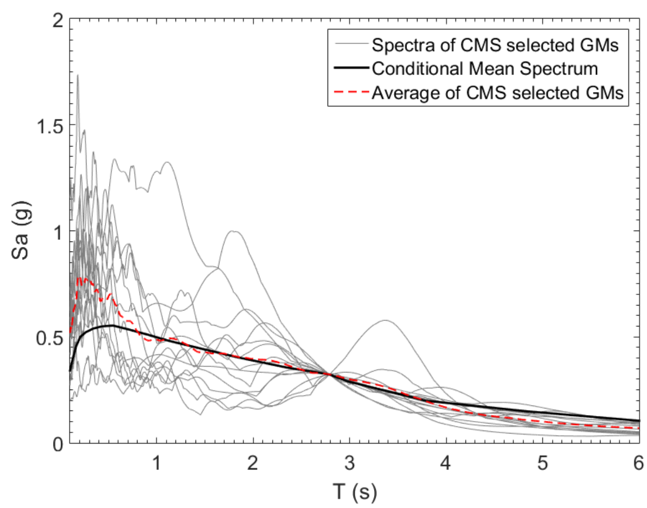

Figure 38. Ground motions selected using CMS method for the 8-story ELF-designed building at the selected site for $T = T_1 = 2.79\ s$.

Table 11. Ground Motion Records used for the $2T_1$ conditioning period for the 8-story frame.

Record No.	Event Name	Station Name	Comp.	Scale Factor	Time Step (s)	Duration (s)
1	St. Elias	Yakutat	1	1.85	0.005	82.97
2	Kocaeli, Turkey	Arcelik	2	1.65	0.005	30.00
3	Hector Mine	Whittier Narrows Dam	2	1.85	0.005	67.00
4	Loma Prieta	Hollister - South & Pine	2	1.82	0.005	59.95
5	Kocaeli, Turkey	Ambarli	1	1.68	0.005	150.40
6	Landers	Yermo Fire Station	1	1.8	0.020	44.00
7	Kocaeli, Turkey	Duzce	1	1.59	0.005	27.18
8	Chi-Chi, Taiwan	CHY026	1	1.56	0.005	95.00
9	Kobe	Amagasaki	1	1.96	0.010	54.00
10	Chi-Chi, Taiwan	CHY093	2	1.96	0.004	130.00
11	Chi-Chi, Taiwan	NSY	1	1.22	0.005	53.00
12	Kobe	Fukushima	2	2	0.010	80.00
13	Loma Prieta	Hollister City Hall	1	2.03	0.005	39.09
14	Northridge	Tarzana - Cedar Hill A	2	2.21	0.020	40.00

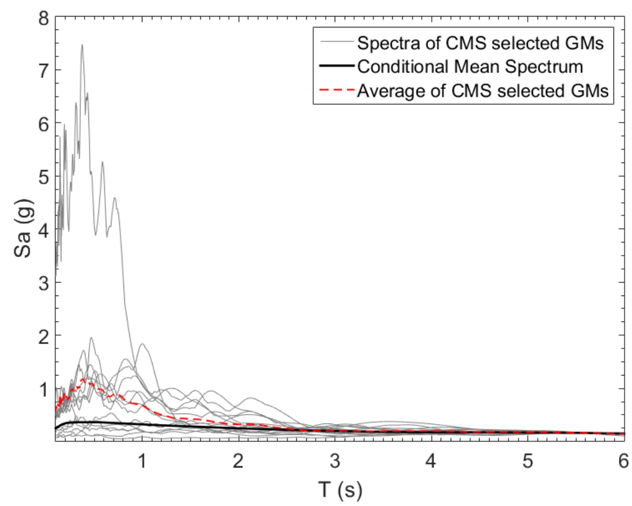

Figure 39. Ground motions selected using CMS method for the 8-story ELF-designed building at the selected site for $T = 2T_1 = 5.58\ s$.

Table 12. Ground Motion Records used for the $0.2T_1$ conditioning period for the 16-story frame.

Record No.	Event Name	Station Name	Comp.	Scale Factor	Time Step (s)	Duration (s)
1	Loma Prieta	Hollister Diff. Array	1	1.64	0.005	39.64
2	Loma Prieta	Hollister - South & Pine	1	1.07	0.005	59.95
3	Chi-Chi, Taiwan	CHY036	1	1.41	0.005	90.00
4	Kobe	Amagasaki	1	1.57	0.010	54.00
5	Northridge	Saticoy	2	1.21	0.010	29.99
6	Northridge	Castaic - Old Ridge Route	2	1.18	0.020	40.00
7	Loma Prieta	Foster City - APEEL 1	2	1.12	0.005	59.99
8	Kobe	Fukushima	2	1.94	0.010	80.00
9	Landers	Clearwater	2	1.64	0.0025	27.96
10	Chi-Chi, Taiwan	TCU045	2	1.66	0.005	90.00
11	Superstition Hills	Westmorland Fire Station	2	1.98	0.005	40.00
12	Superstition Hills	El Centro Imp. Co. Cent	1	1.94	0.005	40.00
13	Kobe	Yae	1	1.58	0.010	89.03
14	Northridge	Sun Valley - Roscoe Blvd	2	1.32	0.010	30.28

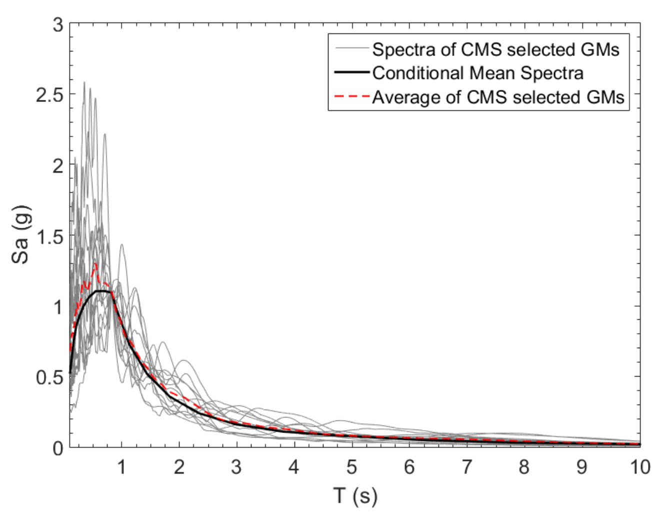

Figure 40. Ground motions selected using CMS method for the 16-Story ELF-designed building at the selected site for $T = 0.2T_1 = 0.824\ s$.

Table 13. Ground Motion Records used for the $0.4T_1$ conditioning period for the 16-story frame.

Record No.	Event Name	Station Name	Comp.	Scale Factor	Time Step (s)	Duration (s)
1	Loma Prieta	Hollister City Hall	2	1.27	0.005	39.09
2	Kobe	Amagasaki	1	1.39	0.010	54.00
3	Kobe	Fukushima	2	1.57	0.010	80.00
4	Loma Prieta	Hollister - South & Pine	1	1.2	0.005	59.95
5	Kocaeli, Turkey	Iznik	2	1.98	0.005	30.00
6	Loma Prieta	Hollister Diff. Array	1	1.84	0.005	39.64
7	Landers	Yermo Fire Station	1	1.47	0.020	44.00
8	Kocaeli, Turkey	Ambarli	2	1.75	0.005	150.40
9	Kocaeli, Turkey	Duzce	2	1.11	0.005	27.18
10	Superstition Hills	El Centro Imp. Co. Cent	2	1.86	0.005	40.00
11	Imperial Valley	Delta	2	1.16	0.010	99.92
12	Superstition Hills	Wildlife Liquef. Array	2	1.97	0.005	44.00
13	Irpinia, Italy	Sturno	1	1.84	0.0024	39.34
14	Palm Springs	Morongo Valley	2	1.32	0.005	20.16

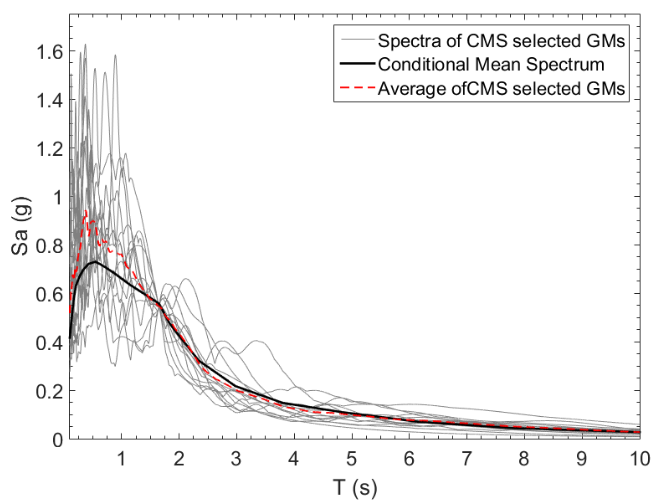

Figure 41. Ground motions selected using CMS method for the 16-Story ELF-designed building at the selected site for $T = 0.4T_1 = 1.648\ s$.

Table 14. Ground Motion Records used for the T_1 conditioning period for the 16-story frame.

Record No.	Event Name	Station Name	Comp.	Scale Factor	Time Step (s)	Duration (s)
1	Chi-Chi, Taiwan	CHY025	1	1.59	0.005	102.00
2	St. Elias	Yakutat	2	1.62	0.005	83.22
3	Hector Mine	San Bernardino - E & Hospitalty	1	2	0.010	60.00
4	Kocaeli, Turkey	Duzce	1	1.21	0.005	27.18
5	Superstition Hills	Wildlife Liquef. Array	1	1.96	0.005	44.00
6	Loma Prieta	Hollister - South & Pine	2	1.98	0.005	59.95
7	Hector Mine	Amboy	2	1.67	0.020	60.00
8	Kobe	Yae	1	1.97	0.010	89.03
9	Manjil, Iran	Abhar	2	1.34	0.010	29.49
10	Irpinia, Italy	Sturno	2	1.42	0.0024	39.34
11	Chi-Chi, Taiwan	CHY094	2	1.87	0.004	100.00
12	Chi-Chi, Taiwan	TCU061	1	1.64	0.005	90.00
13	Loma Prieta	Hollister City Hall	1	2.04	0.005	39.09
14	Westmorland	Parachute Test Site	1	2.01	0.005	40.00

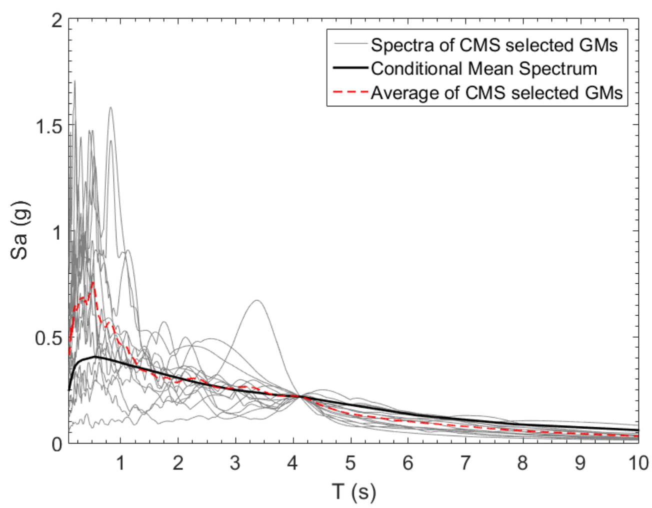

Figure 42. Ground motions selected using CMS method for the 16-Story ELF-designed building at the selected site for $T = T_1 = 4.12\ s$.

Table 15. PEER selected ground motion records used for the 4-story frame.

Record No.	Event Name	Station Name	Comp.	Combined Scale Factor (scaled down)	Time Step (s)	Duration (s)
1	Iwate	Iwadeyama	2	2.36 (1.97)	0.010	60.00
2	Chuetsu-oki	Kawanishi Izumozaki	2	3.01 (2.52)	0.010	60.00
3	Northridge	Hollister - South & Pine	1	2.83 (2.36)	0.010	29.99
4	Chuetsu-oki	Kashiwazaki NPP, Unit 1: ground surface	2	0.72 (0.60)	0.010	70.00
5	Northridge	Santa Monica City Hall	1	2.69 (2.24)	0.020	40.00
6	Kocaeli, Turkey	Duzce	1	2.35 (1.96)	0.005	27.18
7	Smart	SMART1 O08	2	2.95 (2.47)	0.010	60.60
8	Northridge	Sun Valley - Roscoe Blvd	2	2.48 (2.07)	0.010	30.28
9	Loma Prieta	Hollister - South & Pine	1	1.70 (1.42)	0.005	59.99
10	Loma Prieta	Gilroy Array #3	2	2.81 (2.35)	0.005	39.99
11	Landers	Yermo Fire Station	1	2.92 (2.43)	0.020	44.00
12	Westmorland	Parachute Test Site	1	2.99 (2.50)	0.005	41.69
13	Chuetsu-oki, Japan	Nakanoshima Nagaoka	2	2.51 (2.09)	0.010	60.00
14	Superstition Hills	Poe Road (Temp)	1	2.83 (2.37)	0.010	22.30

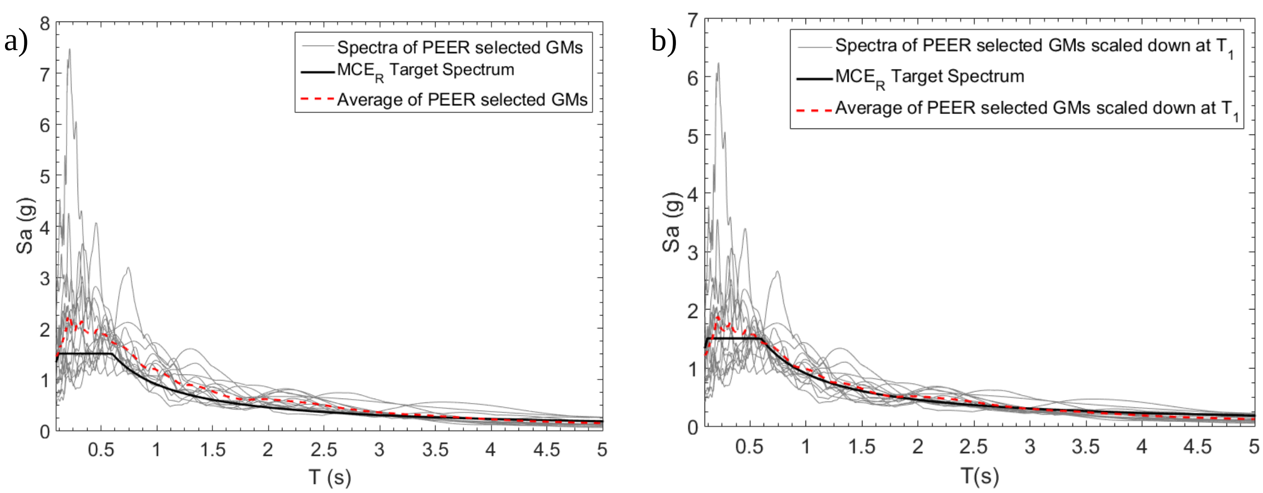

Figure 43. Ground motions selected using a) PEER method and b) PEER method scaling down to match the MCE$_R$ at T_1 for the 4-story ELF-designed building at the selected site.

Table 16. PEER selected ground motion records used for the 8-story frame.

Record No.	Event Name	Station Name	Comp.	Combined Scale Factor (scaled down)	Time Step (s)	Duration (s)
1	Iwate	Iwadeyama	2	2.58 (1.53)	0.01	60.00
2	Landers	Yermo Fire Station	1	2.97 (1.76)	0.02	44.00
3	Chuetsu-oki, Japan	Kashiwazaki NPP, Unit 1: ground surface	2	0.96 (0.57)	0.01	70.00
4	Kocaeli, Turkey	Duzce	1	2.43 (1.44)	0.005	27.185
5	Westmorland	Parachute Test Site	1	3.10 (1.83)	0.005	41.69
6	Loma Prieta	Hollister - South & Pine	1	1.98 (1.17)	0.005	59.99
7	Iwate	Minamikatamachi Tore City	1	2.42 (1.43)	0.01	60.00
8	Loma Prieta	Gilroy Array #3	2	3.37 (2.00)	0.005	39.99
9	Northridge	Saticoy	2	2.05 (1.21)	0.01	29.99
10	Chuetsu-oki, Japan	Kashiwazaki City Center	2	1.28 (0.76)	0.01	60.00
11	St. Elias	Icy Bay	2	3.22 (1.90)	0.005	61.88
12	Northridge	Beverly Hills - 14145 Mulholland	1	2.56 (1.51)	0.01	29.99
13	Chuetsu-oki, Japan	Kariwa	1	0.80 (0.48)	0.01	60.00
14	Manjil, Iran	Abhar	2	2.62 (1.55)	0.01	29.49

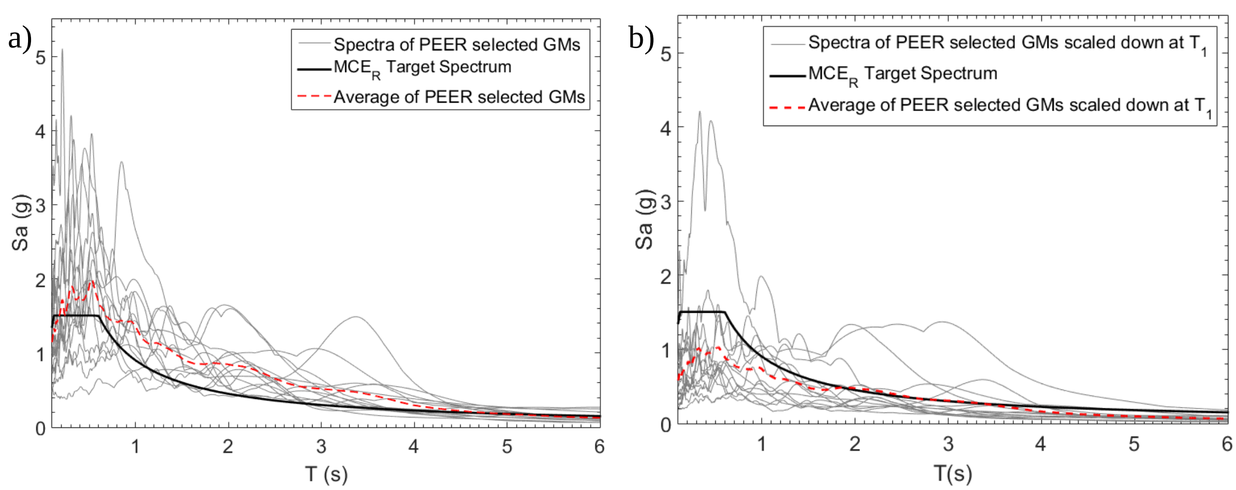

Figure 44. Ground motions selected using a) PEER method and b) PEER method scaling down to match the MCE$_R$ at T_1 for the 8-story ELF-designed building at the selected site.

Table 17. PEER selected ground motion records used for the 16-story frame.

Record No.	Event Name	Station Name	Comp.	Combined Scale Factor (scaled down)	Time Step (s)	Duration (s)
1	Landers	Yermo Fire Station	1	3.80 (1.95)	0.02	44.00
2	Kocaeli, Turkey	Duzce	1	3.11 (1.60)	0.005	27.18
3	Westmorland	Parachute Test Site	1	4.13 (2.12)	0.005	41.69
4	Iwate	Iwadeyama	2	3.90 (2.00)	0.01	60.00
5	Chi-Chi, Taiwan	TCU059	2	3.13 (1.61)	0.005	90.00
6	Loma Prieta	Hollister - South & Pine	1	2.91 (1.50)	0.005	59.99
7	Iwate	Minamikatamachi Tore City	1	3.40 (1.75)	0.01	60.00
8	Chi-Chi, Taiwan	TCU038	1	4.21 (2.16)	0.005	90.00
9	Chuetsu-oki, Japan	Kashiwazaki NPP, Unit 1: ground surface	2	1.60 (0.82)	0.01	70.00
10	Northridge	Saticoy	2	3.35 (1.72)	0.01	29.99
11	Chuetsu-oki, Japan	Kariwa	1	1.01 (0.52)	0.01	60.00
12	Chuetsu-oki, Japan	Kashiwazaki City Center	1	1.86 (0.96)	0.01	60.00
13	Manjil, Iran	Abhar	2	3.69 (1.89)	0.01	29.49
14	Northridge	Beverly Hills - 14145 Mulholland	1	4.41 (2.26)	0.01	29.99

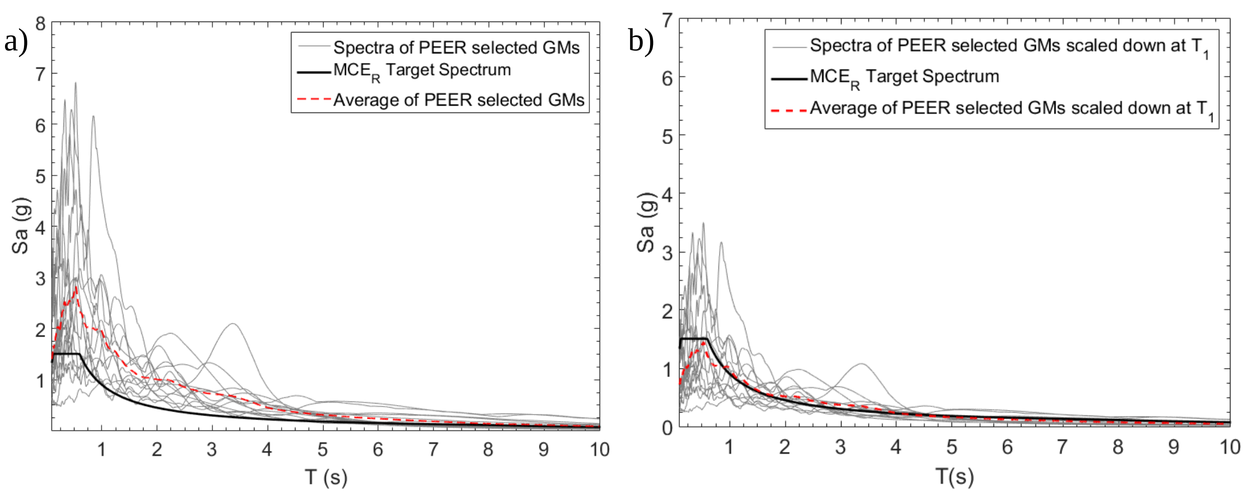

Figure 45. Ground motions selected using a) PEER method and b) PEER method scaling down to match the MCE$_R$ at T_1 for the 16-story ELF-designed building at the selected site.

APPENDIX C:

COMPREHENSIVE SMF RESULTS

This appendix provides the normalized demand-to-capacity ratio, DCR_N, and dispersion results for the entire special moment frame, i.e. all bays, for the reduced beam sections and column hinges of the 4-, 8-, and 16-story frames. These results are calculated by assuming a normal and lognormal distribution.

In Section 5.2, the DCR_N results are first presented for reduced beam sections (RBS) in bay D-E and column hinges (CH) located on column line E for the three buildings used in this study. In this section, a comparison of the CMS and PEER method DCR_N results of the RBS and CH for the other bays of the special moment frames (SMFs) will be presented for the 4-, 8- and 16-story buildings. This section will also present the comparison of the standard deviation (dispersion) of the DCR_N values for the RBS and CH for the CMS and PEER methods.

Figure 46 and Figure 47 present the mean and median DCR_N results of the RBS and CH elements, respectively, computed assuming the DCR_N results are normally and lognormally distributed for the 4-story SMF. In the mean calculation, assuming a normal distribution, all analysis results are used including those that caused "collapse," defined in this study as a roof drift limit of 20 %. For the lognormal distribution, percentiles and the standard deviation are used to calculate the results, as described in section 6.2.3, to avoid using collapse cases in the mean calculation.

Figure 46 shows that the mean for the PEER selected ground motions exceeds the acceptance criteria in all of the bays of the 4-story SMF when all analysis cases are included in the calculation using a normal distribution. Conversely, when using the CMS method, the mean DCR_N results all pass the acceptance criteria for all bays and are lower than the PEER results by a significant amount. The column hinges also show a similar trend with the CMS method providing lower DCR_N results for all column lines in the 4-story SMF, which are presented in Figure 47. As can be seen both the CMS and PEER methods still provide DCR_N results that meet the acceptance criteria for the column elements.

The DCR_N results calculated by assuming a lognormal distribution, by using Eq. (7) and Eq. (8), for the 4-story building are overlaid on the normal distribution results in Figure 46 for the RBS connections and Figure 47 for the column hinges with both labeled as "lognormal mean"; note, these results use the same ground motions for input as the results computed using a normal distribution. As shown in Figure 46 and Figure 47, the mean DCR_N results are lower in all bays and column lines, when using a lognormal distribution, compared to the results calculated using a normal distribution. The mean results are reduced to be much closer to the median, due to using a lognormal distribution. For the RBS connections, as shown in Figure 46, the lower demand to capacity ratios result in both the CMS and PEER methods, producing DCR_N values that pass the acceptance criteria in all bays. For the columns, shown in Figure 47, since the mean DCR_N computed using a normal distribution passed the acceptance criteria for the CMS and PEER methods previously, the use of a lognormal distribution makes a difference by producing mean values closer to the median, similar to the RBS connections.

As mentioned in Section 5.4, the ground motion selection method that produces the lower DCR_N dispersion for the elements of the buildings can be considered more useful for use in the nonlinear dynamic procedure of ASCE/SEI 41-13. The DCR_N dispersion of the

RBS and CH elements for the CMS controlling period is compared to that of the PEER scaled down at T_1. The dispersion of the DCR_N for the RBS connections of the 4-story SMF, shown in Figure 48, shows that the PEER ground motions scaled down at T_1 provide a lower dispersion for almost all the elements in the three bays than the CMS at the controlling period. There is only one RBS element in which the CMS method provides lower dispersion, the 4th floor of Bay D-E. The dispersion of the column hinges provides similar results with a similar number of elements where the CMS provides lower dispersion. Figure 49 presents the DCR_N dispersion of the columns for the 4-story SMF which show that for all the column lines, the upper and lower columns show the PEER scaled down at T_1 ground motions provide lower dispersion. While the middle two columns show the CMS records provides lower dispersion.

For the 8-story frame the mean (computed using the arithmetic average) and median DCR_N results for the RBS, shown in Figure 50, are lower for the CMS method in all three bays of the building for all the elements, especially in the lower half of the frame. Using the arithmetic average, the CMS method only has two beams that do not pass the acceptance criteria, while the PEER method has three beams that do not pass by a margin as large as 3.75 times the acceptance criteria. The DCR_N results for the CH of Figure 51 show the CMS method also provides lower DCR_N values than the PEER method in all the column lines. The DCR_N at the column bases for the PEER method exceeds the acceptance criteria for the 4 column lines, the CMS exceeds the acceptance criteria for only the two exterior column lines of the frame, column lines B and E. However, when the results are computed using a lognormal distribution, shown in Figure 50 for the RBS and Figure 51 for the CH elements, all the elements, except the base columns of the exterior column lines, pass the acceptance criteria for both the CMS and PEER methods.

The DCR_N dispersion of the RBS elements, shown in Figure 52, show that the CMS method at the controlling period also provides lower dispersion in the beams for most of the elements in the 8-story frame when compared to the PEER selected ground motions that are scaled down at T_1. The exceptions occur at the roof of Bay C-D and Bay D-E of the frame. For the CH elements, shown in Figure 53, the dispersion of the CMS method is mostly lower than that of the PEER ground motions scaled down at T_1. At the base column, only the column line B, shows the PEER scaled down at T_1 with lower dispersion among the base columns.

Figure 54 presents the DCR_N for the RBS elements of the 16-story frame, showing the same trend of CMS results being lower than those obtained from the PEER method. Similar to the 8-story frame, the CMS RBS DCR_N values all pass the acceptance criteria while the mean demand in only the upper five floors of the frame pass for the PEER method. However, if a lognormal distribution is used to compute the RBS DCR_N, shown in Figure 54 as well, then the values reduce so that only a few values exceed the acceptance criteria for the PEER method. If the lognormal distribution is used, then all the CMS results are lower than the acceptance criteria. The DCR_N values of the CH elements, shown in Figure 55, have lower DCR_N values with the CMS method when compared to the PEER. The PEER method has a few elements in each bay exceeding the acceptance criteria while the CMS has no element exceeding the criteria. Assuming a lognormal distribution, the DCR_N for CMS and PEER methods are lower than the acceptance criteria for all column elements.

Figure 56 shows the dispersion of the *DCR*$_N$ results for the 16-story building RBS. As can be seen, the CMS method provides lower dispersion values than the PEER method for most RBS elements. The exceptions where the PEER method has lower dispersion tend to occur in the upper floors of the three bays, which is where conditioning periods other than T_1 control. The dispersion of the CH elements, shown in Figure 57 indicate the CMS method provides lower dispersion for most elements. Similar to the RBS elements, the elements where the dispersion is lower for the PEER scaled down at T_1 are usually located in the upper floors where periods other than T_1 control.

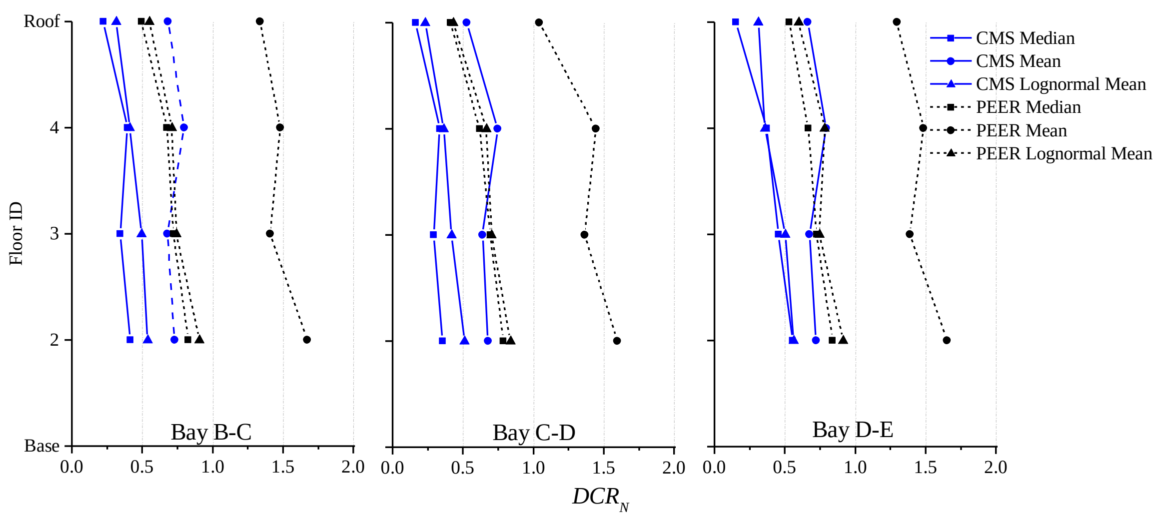

Figure 46. Comparison of max *DCR*$_N$ values of the reduced beam sections computed using an arithmetic mean and a lognormal assumption for ground motions selected using the CMS & PEER methods for the 4-story ELF-designed building. [The "lognormal mean" is calculated using Eq (7), and represents the mean of the max *DCR*$_N$ values assuming the lognormal distribution, see discussion in Section 5.3].

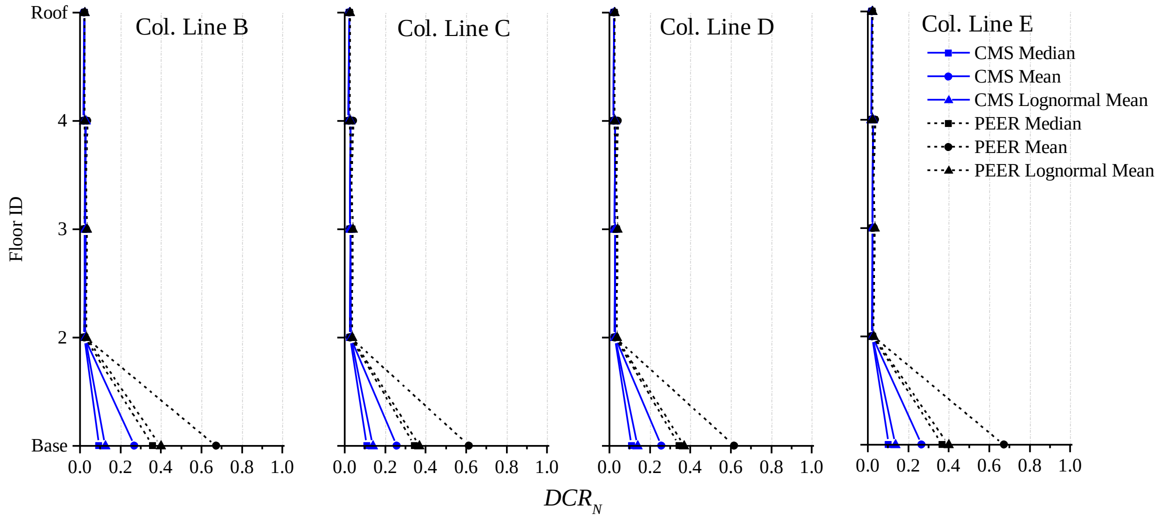

Figure 47. Comparison of max DCR_N values of the column hinges computed using an arithmetic mean and a lognormal assumption for ground motions selected using the CMS & PEER methods for the 4-story ELF-designed building. [The "lognormal mean" is calculated using Eq (7), and represents the mean of the max DCR_N values assuming the lognormal distribution, see discussion in Section 5.3].

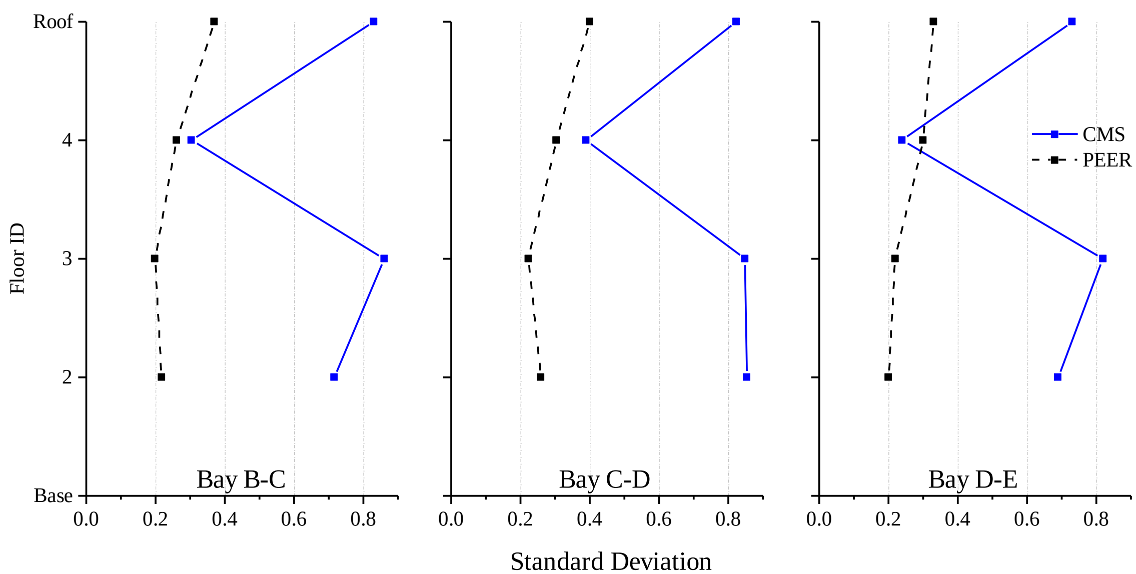

Figure 48. Standard deviation of the DCR_N results for the reduced beam sections of the 4-story ELF designed building using the CMS & PEER ground motions scaled down at T_1.

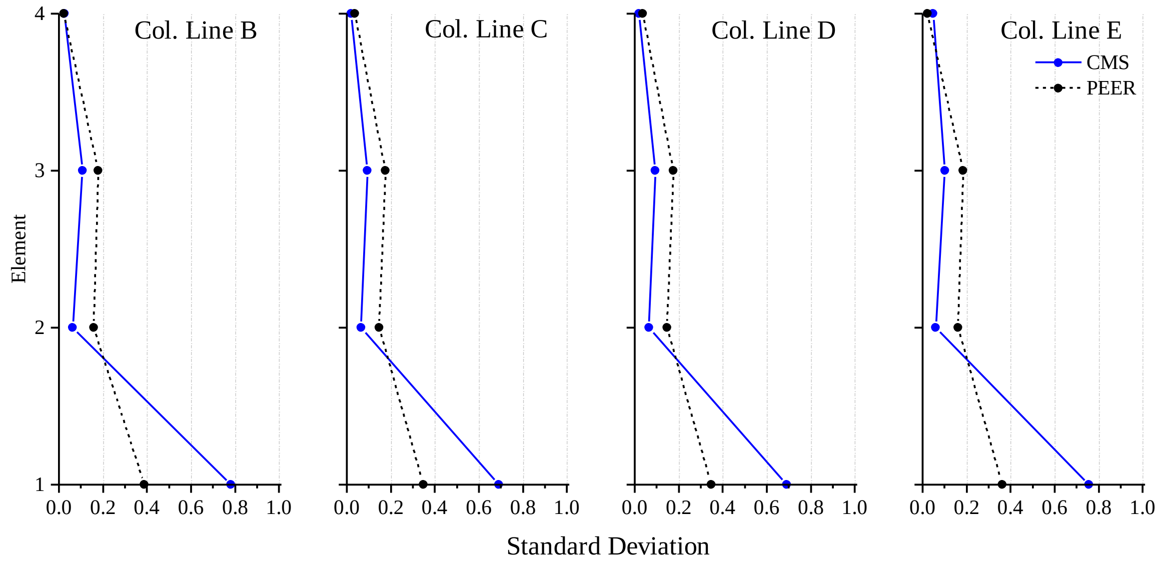

Figure 49. Standard deviation of the DCR_N results for the column hinges of the 4-story ELF designed building using the CMS & PEER ground motions scaled down at T_1.

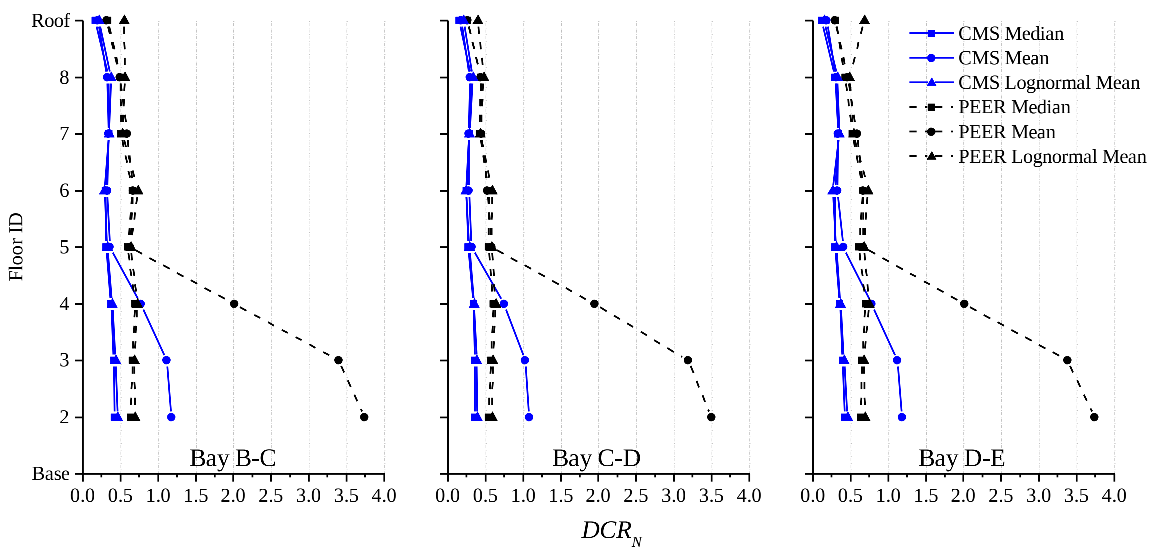

Figure 50. Comparison of max DCR_N values of the reduced beam sections computed using an arithmetic mean and a lognormal assumption for ground motions selected using the CMS & PEER methods for the 8-story ELF-designed building. [The "lognormal mean" is calculated using Eq (7), and represents the mean of the max DCR_N values assuming the lognormal distribution, see discussion in Section 5.3].

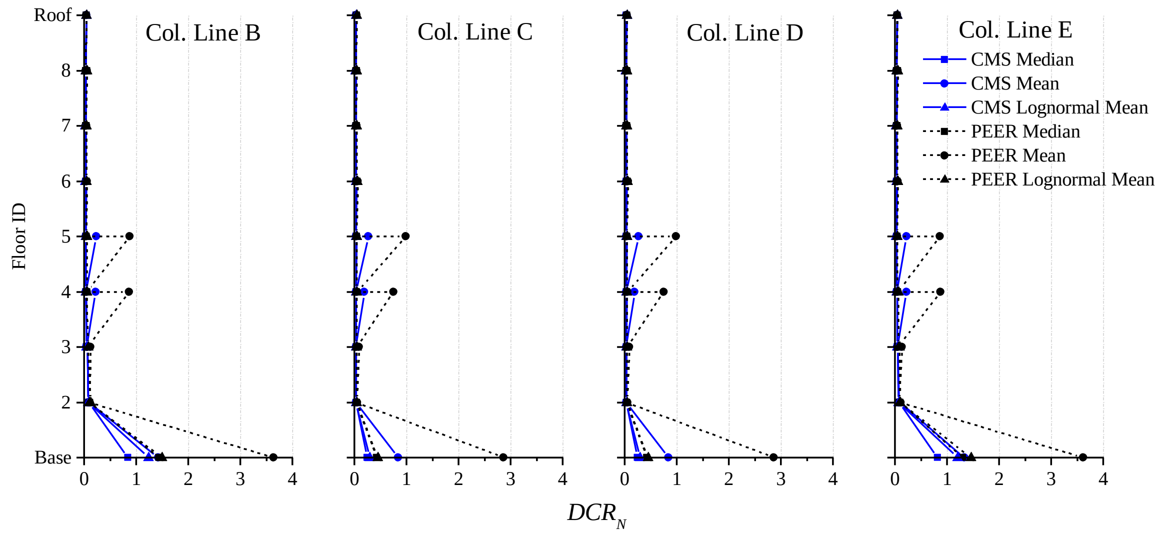

Figure 51. Comparison of max DCR_N values of the column hinges computed using an arithmetic mean and a lognormal assumption for ground motions selected using the CMS & PEER methods for the 8-story ELF-designed building. [The "lognormal mean" is calculated using Eq (7), and represents the mean of the max DCR_N values assuming the lognormal distribution, see discussion in Section 5.3].

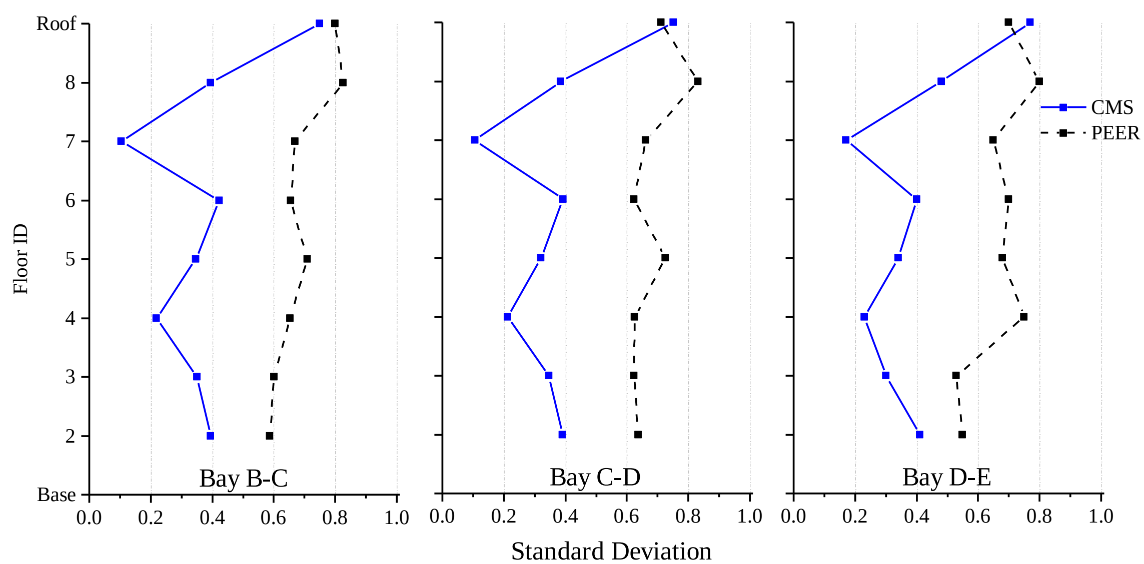

Figure 52. Standard deviation of the DCR_N results for the reduced beam sections of the 8-story ELF designed building using the CMS & PEER ground motions scaled down at T_1.

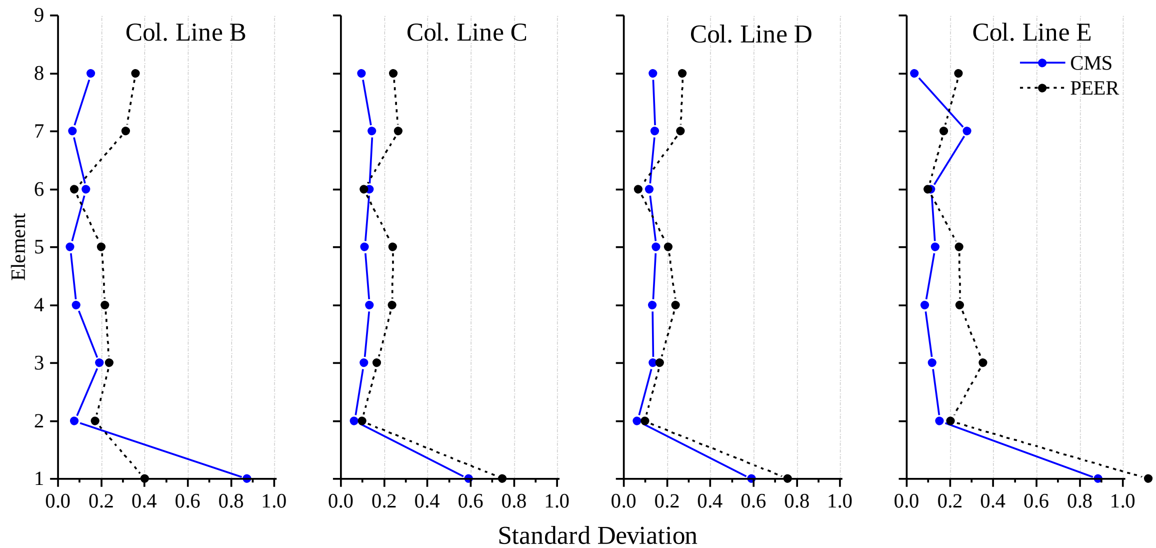

Figure 53. Standard deviation of the DCR_N results for the column hinges of the 8-story ELF designed building using the CMS & PEER ground motions scaled down at T_1.

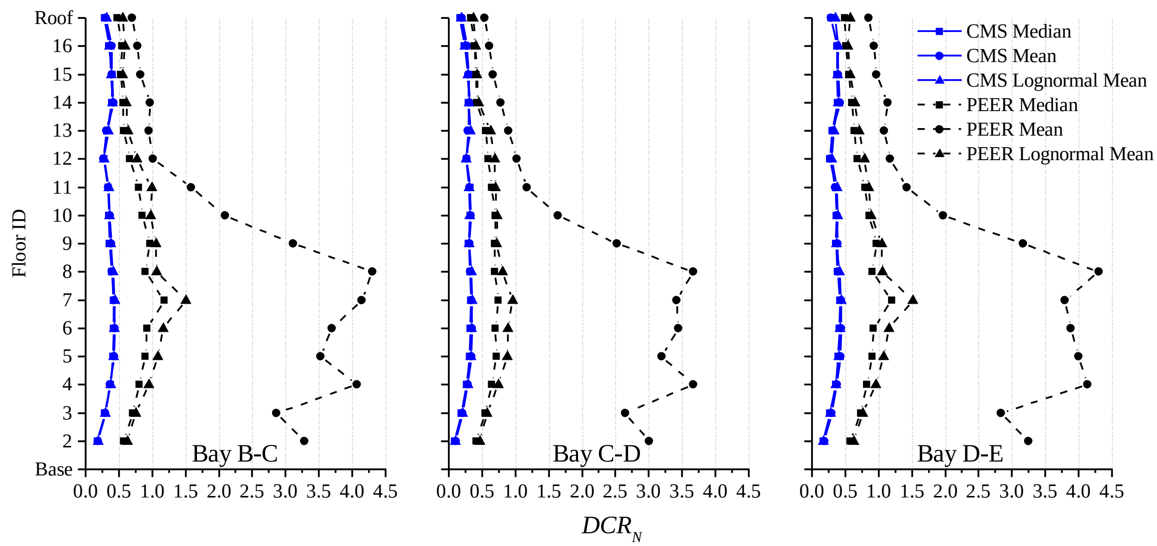

Figure 54. Comparison of max DCR_N values of the reduced beam sections computed using an arithmetic mean and a lognormal assumption for ground motions selected using the CMS & PEER methods for the 16-story ELF-designed building. [The "lognormal mean" is calculated using Eq (7), and represents the mean of the max DCR_N values assuming the lognormal distribution, see discussion in Section 5.3].

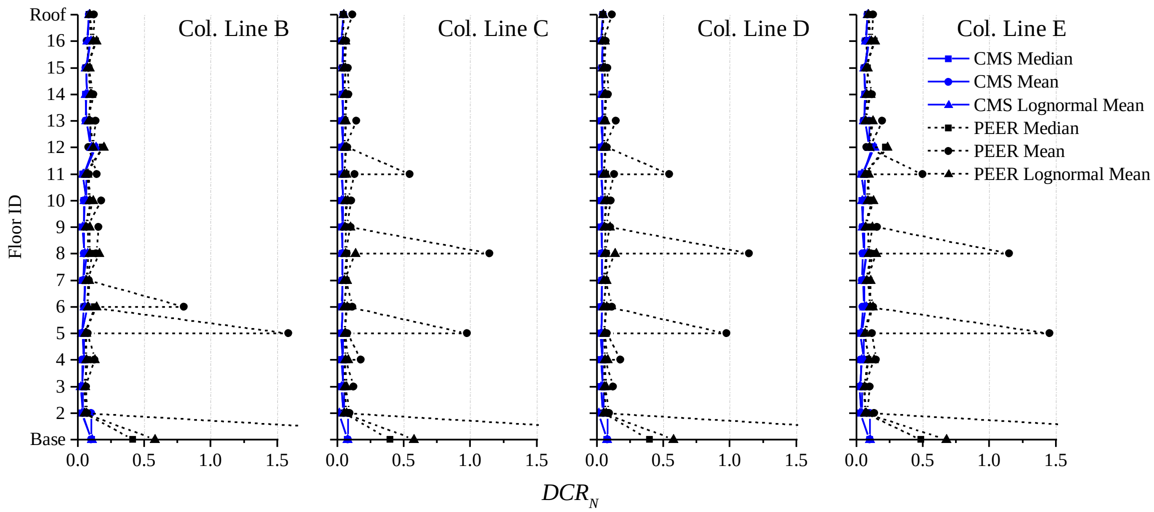

Figure 55. Comparison of max DCR_N values of the column hinges computed using an arithmetic mean and a lognormal assumption for ground motions selected using the CMS & PEER methods for the 16-story ELF-designed building. [The "lognormal mean" is calculated using Eq (7), and represents the mean of the max DCR_N values assuming the lognormal distribution, see discussion in Section 5.3].

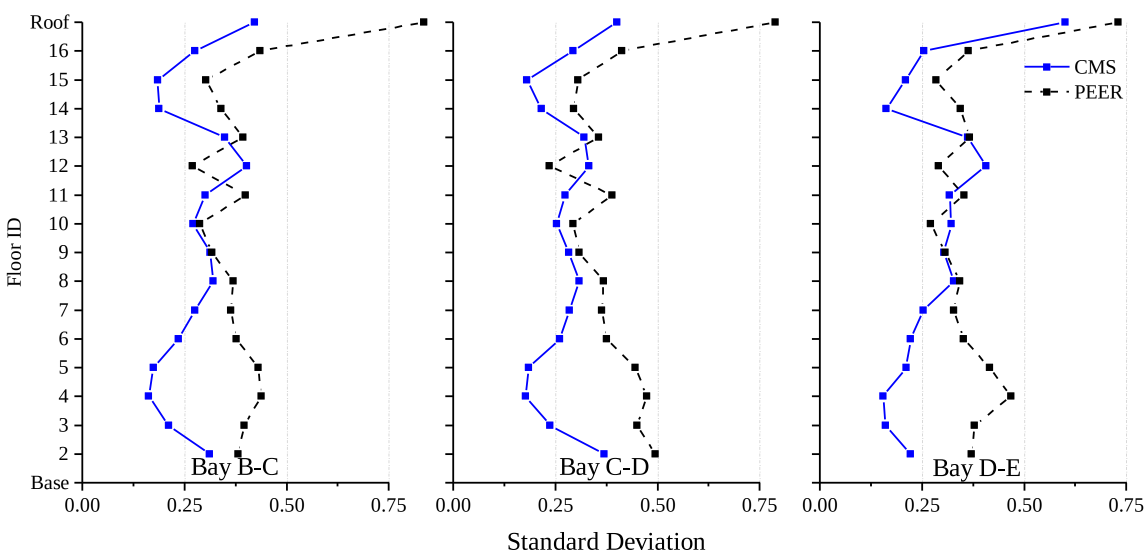

Figure 56. Standard deviation of the DCR_N results for the reduced beam sections of the 16-story ELF designed building using the CMS & PEER ground motions scaled down at T_1.

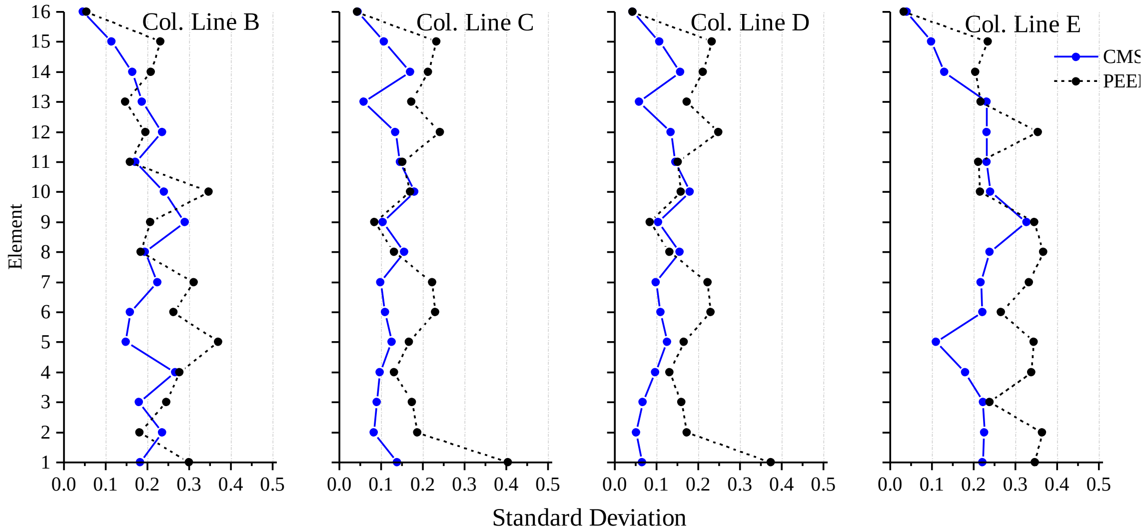

Figure 57. Standard deviation of the DCR_N results for the column hinges of the 16-story ELF designed building using the CMS & PEER ground motions scaled down at T_1.

APPENDIX D:

PROBABILITY DISTRIBUTION OF DCR_N FOR RBS CONNECTIONS

This appendix outlines the statistical test performed on the demand-to-capacity ratio data of the RBS elements and how to interpret the test to determine the underlying distribution associated with the output parameters for the 4-, 8-, and 16-story frames. The results are tabulated for the RBS elements of the three frames.

Previous studies have concluded that the distribution of the spectral accelerations of ground motions can be represented with a lognormal distribution (Baker, 2011; Shome and Cornell, 1999). The response of nonlinear structures is also usually considered to be distributed lognormally (Ibarra and Krawinkler, 2005; Shome and Cornell, 1999), an assumption verified in this appendix. For this research, the response of the building is quantified using the normalized demand to capacity ratio (DCR_N) of the building's elements. To determine the distribution that best fits the DCR_N data obtained, a set of Kolmogorov-Smirnov (K-S) goodness-of-fit tests are conducted to determine the associated data distribution. The data sets are tested to identify which distribution fits the data best between a normal and a lognormal distribution.

The K-S test begins by stating a hypothesis, e.g. assuming a normal or lognormal distribution fits the data. Then, the rest of the test is carried out by comparing the test statistic, known as $D_{n,max}$, to a critical value which is dependent of the significance level. If the test statistic is lower than the critical statistic, then one cannot reject the hypothesis that the assumed distribution fits the data. The test statistic $D_{n,max}$ is calculated with the equation (Ang and Tang, 2007):

$$D_{n,max} = \max|F_x(x_i) - S_n(x_i)|\,\rho(\mathrm{T_i}, \mathrm{T^*})\varepsilon(\mathrm{T^*}) \tag{11}$$

where $F_x(x_i)$ is the theoretical cumulative distribution function, CDF, for the assumed distribution computed using the mean and standard deviation of the data and $S_n(x_i)$ is the step-function also known as the empirical cumulative distribution function (Ang and Tang, 2007). The step-function requires the data to be sorted from smallest to largest and differs depending on the size of the sample. The standard deviation $S_n(x)$ is computed as follows:

$$\begin{aligned} S_n &= 0 && x < x_1 \\ &= \frac{i}{n} && x_i \le x < x_{i+1} \\ &= 1 && x \ge x_n \end{aligned} \tag{12}$$

where $x_1, \dots, x_n$ are the values of the sorted data set, and n is the sample size (Tang and Ang, 2007).

The results of the K-S tests for each building are presented below in Table 18, Table 19, and Table 20 for the 4-, 8-, and 16-story buildings, respectively. The tables present DCR_N results from the CMS and PEER selected ground motions. For the data, a significance level of 1 % is used to determine the value of the critical value for a sample size of 14 realizations from Table A.5 from Ang and Tang (2007). A 1 % significance level is selected because if a stricter significance level were selected, some elements would have rejected the hypothesis of both a normal and lognormal distribution. From the tables of the three frames it can be seen that for some elements the hypothesis of both a normal and lognormal distribution cannot be rejected, but in a majority of the cases a lognormal distribution fits the data better. Thus, in this research the statistical parameters such as the mean and standard deviation are computed using a lognormal distribution for all the elements.

Table 18. Distribution of DCR_N for the RBS connections of the 4-story frame.

4-story frame	CMS at Controlling Period				PEER			
RBS Element	Normal CDF $D_{n,max}$	Lognormal CDF $D_{n,max}$	Critical Value	Best Fitted Distribution	Normal CDF $D_{n,max}$	Lognormal CDF $D_{n,max}$	Critical Value	Best Fitted Distribution
1	0.462	0.221	0.418	Lognormal	0.349	0.290	0.418	Lognormal
2	0.470	0.224		Lognormal	0.338	0.307		Lognormal
3	0.452	0.210		Lognormal	0.346	0.286		Lognormal
4	0.478	0.247		Lognormal	0.466	0.363		Lognormal
5	0.479	0.236		Lognormal	0.462	0.345		Lognormal
6	0.478	0.250		Lognormal	0.468	0.369		Lognormal
7	0.477	0.310		Lognormal	0.450	0.302		Lognormal
8	0.474	0.286		Lognormal	0.460	0.312		Lognormal
9	0.489	0.297		Lognormal	0.418	0.319		Lognormal
10	0.455	0.241		Lognormal	0.443	0.263		Lognormal
11	0.453	0.234		Lognormal	0.444	0.258		Lognormal
12	0.474	0.209		Lognormal	0.420	0.291		Lognormal

Table 19. Distribution of the DCR_N for the RBS connections of the 8-story frame.

8-Story frame	CMS at Controlling Period				PEER			
RBS Element	Normal CDF $D_{n,max}$	Lognormal CDF $D_{n,max}$	Critical Value	Best Fitted Distribution	Normal CDF $D_{n,max}$	Lognormal CDF $D_{n,max}$	Critical Value	Best Fitted Distribution
1	0.487	0.264	0.418	Lognormal	0.386	0.279	0.418	Lognormal
2	0.494	0.267		Lognormal	0.386	0.286		Lognormal
3	0.486	0.270		Lognormal	0.385	0.274		Lognormal
4	0.501	0.318		Lognormal	0.426	0.327		Lognormal
5	0.507	0.331		Lognormal	0.430	0.338		Lognormal
6	0.498	0.299		Lognormal	0.424	0.316		Lognormal
7	0.490	0.325		Lognormal	0.413	0.323		Lognormal
8	0.500	0.347		Lognormal	0.415	0.322		Lognormal
9	0.484	0.318		Lognormal	0.412	0.320		Lognormal
10	0.249	0.161		Lognormal	0.136	0.129		Lognormal
11	0.263	0.151		Lognormal	0.153	0.127		Lognormal
12	0.318	0.220		Lognormal	0.197	0.121		Lognormal
13	0.278	0.154		Lognormal	0.313	0.224		Lognormal
14	0.303	0.186		Lognormal	0.290	0.231		Lognormal
15	0.246	0.119		Lognormal	0.312	0.220		Lognormal
16	0.095	0.116		Normal	0.300	0.199		Lognormal
17	0.071	0.087		Normal	0.202	0.132		Lognormal
18	0.110	0.112		Normal	0.306	0.204		Lognormal
19	0.148	0.127		Lognormal	0.098	0.125		Normal
20	0.173	0.166		Lognormal	0.111	0.150		Normal
21	0.173	0.183		Normal	0.149	0.140		Lognormal
22	0.186	0.211		Normal	0.138	0.136		Lognormal
23	0.155	0.182		Normal	0.116	0.084		Lognormal
24	0.238	0.219		Lognormal	0.175	0.147		Lognormal

Table 20. Distribution of the DCR_N for the RBS connections of the 16-story frame.

16-story frame	CMS at Controlling Period				PEER			
RBS Element	Normal CDF $D_{n,max}$	Lognormal CDF $D_{n,max}$	Critical Value	Distribution	Normal CDF $D_{n,max}$	Lognormal CDF $D_{n,max}$	Critical Value	Distribution
1	0.178	0.118	0.418	Lognormal	0.481	0.360	0.418	Lognormal
2	0.209	0.139		Lognormal	0.479	0.351		Lognormal
3	0.230	0.155		Lognormal	0.481	0.369		Lognormal
4	0.192	0.137		Lognormal	0.496	0.307		Lognormal
5	0.216	0.151		Lognormal	0.526	0.386		Lognormal
6	0.212	0.147		Lognormal	0.516	0.340		Lognormal
7	0.272	0.213		Lognormal	0.455	0.304		Lognormal
8	0.265	0.203		Lognormal	0.462	0.302		Lognormal
9	0.226	0.172		Lognormal	0.459	0.316		Lognormal
10	0.209	0.159		Lognormal	0.420	0.334		Lognormal
11	0.201	0.151		Lognormal	0.431	0.336		Lognormal
12	0.213	0.157		Lognormal	0.437	0.289		Lognormal
13	0.169	0.112		Lognormal	0.404	0.283		Lognormal
14	0.143	0.109		Lognormal	0.421	0.317		Lognormal
15	0.190	0.139		Lognormal	0.414	0.286		Lognormal
16	0.124	0.103		Lognormal	0.424	0.299		Lognormal
17	0.126	0.114		Lognormal	0.418	0.362		Lognormal
18	0.181	0.175		Lognormal	0.409	0.295		Lognormal
19	0.226	0.224		Lognormal	0.453	0.266		Lognormal
20	0.225	0.220		Lognormal	0.456	0.334		Lognormal
21	0.185	0.172		Lognormal	0.454	0.272		Lognormal
22	0.222	0.169		Lognormal	0.468	0.290		Lognormal
23	0.216	0.167		Lognormal	0.493	0.374		Lognormal
24	0.220	0.167		Lognormal	0.454	0.272		Lognormal
25	0.153	0.121		Lognormal	0.412	0.241		Lognormal
26	0.157	0.126		Lognormal	0.501	0.326		Lognormal
27	0.177	0.122		Lognormal	0.455	0.341		Lognormal
28	0.148	0.108		Lognormal	0.393	0.272		Lognormal
29	0.161	0.116		Lognormal	0.460	0.258		Lognormal
30	0.177	0.122		Lognormal	0.433	0.286		Lognormal

Table 20. (continued)

16-story frame	CMS at Controlling Period				PEER			
RBS Element	Normal CDF $D_{n,max}$	Lognormal CDF $D_{n,max}$	Critical Value	Distribution	Normal CDF $D_{n,max}$	Lognormal CDF $D_{n,max}$	Critical Value	Distribution
31	0.118	0.100	0.418	Lognormal	0.444	0.225	0.418	Lognormal
32	0.138	0.086		Lognormal	0.410	0.226		Lognormal
33	0.123	0.109		Lognormal	0.471	0.266		Lognormal
34	0.174	0.155		Lognormal	0.454	0.229		Lognormal
35	0.188	0.177		Lognormal	0.464	0.256		Lognormal
36	0.149	0.128		Lognormal	0.476	0.272		Lognormal
37	0.244	0.209		Lognormal	0.425	0.204		Lognormal
38	0.207	0.168		Lognormal	0.464	0.275		Lognormal
39	0.274	0.249		Lognormal	0.455	0.237		Lognormal
40	0.204	0.155		Lognormal	0.416	0.247		Lognormal
41	0.160	0.158		Lognormal	0.468	0.306		Lognormal
42	0.279	0.240		Lognormal	0.454	0.282		Lognormal
43	0.238	0.174		Lognormal	0.352	0.233		Lognormal
44	0.236	0.167		Lognormal	0.424	0.231		Lognormal
45	0.218	0.168		Lognormal	0.410	0.255		Lognormal
46	0.205	0.114		Lognormal	0.292	0.150		Lognormal
47	0.211	0.129		Lognormal	0.377	0.166		Lognormal
48	0.218	0.168	0.418	Lognormal	0.385	0.204	0.418	Lognormal

APPENDIX E:

COMPARISON OF DCR_N RESULTS WITH AN ALTERNATIVE METHOD

In this appendix the RBS and column hinge (CH) DCR_N results of the 8-story moment frame for the CMS and PEER methods are compared with those of a third, alternative ground motion selection procedure used in the previous NIST study by Harris and Speicher (2015). Note, the results are only shown for the CP building performance level at the BSE-2 seismic hazard level. For the CHs, the fact that some may be considered force-controlled and, therefore should be checked against yield, is reflected in the results.

Many selection procedures are available for use in the NDP of ASCE/SEI 41-13, this study focuses on two methods outlined in Chapter 2. The results of those two methods are compared with those of the third alternative method used in Harris and Speicher (2015) to provide more insight on the effect of ground motion selection. The alternative method is similar to the PEER method, but with slight differences. The key differences between the three methods are presented in Table 21. As shown, the three methods differ on the database used for record selection and error calculation. The difference in database can have an impact in the results because of the different data accessible to each method. While the alternative method has access to 44 records in the FEMA P-695 dataset, the PEER method has access to thousands of records which, in theory, should allow the method to fit the spectrum better due to the greater number of ground motion records that are accessible. As for the error equations used, the alternative method provides the simplest to implement error equation and is applied in a similar manner as the PEER method. The alternative error equation evaluates the error at each period in 0.01 second increments between the $0.2T_1 - 1.5T_1$ period range, whereas the $0.2T_1 - 2T_1$ range is used in the PEER method, and is summed to select the records with the least amount of total error. A combination of the differences in error calculation and database size is the cause of the difference in average spectrum, seen in

Figure 58, and ultimately the differences in *DCR*$_N$. The average spectra of ground motions selected by the three methods for the 8-story moment frame are shown in Figure 58.

Figure 59 shows the RBS *DCR*$_N$ results of the 8-story SMF for the three methods at the CP performance level. The alternative method results in lower mean *DCR*$_N$ than the PEER method in the lower floors but larger in the upper floors while the CMS method has the lowest mean *DCR*$_N$ of the three methods. A majority of the median *DCR*$_N$ are lower for the alternative method in comparison to the PEER results, but are always larger when compared with the CMS method. The reason the alternative method results in *DCR*$_N$ between the other two selection methods is because the average spectra is also between the average of the PEER and CMS spectra at periods larger than approximately 1.0 seconds which includes T_1, as shown in Figure 60 presents the *DCR*$_N$ results for the CH of the 8-story SMF at the CP performance level. Similar to the RBS elements the largest mean *DCR*$_N$ is produced by the PEER method followed by the alternative and CMS methods, respectively. The PEER and alternative methods have results that exceed the acceptance criteria in all column lines while the CMS has results exceeding the criteria in the two outer column lines B and E. The median *DCR*$_N$ results are the largest for alternative method with the PEER having the second largest and CMS method with the lowest. The difference can be seen more clearly at the base of the frame. The CMS method is the only method in which no median DCR_N values are larger than the acceptance criteria. The alternative and PEER methods both produce median DCR_N values greater than unity in the outer column lines B and E. Overall, the CMS method results in lowest DCR_N even when compared to other selection methods in the RBS and CH elements.

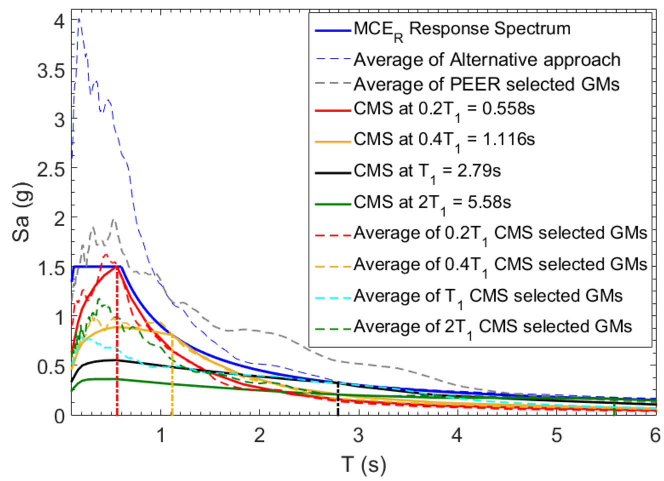

Figure 58. Comparison between the averages and target spectra of the selected ground motions using the CMS, PEER, and alternative methods for the 8-story building.

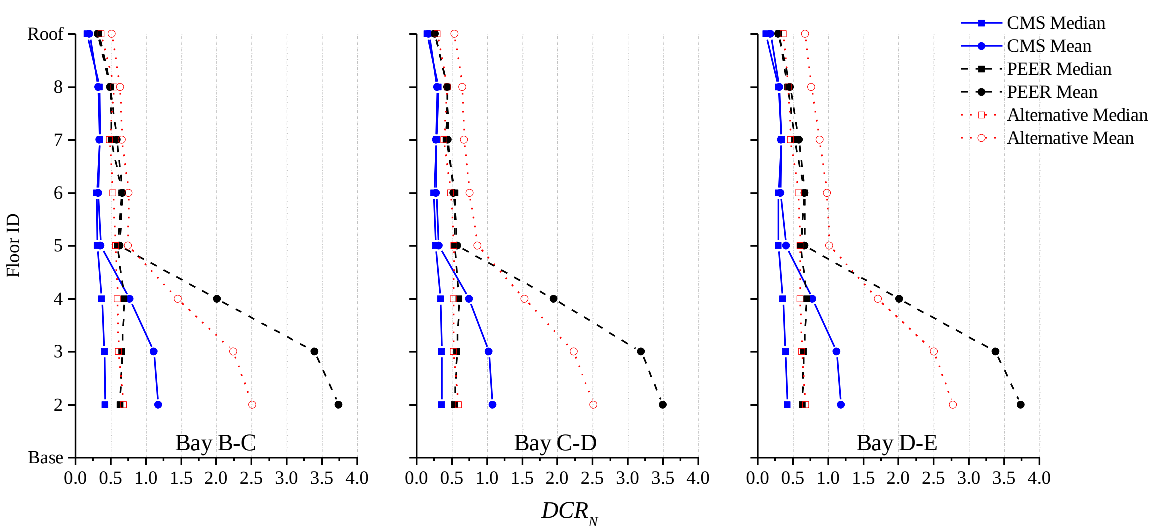

Figure 59. Comparison of max DCR_N values of beams computed for GMs selected using the CMS, PEER, and alternative methods for the 8-story building.

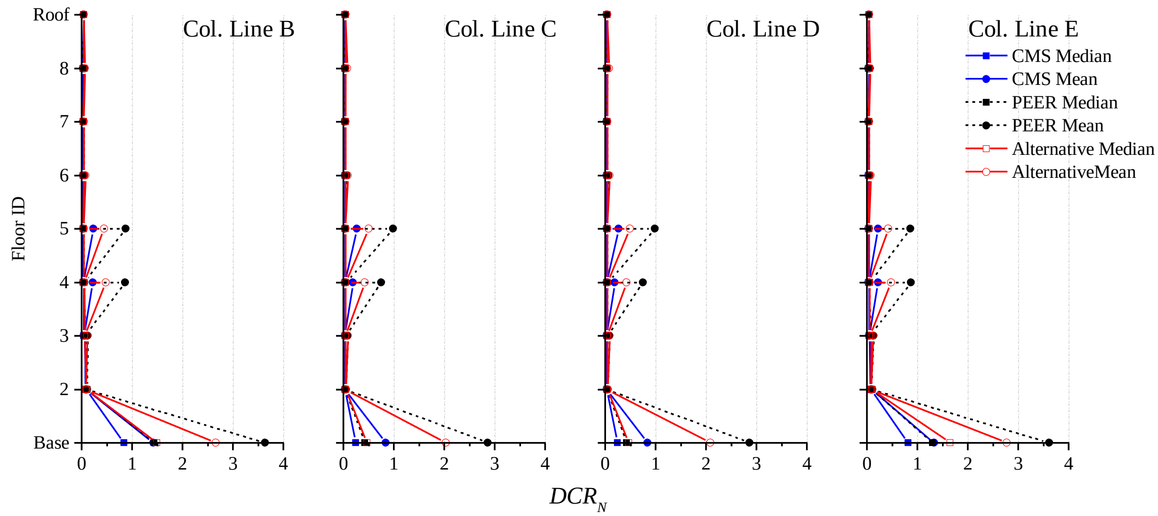

Figure 60. Comparison of max DCR_N values of the column hinges computed for GMs selected using the CMS, PEER, and alternative ground motion selection methods for the 8-story building.

Table 21. Differences in ground motion database, target spectrum, and error calculation used between the CMS, PEER, and alternative methods.

	CMS Method	PEER Method	Alternative Method
Ground Motion Database	PEER NGA-West 2	PEER NGA-West 2	FEMA P-695 Subset
Target Spectrum	Conditional Mean Spectrum (CMS)*	Maximum Considered Earthquake (MCE_R)	Maximum Considered Earthquake (MCE_R)
Error Used	Sum of Squared Error (SSE)	Mean Square Error (MSE)	Percent Error
Equation used for calculating error	$\sum_{j=1}^{n}\left(lnS_a(T_j) - lnS_{a,CMS}(T_j)\right)^2$	$\frac{\left(\sum_i w(T_i)\{\ln[S_a^{target}(T_i)] - \ln[f * S_a^{record}(T_i)]\}^2\right)}{\sum_i w(T_i)}$	$\sum_{j=1}^{n}\left(1 - \frac{S_{a,greater}}{S_{a,lesser}}\right)$
Period range for minimizing error	All periods for which the CMS is calculated	$0.2T_1 - 2T_1$	$0.2T_1 - 1.5T_1$

*The CMS uses a single value on the MCE_R as a starting point to create the CMS and is the point where all the ground motions are scaled to have the same spectral acceleration, thus the CMS method scales to the MCE_R implicitly.

REFERENCES

Adam, C., Kampenhuber, D., Ibarra, L.F., Tsantaki, S., 2016. Optimal Spectral Acceleration-based Intensity Measure for Seismic Collapse Assessment of P-Delta Vulnerable Frame Structures. Journal of Earthquake Engineering 21(7), 1189-1195. doi:10.1080/13632469.2016.1210059

AISC, 2010. Seismic Provisions for Structural Steel Buildings, (ANSI/AISC 341-10). American Institute of Steel Construction, Chicago, IL.

ASCE, 2016. Minimum Design Loads for Buildings and Other Structures Draft, 7th ed. American Society of Civil Engineers, Reston, VA.

ASCE, 2014. Seismic Evaluation and Retrofit of Existing Buildings, 41st ed. American Society of Civil Engineers, Reston, VA.

ASCE, 2010. Minimum Design Loads for Buildings and Other Structures, 7th ed. American Society of Civil Engineers, Reston, VA.

Baker, J.W., 2016. Baker Research Group http://web.stanford.edu/~bakerjw/gm_selection.html (accessed 9.9.16).

Baker, J.W., 2011. Conditional Mean Spectrum: Tool for ground motion selection. Journal of Structural Engineering. 137, 322–331.

Campbell, K.W., Bozorgnia, Y., 2008. NGA Ground Motion Model for the Geometric Mean Horizontal Component of PGA, PGV, PGD and 5% Damped Linear Elastic Response Spectra for Periods Ranging from 0.01 to 10 *s*. Earthquake Spectra 24, 139–171. doi:10.1193/1.2857546

CSI, 2011. PERFORM 3D. Computers and Structures, Inc, Berkeley, California.

Harris, John L., Speicher, M.S., 2015. Assessment of First Generation Performance-Based Seismic Design Methods for New Steel Buildings, Volume 1: Special Moment Frames (NIST TN 1863-1). National Institute of Standards and Technology. http://dx.doi.org/10.6028/NIST.TN.1863-1.

Haselton, C.B., Baker, J.W., Bozorgnia, Y., Goulet, C.A., Kalkan, E., Luco, N., Shantz, T., Shome, N., Stewart, J.P., Tothong, P., others, 2009. Evaluation of ground motion selection and modification methods: Predicting median interstory drift response of buildings. PEER Rep. 2009/01, Pacific Earthquake Engineering Research Center, Berkeley, CA.

Ibarra, L.F., Krawinkler, H., 2005. Global collapse of frame structures under seismic excitations. Report No. 152, Pacific Earthquake Engineering Research Center, Berkeley, CA.

International Code Council (ICC), 2012. 2012 International Building Code. ICC, Washington, D.C.

Jayaram, N., Lin, T., Baker, J.W., 2011. A Computationally Efficient Ground-Motion Selection Algorithm for Matching a Target Response Spectrum Mean and Variance. Earthq. Spectra 27, 797–815.

Kalkan, E., Chopra, A.K., 2010. Practical guidelines to select and scale earthquake records for nonlinear response history analysis of structures. US Geological Survey, Open-File Report 1068, Reston, Virginia

Krawinkler, H., 1978. Shear in beam-column joints in seismic design of steel frames. Engineering Journal 15, 82-91.

Lin, T., Haselton, C.B., Baker, J.W., 2013. Conditional spectrum-based ground motion selection. Part I: Hazard consistency for risk-based assessments. Earthquake Engineering and Structural Dynamics 42, 1847–1865.

NIST, 2011. Selecting and scaling earthquake ground motions for performing response history analyses. GCR 11-917-15, National Institute of Standards and Technology, Gaithersburg, Maryland.

OpenSHA, 2016. Applications. http://www.opensha.org/apps (accessed 9.9.16).

PEER, 2016. PEER Ground Motion Database - PEER Center. http://ngawest2.berkeley.edu/ (accessed 9.9.16).

Sattar, S., 2018. Evaluating the consistency between prescriptive and performance-based seismic design approaches for reinforced concrete moment frame buildings. Engineering Structures 174, 919–931. https://doi.org/10.1016/j.engstruct.2018.07.080

Sattar, S., Liel, A.B., Martinelli, P., 2013. Quantification of Modeling Uncertainties Based on the Blind Prediction Contest Submissions, ASCE Structures Congress Proceedings, pp. 1997–2008. https://doi.org/10.1061/9780784412848.175

Shome, N., Cornell, C.A., 1999. Probabilistic seismic demand analysis of nonlinear structures.

Speicher, M.S., Harris, J.L., 2016a. Collapse Prevention seismic performance assessment of new eccentrically braced frames using ASCE 41. Engineering Structures. 117, 344–357. http://dx.doi.org/10.1016/j.engstruct.2016.02.018.

Speicher, M.S., Harris, J.L., 2016b. Collapse prevention seismic performance assessment of new special concentrically braced frames using ASCE 41. Engineering Structures. 126, 652-666. http://dx.doi.org/10.1016/j.engstruct.2016.07.064.

Tang, W.H., Ang, A., 2007. Probability Concepts in Engineering: Emphasis on Applications to Civil & Environmental Engineering. Wiley.

USGS, 2016a. Custom Vs30 Mapping. http://earthquake.usgs.gov/hazards/apps/vs30/custom.php

USGS, 2016b. 2008 Interactive Deaggregations. http://geohazards.usgs.gov/deaggint/2008/ (accessed 9.9.16).

USGS, 2016c. U.S. Seismic Design Maps. http://earthquake.usgs.gov/designmaps/us/application.php (accessed 9.9.16).